Meshfree Methods: Progress Made After 20 Years

Jiun-Shyan Chen

Prager Professor, Dept. of Structural Engineering, Univ. of California, San Diego, 9500 Gilman Dr., La Jolla, CA 92093 (corresponding author). E-mail: js-chen@ucsd.edu

Michael Hillman

Kimball Assistant Professor, Dept. of Civil and Environmental Engineering, Pennsylvania State Univ., University Park, PA 16802.

Sheng-Wei Chi

Assistant Professor, Dept. of Civil and Materials Engineering, Univ. of Illinois at Chicago, 842 W. Taylor St., Chicago, IL 60607.

Abstract

The finite difference method (FDM) and the finite element method (FEM) rely on a mesh (or stencil) to construct the local approximation of functions and their derivatives for solving partial differential equations (PDEs). A few drawbacks are commonly encountered in these methods:

- time consuming in generating a quality mesh in arbitrary geometry for desired accuracy,
- difficult in constructing approximations with arbitrary order of continuity, making the solution of PDEs with higher order differentiation or problems with discontinuities difficult to solve,
- tedious in performing *h*- or *p*-adaptive refinement, and
- ineffective in dealing with mesh entanglement related difficulties (such as those in large deformation and fragment-impact problems).

Meshfree methods all share a common feature that alleviate or eliminate the above issues: *the approximation of unknowns in the PDE are constructed based on scattered points without mesh connectivity*. As shown in Figure 1, the approximation function at a point in FEM is constructed at the element-level natural coordinate and then transformed to the global Cartesian coordinate, whereas meshfree approximation functions are constructed using only nodal data in the global Cartesian coordinates directly. These compactly supported meshfree approximation functions form a partition of unity subordinate to the open cover of the domain with controllable orders of continuity and completeness, independent from one another. Using this class of approximation functions, it becomes possible to relax the strong tie between the quality of the discretization and the quality of approximation in FEM, and the procedures in *h*-adaptivity are significantly simplified. Special basis functions can be embedded in the approximation to capture essential characteristics of the PDE at hand, and arbitrary discontinuities can be introduced into the approximation as well.

In the past 20 years, meshfree methods have emerged into a new class of computational methods with considerable success. In addition, a significant amount of progress has been made in addressing the major shortcomings that were present in these methods at the early stages of their development. For instance, essential boundary conditions are almost trivial to enforce by employing the techniques now available, and the need for high order quadrature has been circumvented with the development of advanced techniques, essentially eliminating the previously existing bottleneck of computational expense in meshfree methods. Given the proper treatment, nodal integration can be made accurate and free of spatial instability, making it possible to eliminate the need for a mesh entirely. Meshfree collocation methods have also undergone significant development, which also offer a truly meshfree solution. This paper gives an overview of many classes of meshfree methods and their applications, and several advances are described in detail.

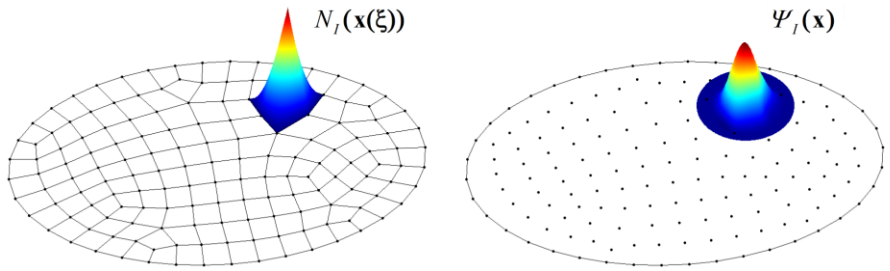

Figure 1. (a) Patching of a finite element shape function from local element domains, and (b) a meshfree approximation function constructed directly in the global Cartesian coordinates.

Acronym Appendix

CPDI – convected particle domain interpolation
C-SPH – corrected SPH
DEM – diffuse element method
DNI – direct nodal integration
EFG – element free Galerkin
FEM – finite element method
FMM – free mesh method
FPM – finite point method
GFD – generalized finite difference
GFEM – generalized finite element method
GI – Gauss integration
GIMP – generalized interpolation material point
GRKCM – gradient RKCM
HPC – *hp* clouds
IGC – isogeometric collocation
KC – kernel contact
L-RBCM – localized RBCM
LRPIM – local radial point interpolation method
LS – least squares
MaxEnt – maximum entropy
MFEM – meshless finite element method
MFS – method of finite spheres
MLPG – meshless local Petrov-Galerkin
MLS – moving least squares
MLSPH – moving least squares particle hydrodynamics
MPM – material point method
MPS – moving particle semi-implicit
MQ – multiquadratics
M-SCNI – modified SCNI
M-SNNI – modified SNNI
NEM – natural element method
NSNI – naturally stabilized nodal integration
NURBS – non-uniform rational B-splines
OTM – optimal transport meshfree
PFEM – particle finite element method
PFEM-2 – second generation PFEM
PPU – particle partition of unity method
PU – partition of unity
PUM – partition of unity method
RBCM – radial basis collocation method
RBF – radial basis function
RK – reproducing kernel
RKCM – Reproducing kernel collocation method
RKPM – reproducing kernel particle method
RPIM – radial point interpolation method
SCNI – stabilized conforming nodal integration
SFEM – smoothed finite element method
SGFEM – stable GFEM
SLRKPM – semi-Lagrangian RKPM
SNNI – stabilized nonconforming nodal integration
SPH – smoothed particle hydrodynamics
VCI – variationally consistent integration
VC-MSNNI – variationally consistent MSNNI
VC-NSNI – variationally consistent NSNI
WLS – weighted least squares
XEFG – extended EFG
XFEM – extended finite element method
XIGA – extended IGA

1. Introduction

Meshfree methods evolved from the mesh-based finite element methods and emerged into a new class of numerical methods for solving partial differential equations (PDEs) using a point-based approximation and discretization. Generally speaking, meshfree methods have been developed under two branches of formulations:

1. The Galerkin meshfree methods based on the weak form of PDEs. While no mesh is needed in the construction of the approximation, domain integration is required, and special techniques to enforce essential boundary conditions are needed. Advances in domain integration and enforcement of boundary conditions are discussed in Section 3.
2. The collocation meshfree methods based on the strong form of PDEs. Due to the ease of constructing smooth meshfree approximations, PDEs can be solved directly at the collocation points without special domain integration and essential boundary condition procedures, as will be presented in Section 4.

A wide variety of meshfree methods have been proposed over the years. Table 1 summarizes the attributes of some selected methods, along with some mesh-based methods for comparison. The table is roughly ordered by the dates the methods were proposed (or when the first robust version was proposed), which also gives some historical perspective. In Table 2, an alternative analysis is presented and made slightly more precise, where these methods are shown at the intersection of the solution method (columns) and the approximation employed (rows). In this paper, we hope to elucidate the relationship between the various meshfree methods, and present advancements that have been made over the years.

Method	Approximation Function												Solution Scheme (Discretization)								
	Local											Global	Weak form					Strong form			Lagrangian-Eulerian form
	With Polynomial Reproduction (PR)									without PR			Bubnov-Galerkin		Petrov-Galerkin						
	Local Polynomials	MLS/RK		WLS	Enriched		Natural neighbor	Maximum Entropy	Splines/NURBS	Smooth Kernel	Local RBF	RBF	Gauss integration	Stabilized Integration	Point Collocation	Gauss integration	Variationaly Consistent	Point Collocation	Subdomain Collocation	Weighted Collocation	
		Direct	Diffuse		Polynomials	MLS/RK (PU)															
FEM[1] [1], SFEM[1] [2]	•												•	•							
SPH[2,3] [3,4]										•					•						
GFD [5,6]			•															•			
RBCM [7–10]											•	•						•	•	•	
DEM [11]			•										•								
EFG [12–14], XEFG [15,16]		•				•							•	•							
MPM [17,18], GIMP [19], CPDI [20], PFEM-2 [21,22]	•																				•
RKPM [23,24], SLRKPM[3] [25]		•											•	•							
GFEM [26,27], XFEM [28,29]					•								•								
MPS[4] [30]				•														•			
PUM [31,32]	•				•	•							•								
hp clouds [33,34]						•							•								
FPM [35]				•														•			
FMM[3] [36]	•												•								
C-SPH/MLSPH[2,3] [37]		•													•						
MLPG [38]		•								•						•					
NEM [39,40]							•						•								
PPU [41]						•							•								
MFS [42]						•							•								
RKCM [43,44], GRKCM [45]		•	•															•		•	
Meshless SCNI [46–48]		•												•							
LRPIM [49]	•									•	•					•					
RPIM [50]	•										•		•								
MFEM[3] [51], PFEM[3] [52,53]							•						•								
MaxEnt [54,55]								•					•								
IGA[1] [56,57]									•				•				•				
Peridynamics[5] [58,59]			•															•			
OTM[3] [60]								•					•								
Meshless VCI[6] [61]		•											•	•	•		•				

[1]Mesh-based; [2]Considered weak form here due to weakened approximation requirements; [3]Continually reconstructed; [4]WLS-type approximation of pair-wise gradients; [5]Employs diffuse derivatives [62]; [6]Can construct for any integration.

Table 1. Attributes of selected mesh-based and mesh-free methods.

					Solution Scheme (Discretization)	
					Weak form	**Strong form**
Approximation Function	Local Polynomial	Lagrangian mesh	No enrichment	Direct derivatives	FEM [1]	
				Smoothed derivatives	SFEM [2]	
			Enriched		GFEM [26,27], XFEM [28,29]	
		Continually reconstructed			FMM [36]	
		Eulerian mesh, Lagrangian points	Points carry history and mass		MPM [17,18], GIMP [19], CPDI [20]	
			Points carry history		PFEM-2 [21,22]	
	Spline / NURBS	No enrichment			IGA [56,57]	IGC [63]
		Enriched			XIGA [64,65]	
	MLS	No enrichment	Direct derivatives		EFG [12–14], MLPG [38], MLSPH/C-SPH [37]	
			Diffuse derivatives[1]		DEM [11]	Peridynamics[2] [58,59], GFD [5,6]
			VCI derivatives		Meshless VCI [61], Meshless SCNI [46,47]	
		Enriched			XEFG [15,16]	
	RK	Lagrangian	Smoothed derivatives		Meshless SCNI [46,47]	
			Direct derivatives		RKPM [23,24]	RKCM [43,44]
			Diffuse derivatives[1]			GRKCM [45]
		Continually reconstructed			SLRKPM [25]	
	PU	Polynomial enriched			*hp* clouds [33,34], MFS [42]	
		Polynomial and/or other enriched			PUM [31,32], PPU [41]	
	MaxEnt	Lagrangian			MaxEnt method [54,55]	
		Continually reconstructed			OTM [60]	
	Natural neighbor	Lagrangian			NEM [39,40]	
		Continually reconstructed			MFEM [51], PFEM [52,53]	
	Radial basis functions				RPIM [50], LRPIM [49]	RBCM [7,8]
	Weighted least squares					FPM [35]
	Kernel approximation				SPH[3] [3,4]	
	WLS of pair-wise gradients					MPS [30]

[1]Implicit, diffuse and synchronized derivatives, and generalized finite differences are equivalent, see Section 2.6; [2]Employs diffuse derivatives [62]; [3]Considered weak form here due to weakened approximation requirements.

Table 2. Methods shown at intersection of approximation function and solution method.

1.1 Early Development

The early development of meshfree methods can be traced back to smoothed particle hydrodynamics (SPH) by Lucy [3] and Gingold and Monaghan [4] for astrophysics modeling. SPH was formulated by kernel estimation [66,67] of conservation equations. The method later gained traction in solid mechanics as a way to solve problems difficult for mesh-based methods such as fragment-impact problems [68–71]. The accuracy, tensile instability, and spatial instability of SPH have been examined [23,72–74], and formulations have been proposed to correct the deficiencies in SPH [37,70,75–77]. These later enhancements of SPH have motivated the development of many more modern meshfree methods. A prime example is the introduction of RKPM [23] as a correction of SPH for enhanced consistency and stability.

Another branch of numerical methods for solving PDEs which do not rely on a grid structure is the class of generalized finite difference (GFD) methods. One of the earliest finite difference methods using scattered points is due to Jenson [78]. A difficulty associated with this method, however, was the selection of an appropriate "star" (collection of neighbors) such that the resulting matrix for determining weights at a point is not singular, analogous to the moving least-squares (MLS) requirements (this is in fact, not a coincidence, see Section 2). Perrones and Kao introduced an algorithm [79] to avoid this difficulty, and also improved the accuracy of mixed derivatives. A robust GFD method by Liszka and Orkisz [5,6] considered an arbitrary number of neighbors for higher accuracy and matrix stability, resulting in an overdetermined system solved by weighted least-squares. In meshfree terminology, this method employs second order basis with diffuse derivatives for the solution of the strong form of the problem, see Section 2.6. In [6], Liszka formalized the inclusion of the approximation of the primary variable in [5] and independently arrived at the moving least-squares (MLS) approximation [80] by Lancaster and Salkauskas. Many modern meshfree methods originate from the employment of this approximation for solving PDEs.

1.2 Galerkin Meshfree Methods

The diffuse element method (DEM) [11] employed a MLS approximation for the Galerkin solution of boundary value problems for the first time. The authors apparently also independently derived the MLS approximation [80]. In this method, derivatives in the weak form are approximated by the differentiation of a certain portion of the basis functions, which are considered "diffuse derivatives". Section 2.6 gives and in depth discussion on the relationship between diffuse derivatives and several other meshfree approximations.

Thereafter, Belytschko et al. [12–14] introduced the element-free Galerkin (EFG) method as an improvement of DEM. They introduced Lagrange multipliers to enforce boundary conditions, and used the full derivative of the MLS approximation functions in the Galerkin solutions of PDEs. Further, they introduced higher order quadrature based on a background mesh to achieve enhanced accuracy in the Galerkin solution. They showed that with these improvements, EFG gave superior

accuracy over employing diffuse derivatives and enforcing boundary conditions on nodal coefficients. Taking advantage of the ability to embed discontinuities into the approximation without remeshing, as well as straightforward *h*-refinement, EFG was effectively applied to fracture mechanics problems [13,81,82].

Motivated by wavelet analysis, Liu et al. [23] introduced the reproducing kernel particle method (RKPM) based on the reproducing kernel (RK) approximation, around the same time as the EFG method was proposed (see Table 1). They demonstrated that the discrete version of the RK kernel estimate offered favorable properties over DEM and SPH, and could serve as a correction to SPH, which is particularly inaccurate near boundaries. It was shown by Chen et al. [24] that the discretizations of the continuous form of the RK approximation and the moment matrix needs to be done in a consistent manner in order to preserve polynomial reproducibility. They then introduced a direct discrete reproducing kernel approximation [83] to avoid the trouble of determining the integration weights based on the continuous RK approximation. Error and convergence estimates for RKPM with monomial bases have since been well established [84–87]. Based on the RKPM method, a multiresolution extension has been proposed [84,88–90], as well as a related framework which can yield synchronized convergence and a hierarchical partition of unity [91–93]. RKPM has been shown to be particularly effective for large deformation problems [24,94–99], smooth contact [100–102], multi-body contact, and fragment-impact problems [103–105], among others (see Section 6). Adaptive refinement can also be implemented with relative ease compared to the conventional mesh-based methods [88,90,106–108].

One major difference between meshfree and finite element approximations is that the meshfree approximations such as MLS and RK are constructed without the need of mesh topology and they are typically rational functions. Domain integration of the weak form poses considerable complexity in the Galerkin meshfree method. Employment of Gauss quadrature rules yields integration errors when background calls do not coincide with the shape function supports [109]. Direct nodal integration, on the other hand, results in rank deficiency and loss of accuracy. The above mentioned EFG and RKPM methods with Gauss quadrature or nodal integration do not pass the linear patch test for non-uniform point distributions. A stabilized conforming nodal integration (SCNI) [46] has been introduced to ensure passing the linear patch test and to remedy rank deficiency of direct nodal integration. More recently, an extension of SCNI for quadratic basis functions has been proposed [110]. A generalization of conditions for passing the linear patch test (for Galerkin exactness) to arbitrary order has also been recently introduced under the framework of variational consistency [61]. A variationally consistent integration (VCI) approach has been proposed that can be used as a correction of any quadrature rules to achieve optimal rates of convergence. Stabilization of nodal integration has also been proposed, including adding a residual of the equilibrium equation to the nodally integrated potential energy functional [111], the stress point method by taking derivatives away from the nodal points [75], and an approach based on an iterative correction of nodal integration for passing the patch test in conjunction with a least-squares type stabilization [77]. An in depth discussion of progress made on quadrature will be presented in Section 3.3.

A series of meshfree methods have emerged based on the partition of unity (PU) framework by Melenk and Babuška [31,32]. For a general survey of mathematical results concerning PU methods, see [112]. In [33], Duarte and Oden introduced a meshfree method called *hp* clouds based on PU, where the MLS approximations were enriched *extrinsically* (adding additional degrees of freedom in the PU approximation) with higher order complete polynomials. This gave the ability to perform *p*-adaptivity since bases could vary in space, in contrast to the MLS-based methods where this would introduce a discontinuity. The completeness of the approximation depends on the order of the complete monomials in the higher order enrichment. They also proposed *p*-refinement in the enrichment of MLS with constant bases (using the Shepard function [113]). In [114], this concept was extended to FEM for an *hp* finite element method. An important offshoot of the PU method is the celebrated XFEM [28,29] which is an active area of research in finite elements.

In [27,115,116], the partition of unity finite element method was redesigned in a more general fashion and was labeled GFEM. Efforts have been devoted to algorithms that ease the linear dependency which can occur in PU methods, and adaptive integration techniques have been proposed to enhance integration of enrichment functions [116]. A GFEM implementation has been proposed where meshes that are completely independent of geometry can be employed by using automatic generation of domain-conforming integration cells, with "hand-book" enrichments for features like corners, which greatly alleviates difficulty in meshing for solving PDEs on complex domains [27,115]. Thus, opposite to many meshfree Galerkin methods, the approximation is mesh-based but the integration scheme is meshfree. More recently, stable GFEM (SGFEM) was proposed in [117,118] that gives far better conditioning of the stiffness matrix than GFEM. An approach where a local solution can be embedded in the global solution under the framework of partition of unity to achieve computational efficiency and accuracy has also been recently introduced [119,120]. In this global-local approach, the local solution is "patched" together by the global partition of unity functions. This method has been applied to fracture modeling [121–123].

Based on the partition of unity methods, Griebel and Schweitzer [41] introduced the particle-partition of unity method, which considered the aspects of constructing a meshfree partition of unity method under an arbitrary distribution of points. They systematically examined issues such as quadrature and constructing a PU subordinate to open cover [124], solvers and parallelization [125,126], and boundary conditions in this non-interpolatory method [127].

In Galerkin meshfree methods, integration of the weak form often performed by a background mesh (cf. [12]). The *Meshless local Petrov-Galerkin* (MLPG) method [38,128] introduced by Atluri and Zhu [38] employed a *local weak form* for an MLS-based meshfree method, where the weak form is formulated in local domains and avoids background cell integration. The local domain was selected to coincide with supports of test functions, resulting in each row of the stiffness matrix being integrated over the local support of the test functions. They have also extended this method to a boundary integral technique in [129]. De and Bathe introduced the method of finite spheres [42,130]

as a special case of MLPG, with additional modifications to improve boundary condition enforcement and quadrature.

A number of other Galerkin meshfree methods have been introduced, and here we name a few for the sake of brevity. The natural element methods (NEMs) [39,40] employ natural neighbor interpolation, based on Voronoi diagrams of a set of arbitrarily distributed points. This includes the Sibson Interpolants [131] and Laplace interpolants (non-Sibsonian interpolants) [132], which are positive functions with partition of unity and first order completeness. The radial point interpolation method (RPIM) [50] uses a combination of radial and polynomial basis functions, which gives completeness, the interpolation property, and offers efficient derivative computation. The local RPIM (LRPIM) [49] employs the same approximation, but with a local weak form for a method without background cells. Convex approximations for meshfree computation based on the principle of maximum entropy (MaxEnt) [133] to achieve unbiased statistical influence of nodal data have been proposed for the Galerkin solution of PDEs [54,55]. The approximation functions constructed by maximum entropy (a measure of uncertainty) subjected to monomial reproducibility constraints are positive, can interpolate affine functions exactly, and have a weak Kronecker-delta property at the boundary. Li, Ortiz, and co-workers proposed the optimal transport meshfree (OTM) method [60] which utilizes maximum entropy approximations under the framework of optimal transport theory [134]. In order to discretize the equations, material points are employed for mass transport, and MaxEnt is employed for mapping of configurations. The MaxEnt approximation is continually reconstructed and has been applied to fragment-impact problems [135,136]. Recently, higher order versions of maximum entropy approximations have been developed in [137–140]. This approximation, as well as the RK and MLS approximations, were recently generalized under a unified framework in [141], and have been employed for convex approximations and the weak Kronecker-delta property in the meshfree method [142–144].

Several other methods employ a mesh in an unconventional sense to alleviate mesh distortion difficulties in the mesh-based methods. The material point method [17,18,145], which originated from the Particle-in-cell methods [146–148], uses an Eulerian background mesh for discretization of PDEs while the masses, stresses and state variables live and are updated at Lagrangian points. The generalization of MPM in [19] to the generalized interpolation material point (GIMP) method avoids the cell-crossing instability due to rough interpolation functions in MPM by employing particle functions which smooth the grid approximation. The convected particle domain interpolation (CPDI) method has been developed to improve GIMP by allowing the particle domains to distort for more accuracy under shear deformation and large rotations [20]. CPDI also incorporates a modification to the background discretization to avoid the expensive integration that would be necessary for integrating over the distorted particle domains. The free mesh method [36] reconstructs nodal connectivity of a point cloud for FEM computation on the fly. Similarly, the meshless finite element method [51] and the particle finite element method (PFEM) [52,53] reconstruct Delaunay tessellations [149] which give bounded $O(n)$ time for efficiency, and use non-Sibsonian interpolation

[132]. In more recent developments, a second generation of PFEM (PFEM-2) has been proposed which uses a fixed mesh that allows much larger time steps and avoids mesh reconstruction [21,22].

1.3 Collocation Meshfree Methods

An alternative approach to address domain integration issues in the Galerkin meshfree method is by collocation of strong forms. In fact, collocation methods have been around seven decades [150–153]. Although methods for interpolation of scattered data existed for at least five decades (cf. [154] and references therein), it appears that employing them for strong form collocation methods for solving PDEs did not emerge until Kansa's seminal work [7,8]. The radial basis collocation method (RCBM) [7,8] employs radial basis functions in the numerical solution of PDEs using strong form collocation. The originator of the radial basis function (RBF) is Hardy [155,156] who introduced them for interpolation problems. Hardy [156] showed that multiquadric RBFs is related to a consistent solution of the biharmonic potential problem and thus have a physical foundation. Buhmann and Micchelli [157] and Chiu et al. [158] have shown that RBFs are related to prewavelets (wavelets that do not have orthogonality properties). Madych and Nelson [159] proved that multiquadric RBFs and its partial derivatives have exponential convergence. Franke and Schaback [160] provided some theoretical foundation of the RBF method for solving PDEs. Wendland [161] derived error estimates for the solution of smooth problems. Hu et al. [162] presented a radial basis collocation method including combined and alternative schemes for singularity problems. Cecial et al. [163] proposed a numerical scheme for Hamilton–Jacobi equations. Li [164] developed a mixed method for fourth-order elliptic and parabolic problems by using radial basis functions. More recently, Hu et al. derived weights for the collocation equations [10] for optimal convergence. Methods for incorporating weak and strong discontinuities have also been proposed [165,166], and mixed formulations have been developed for constraint problems [167].

Most RBFs with collocation lead to very ill-conditioned discrete systems. Wong et al. [9] suggested the use of multi-zone decomposition of the domain. Kansa and Hon [168] observed that the condition numbers of the discrete system of direct collocation methods can be greatly reduced by the domain decomposition. The shape parameter of a RBF determines the locality of the RBF function and thus greatly influences the linear dependency and in turn the condition number of the discrete system as reported by Schaback and Hon [169]. Localized RBFs have been introduced by Wendland [170] and truncated multiquadric RBFs have been proposed by Kansa and Hon [168] to reduce the bandwidth of the discrete system. Global and local RBFs have been investigated by Fasshauer [171] and smoothing methods and multilevel algorithms have been suggested. More recently, introducing compactly supported partition of unity functions in conjunction with RBFs has been proposed to alleviate ill conditioning while maintaining exponential convergence [172].

Alternatively, approximations such as MLS or RK can be employed for the collocation solution of PDEs, which naturally introduces compactly supported approximations. The finite point method [35,173,174] by Oñate and co-workers in [35] employs weighted least-squares approximations at

each node. Collocation methods based on the RK approximation have also been introduced [43,44]. Hu et al. [44] have shown that strong form collocation methods based on approximations with monomial reproducing conditions exhibit algebraic convergence rates. In [45], implicit gradients [92,93] were introduced to ease the burden of computing second order derivatives of RK shape functions in the collocation of second order PDEs.

The moving particle semi-implicit method [30] has been proposed as an improvement of SPH in the simulation of incompressible fluids. A Lagrangian description is utilized such that the tracking of free surfaces is handled naturally. Derivative approximations based on a weighted average of gradients calculated for each particle pair is employed to solve the Navier-Stokes equation explicitly, and the Poisson problem for pressure is solved implicitly. This method has been applied to the analysis of dam breaking [30], breaking waves [175], and vapor explosions [176], among others. More recently, several stability enhancements have been proposed for this method [177–180].

A strong form-based meshfree method Peridynamics [58] has been proposed based on the reformulation of governing solid mechanics equations into non-local integral equations [181]. Since the governing equations do not contain derivatives, the formulation accommodates the presence of discontinuities without modification. This method has been shown to be a simple and effective approach in modeling fracture and fragmentation as it does not employ explicit tracking of cracks or enrichment functions. A state-based Peridynamics (a generalization of the original bond-based method) was proposed in [59] that allows standard constitutive models to be employed with the method. Recently, plasticity, viscoplasticity as well as continuum damage mechanics have been incorporated in this context [182–184]. Peridynamics has been shown to converge to the local model when the length-scale goes to zero [185]. Very recently, this method has been shown to be related to classical meshfree methods in [62], where it was shown that for uniform discretizations, the deformation gradient in Peridynamics is equivalent to one constructed by implicit gradients with quadratic basis, or Savitzky–Golay Filters [186].

This paper is organized as follows. We first introduce MLS and RK type approximations in Section 2 to demonstrate the unique properties of this class of approximations that relies only on a point discretization, and elucidate the relationship between several meshfree approximations commonly employed. For consistency in presenting the procedures of formulating discrete meshfree equations, and to introduce the recent advances in meshfree solution procedures and their applications, the RK approximation is generally employed throughout the paper although other type of meshfree approximations are available as described above. In Section 3, the Galerkin meshfree method is presented, and the associated approaches for imposing the essential boundary conditions are discussed. Recent advances in domain integration and the associated convergence, stability, and efficiency issues are also addressed. An alternative approach for solving PDEs by strong form collocation with meshfree approximations is presented in Section 4. The well-established radial basis collocation method and the most recent reproducing kernel collocation methods are discussed, and their convergence and stability properties are outlined. Various meshfree formulations for large deformation problems are

introduced in Section 5, and the recent developments of meshfree-based kernel contact formulations and numerical algorithms are also presented. Several application problems in hyperelasticity, plasticity, damage, contact, and fragment-impact are given in Section 6 to demonstrate the effectiveness of meshfree methods compared to the conventional finite element methods. The paper is concluded with closing remarks and outlook in Section 7.

2. Meshfree Approximation Functions

In this section, we review several approximation functions employed in meshfree methods. Although there are many, for brevity we have chosen a few as representative of meshfree approximations as they form the basis for many Galerkin- and collocation-based meshfree methods.

2.1 Approximations Based on Least-Squares Methods

Let the domain of interest $\bar{\Omega} = \Omega \cup \partial\Omega$ be discretized by a set of Np points $S = \{\mathbf{x}_1, \cdots, \mathbf{x}_{Np} \,|\, \mathbf{x}_I \in \bar{\Omega}\}$ with corresponding point numbers that form a set $Z = \{I \,|\, \mathbf{x}_I \in S\}$. We begin with the weighted least-squares approximation of a set of sample data $\{(\mathbf{x}_I, u_I)\}_{I \in Z}$ near $\bar{\mathbf{x}}$, denoted by $u^h_{\bar{\mathbf{x}}}(\mathbf{x})$, which can be expressed as:

$$u^h_{\bar{\mathbf{x}}}(\mathbf{x}) = \sum_{i=1}^{n} p_i(\mathbf{x}) b_i(\bar{\mathbf{x}}) = \mathbf{p}(\mathbf{x})^{\mathrm{T}} \mathbf{b}(\bar{\mathbf{x}}), \tag{1}$$

where $\{p_i(\mathbf{x})\}_{i=1}^n$ are the basis functions and $\{b_i(\bar{\mathbf{x}})\}_{i=1}^n$ are the corresponding coefficients that are functions of the local position $\bar{\mathbf{x}}$. The coefficients $\{b_i(\bar{\mathbf{x}})\}_{i=1}^n$ are obtained by the minimization of a weighted least-squares measure, sampled at the discrete points in *S*:

$$J_{\bar{\mathbf{x}}} = \sum_{I \in Z} w_a(\bar{\mathbf{x}} - \mathbf{x}_I) \left(\mathbf{p}^{\mathrm{T}}(\mathbf{x}_I) \mathbf{b}(\bar{\mathbf{x}}) - u_I \right)^2, \tag{2}$$

where $w_a(\bar{\mathbf{x}} - \mathbf{x}_I)$ is the weight function with compact support $\omega_I = \{\mathbf{x} \,|\, w_a(\mathbf{x} - \mathbf{x}_I) \neq 0\}$, and the support size is denoted as "*a*". Let us now define a set of point numbers of neighbors of $\mathbf{x}$ as $G_{\mathbf{x}} = \{I \,|\, w_a(\mathbf{x} - \mathbf{x}_I) \neq 0\}$, the cardinality of which defines the *m* neighbors of $\mathbf{x}$ whose weight functions $w_a(\mathbf{x} - \mathbf{x}_I)$ are non-zero at $\mathbf{x}$.

Minimization of $J_{\bar{\mathbf{x}}}$ with respect to $\mathbf{b}(\bar{\mathbf{x}})$ leads to:

$$\begin{aligned} \mathbf{b}(\bar{\mathbf{x}}) &= \mathbf{A}(\bar{\mathbf{x}})^{-1} \sum_{I \in G_{\bar{\mathbf{x}}}} w_a(\bar{\mathbf{x}} - \mathbf{x}_I) \mathbf{p}(\mathbf{x}_I) u_I, \\ \mathbf{A}(\bar{\mathbf{x}}) &= \sum_{I \in G_{\bar{\mathbf{x}}}} \mathbf{p}(\mathbf{x}_I) \mathbf{p}^{\mathrm{T}}(\mathbf{x}_I) w_a(\bar{\mathbf{x}} - \mathbf{x}_I). \end{aligned} \tag{3}$$

Substituting (3) into the local approximation in (1) the weighted least squares (WLS) approximation can be expressed as:

$$
\begin{aligned}
u^h_{\bar{\mathbf{x}}}(\mathbf{x}) &= \sum_{I \in G_{\bar{\mathbf{x}}}} \Psi_I(\bar{\mathbf{x}}, \mathbf{x}) u_I, \\
\Psi_I(\bar{\mathbf{x}}, \mathbf{x}) &= \mathbf{p}(\mathbf{x})^{\mathrm{T}} \mathbf{A}(\bar{\mathbf{x}})^{-1} \mathbf{p}(\mathbf{x}_I) w_a(\bar{\mathbf{x}} - \mathbf{x}_I).
\end{aligned}
\tag{4}
$$

The WLS approximation constructs a polynomial function (as a function of $\mathbf{x}$) which is a least-squares fit of the local data near $\bar{\mathbf{x}}$, with each data point weighted with $w_a(\bar{\mathbf{x}} - \mathbf{x}_I)$. In the finite point method [35], the WLS approximation is employed at each nodal point (setting $\bar{\mathbf{x}} = \mathbf{x}_I$ for each node *I*).

Now, we come to an interesting case: let $\bar{\mathbf{x}} \to \mathbf{x}$ in (1)-(3). The approximation is then no longer defined with respect to some point in the domain $\bar{\mathbf{x}}$, but is only a function of $\mathbf{x}$, and thus we obtain a global approximation in contrast to WLS. Essentially, for any given point $\mathbf{x}$, one finds a weighted least squares fit of the local data, but it is never evaluated anywhere else like in WLS. This approximation is termed the moving-least squares (MLS) approximation [80], which is obtained by letting $\bar{\mathbf{x}} \to \mathbf{x}$ in (1)-(3):

$$
\begin{aligned}
u^h(\mathbf{x}) &= \sum_{I \in G_{\mathbf{x}}} \Psi_I(\mathbf{x}) u_I, \\
\Psi_I(\mathbf{x}) &= \mathbf{p}(\mathbf{x})^{\mathrm{T}} \mathbf{A}(\mathbf{x})^{-1} \mathbf{p}(\mathbf{x}_I) w_a(\mathbf{x} - \mathbf{x}_I), \\
\mathbf{A}(\mathbf{x}) &= \sum_{I \in G_{\mathbf{x}}} \mathbf{p}(\mathbf{x}_I) \mathbf{p}^{\mathrm{T}}(\mathbf{x}_I) w_a(\mathbf{x} - \mathbf{x}_I).
\end{aligned}
\tag{5}
$$

Remarks 2.1

1. By setting $w_a(\bar{\mathbf{x}} - \mathbf{x}_I) = 1$, one obtains the least-squares (LS) approximation:

$$
\begin{aligned}
u^h(\mathbf{x}) &= \sum_{I \in Z} \Psi_I(\mathbf{x}) u_I, \\
\Psi_I(\mathbf{x}) &= \mathbf{p}(\mathbf{x})^{\mathrm{T}} \mathbf{A}^{-1} \mathbf{p}(\mathbf{x}_I), \\
\mathbf{A} &= \sum_{I \in Z} \mathbf{p}(\mathbf{x}_I) \mathbf{p}^{\mathrm{T}}(\mathbf{x}_I).
\end{aligned}
\tag{6}
$$

2. The relationship between the least squares (LS), weighted least squares (WLS), and moving least squares (MLS) approximations is summarized in the following table [187].

	Approximation	Least-squares measure	Least-squares approximation
LS	$u^h(\mathbf{x}) = \mathbf{p}(\mathbf{x})^T \mathbf{b}$	$J = \sum_{I \in Z} \left(\mathbf{p}^T(\mathbf{x}_I)\mathbf{b} - u_I \right)^2$	$u^h(\mathbf{x}) = \mathbf{p}(\mathbf{x})^T \mathbf{A}^{-1} \sum_{I \in Z} \mathbf{p}(\mathbf{x}_I) u_I$ $\mathbf{A} = \sum_{I \in Z} \mathbf{p}(\mathbf{x}_I)\mathbf{p}^T(\mathbf{x}_I)$
WLS	$u^h_{\bar{\mathbf{x}}}(\mathbf{x}) = \mathbf{p}(\mathbf{x})^T \mathbf{b}(\bar{\mathbf{x}})$	$J_{\bar{\mathbf{x}}} = \sum_{I \in G_{\bar{\mathbf{x}}}} w_a(\bar{\mathbf{x}} - \mathbf{x}_I) \left(\mathbf{p}^T(\mathbf{x}_I)\mathbf{b}(\bar{\mathbf{x}}) - u_I \right)^2$	$u^h_{\bar{\mathbf{x}}} = \mathbf{p}(\mathbf{x})^T \mathbf{A}^{-1}(\bar{\mathbf{x}}) \sum_{I \in G_{\bar{\mathbf{x}}}} \mathbf{p}(\mathbf{x}_I) w_a(\bar{\mathbf{x}} - \mathbf{x}_I) u_I$ $\mathbf{A}(\bar{\mathbf{x}}) = \sum_{I \in G_{\bar{\mathbf{x}}}} \mathbf{p}(\mathbf{x}_I)\mathbf{p}^T(\mathbf{x}_I) w_a(\bar{\mathbf{x}} - \mathbf{x}_I)$
MLS	$u^h(\mathbf{x}) = \mathbf{p}(\mathbf{x})^T \mathbf{b}(\mathbf{x})$	$J_{\mathbf{x}} = \sum_{I \in G_{\mathbf{x}}} w_a(\mathbf{x} - \mathbf{x}_I) \left(\mathbf{p}^T(\mathbf{x}_I)\mathbf{b}(\mathbf{x}) - u_I \right)^2$	$u^h(\mathbf{x}) = \mathbf{p}(\mathbf{x})^T \mathbf{A}(\mathbf{x})^{-1} \sum_{I \in G_{\mathbf{x}}} \mathbf{p}(\mathbf{x}_I) w_a(\mathbf{x} - \mathbf{x}_I) u_I$ $\mathbf{A}(\mathbf{x}) = \sum_{I \in G_{\mathbf{x}}} \mathbf{p}(\mathbf{x}_I)\mathbf{p}^T(\mathbf{x}_I) w_a(\mathbf{x} - \mathbf{x}_I)$

Table 3. Comparison of LS, WLS, and MLS Approximations

3. In the case that $m = n$ minimization of (2) leads to the solution $\mathbf{p}^{\mathrm{T}}(\mathbf{x}_I)\mathbf{b}(\mathbf{x}_I) = u_I$, equivalent to enforcing interpolation of the data. In this context, as shown in [11] the finite element approximation can be interpreted as a least-squares fit of the nodal values in each element with $m = n$.
4. In the case $m > n$ a weighted least-squares fit of the data is obtained. This means that the MLS functions $\{\Psi_I(\mathbf{x})\}_{I \in Z}$ are not interpolants, and u_I is not the nodal value of $u^h(\mathbf{x})$, i.e., $u^h(\mathbf{x}_I) \neq u_I$. The imposition of Dirichlet boundary conditions in the Galerkin approximation requires a different approach than in FEM, and will be discussed in Section 3.1.
5. Choosing constant basis $\mathbf{p}(\mathbf{x}) = \{1\}$ in MLS results in a Shepard function [113].
6. The order of continuity in the weight function determines the order of continuity in the MLS approximation. The weight function is directly analogous to the kernel function in the RK approximation, so we defer the discussion of constructing weights to Section 2.4.
7. If the basis function vector consists of complete monomials, that is, $\mathbf{p}^{\mathrm{T}}(\mathbf{x}) = \{\mathbf{x}^\alpha\}^n_{|\alpha|=0}$, $\mathbf{x}^\alpha \equiv x_1^{\alpha_1} \cdot x_2^{\alpha_2} \cdot \ldots \cdot x_d^{\alpha_d}$, $|\alpha| = \sum_{i=1}^d \alpha_i$, then the approximation in (5) is n^{th} order complete:

$$\sum_{I \in G_{\mathbf{x}}} \Psi_I(\mathbf{x})\mathbf{p}(\mathbf{x}_I) = \mathbf{p}(\mathbf{x}). \qquad (7)$$

8. At any given point $\mathbf{x}$, a sufficient number of points' weight functions need to cover $\mathbf{x}$ for $\mathbf{A}(\mathbf{x})$ to be invertible. In addition, the points' position cannot be collinear (or coplanar in three dimensions) so that a linearly dependent system is avoided, see Reference [85] for details.
9. For better conditioning of $\mathbf{A}(\mathbf{x})$, MLS with shifted and normalized bases can be considered:

$$\Psi_I(\mathbf{x}) = \mathbf{p}(\mathbf{0})^{\mathrm{T}}\,\mathbf{A}(\mathbf{x})^{-1}\mathbf{p}\left(\frac{\mathbf{x}-\mathbf{x}_I}{a}\right)w_a(\mathbf{x}-\mathbf{x}_I),$$
$$\mathbf{A}(\mathbf{x}) = \sum_{I\in G_{\mathbf{x}}}\mathbf{p}\left(\frac{\mathbf{x}-\mathbf{x}_I}{a}\right)\mathbf{p}^{\mathrm{T}}\left(\frac{\mathbf{x}-\mathbf{x}_I}{a}\right)w_a(\mathbf{x}-\mathbf{x}_I). \tag{8}$$

The MLS approximation in (5) was first introduced for surface fitting through a given data set $\{(\mathbf{x}_I, u_I)\}_{I\in Z}$ [6,80]. This approach was later rediscovered in the diffuse element method [11] for solving PDEs, where $\Psi_I(\mathbf{x})$ is used as an approximation function, and u_I in (5) became the unknown coefficients to be solved by the Galerkin procedure. In the diffuse element method, derivatives in the weak form are approximated by the differentiation of the basis functions in (1), which are considered "diffuse derivatives", which will be discussed further in Section 2.6.

The celebrated element free Galerkin method by Belytschko, Lu, and Gu [12–14], which is regarded as the pioneering work that popularized meshfree methods, is an improvement of DEM where the full derivatives of the MLS approximation are used in the Galerkin method. The MLS approximation is also employed in MLPG [38], moving least squares particle hydrodynamics (MLSPH) [37], moving least squares RKPM [85,188], *hp* clouds [33,34], the finite point method [35], among others (see Table 1).

2.2 Kernel Estimate

The concept of a kernel estimate (KE) was first introduced by Lucy [3] and Gingold and Monaghan [4] as a starting point of formulating SPH. Although in SPH the kernel estimate is applied directly to a PDE, the smoothing function used in this process plays the same role as the test function in the Galerkin approximation. To examine the completeness in the KE, here we consider the kernel estimate of a function $u(\mathbf{x})$, denoted by $u^h(\mathbf{x})$, as

$$u^h(\mathbf{x}) = \int_{\mathbb{R}^d} u(\mathbf{s})\varphi_a(\mathbf{x}-\mathbf{s})\mathrm{d}\mathbf{s}, \tag{9}$$

where $\varphi_a(\mathbf{x})$ is a kernel function (called a smoothing function in SPH) with support measure a. If the compactly supported kernel $\varphi_a(\mathbf{x})$ mimics a delta function:

1. $\varphi_a(\mathbf{x}) \to \delta(\mathbf{x})$ as $a \to 0$,
2. $\int \varphi_a(\mathbf{x})\mathrm{d}\Omega = 1$,

then the kernel estimate of a function when $a \to 0$ can be obtained by replacing $\varphi_a(\mathbf{x}-\mathbf{s})$ by $\delta(\mathbf{x}-\mathbf{s})$ in (9), and thus $u^h(\mathbf{x}) \to u(\mathbf{x})$ as $a \to 0$.

Considering a finite domain, the integration in (9) can then be carried out numerically at the set of points *S*, as before, as

$$\begin{aligned} u^h(\mathbf{x}) &= \int_{\Omega} \phi_a(\mathbf{x}-\mathbf{s})u(\mathbf{s})\mathrm{d}\mathbf{s} \\ &\simeq \sum_{I\in G_{\mathbf{x}}} \phi_a(\mathbf{x}-\mathbf{x}_I)\Delta V_I u_I . \end{aligned} \tag{10}$$

The approximation in (10) can be written in terms of KE shape functions $\Psi_I(\mathbf{x})$:

$$\begin{aligned} u^h(\mathbf{x}) &= \sum_{I\in G_{\mathbf{x}}} \Psi_I(\mathbf{x}) u_I , \\ \Psi_I(\mathbf{x}) &= \phi_a(\mathbf{x}-\mathbf{x}_I)\Delta V_I . \end{aligned} \tag{11}$$

For kernels with properties such as normalization and symmetry, the KE approximation can satisfy partition of unity or even first order completeness under certain conditions such as in uniform node distributions of the interior of the domain. However, near the boundary and in irregular node distributions, partition of unity is not satisfied in general, as illustrated in Figure 2. This has motivated the development of several corrections to SPH (there are numerous reviews, we refer to [189] for more details) and alternative meshfree methods such as RKPM.

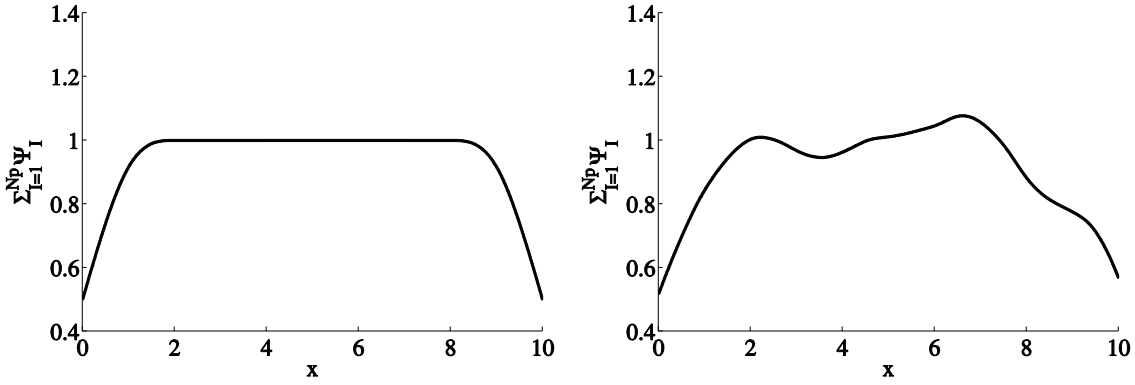

(a) (b)

Figure 2. Partition of unity check ($\sum_{I\in G_{\mathbf{x}}} \Psi_I(\mathbf{x}) = 1$) of KE approximation in (a) uniform discretization, and (b) non-uniform discretization.

2.3 Reproducing Kernel Approximation

The reproducing kernel particle method [23,24,190] was formulated based on the reproducing kernel (RK) approximation under the Galerkin framework. The RK approximation [23,190] was proposed for solving PDEs to improve the accuracy of the SPH method for finite domain problems. In

this method, the kernel function in the kernel estimate was modified by introducing a correction function to allow reproduction of various functions:

$$\begin{aligned} u^h(\mathbf{x}) &= \int_\Omega \Phi(\mathbf{x}, \mathbf{x}-\mathbf{s}) u(\mathbf{s}) \mathrm{d}\mathbf{s}, \\ \Phi(\mathbf{x}, \mathbf{x}-\mathbf{s}) &= \phi_a(\mathbf{x}-\mathbf{s}) C(\mathbf{x}, \mathbf{x}-\mathbf{s}), \\ C(\mathbf{x}, \mathbf{x}-\mathbf{s}) &= \mathbf{P}^{\mathrm{T}}(\mathbf{x}-\mathbf{s}) \mathbf{c}(\mathbf{x}), \end{aligned} \tag{12}$$

where $C(\mathbf{x}, \mathbf{x}-\mathbf{s})$ is a correction function. The vector $\mathbf{P}(\mathbf{x}-\mathbf{s})$ forms a basis, while the coefficients $\mathbf{c}(\mathbf{x})$ are solved for by considering the Taylor expansion of $u(\mathbf{s})$:

$$u(\mathbf{s}) = \sum_{|\alpha|=0}^{\infty} \frac{(-1)^\alpha}{\alpha!} (\mathbf{x}-\mathbf{s})^\alpha \partial^\alpha u(\mathbf{x}), \tag{13}$$

where α is a multi-index with the notation $\alpha = (\alpha_1, \alpha_2, \ldots \alpha_d)$, $|\alpha| = \alpha_1 + \alpha_2 + \ldots + \alpha_d$, $\mathbf{x}^\alpha = x_1^{\alpha_1} \cdot x_2^{\alpha_2} \cdot \ldots \cdot x_d^{\alpha_d}$, $\alpha! = \alpha_1! \alpha_2! \cdots \alpha_d!$, and $\partial^\alpha = \partial^{\alpha_1} \partial^{\alpha_2} \cdots \partial^{\alpha_d} / \partial x_1^{\alpha_1} \partial x_2^{\alpha_2} \cdots \partial x_d^{\alpha_d}$. Substituting (13) into the kernel estimation in (12) leads to

$$\begin{aligned} u^h(\mathbf{x}) &= \tilde{m}_0(\mathbf{x}) u(\mathbf{x}) + \sum_{|\alpha|=1}^{\infty} \frac{(-1)^\alpha}{\alpha!} \tilde{m}_\alpha(\mathbf{x}) \partial^\alpha u(\mathbf{x}), \\ \tilde{m}_0(\mathbf{x}) &= \int_\Omega \Phi(\mathbf{x}, \mathbf{x}-\mathbf{s}) \mathrm{d}\mathbf{s}, \\ \tilde{m}_\alpha(\mathbf{x}) &= \int_\Omega (\mathbf{x}-\mathbf{s})^\alpha \Phi(\mathbf{x}, \mathbf{x}-\mathbf{s}) \mathrm{d}\mathbf{s}. \end{aligned} \tag{14}$$

For n^{th} order completeness, we have the following conditions on the *moments* $\tilde{m}_\alpha(\mathbf{x})$:

$$\begin{aligned} &\tilde{m}_0(\mathbf{x}) = 1, \\ &\tilde{m}_\alpha(\mathbf{x}) = 0, \qquad |\alpha| = 1, \ldots, n. \end{aligned} \tag{15}$$

These conditions can be expressed as:

$$\left\{ \int_\Omega \mathbf{P}(\mathbf{x}-\mathbf{s}) \mathbf{P}^{\mathrm{T}}(\mathbf{x}-\mathbf{s}) \mathrm{d}\mathbf{s} \right\} \mathbf{c}(\mathbf{x}) = \mathbf{P}(\mathbf{0}). \tag{16}$$

Solving for $\mathbf{c}(\mathbf{x})$, one obtains the continuous reproducing kernel approximation:

$$
\begin{aligned}
u^h(\mathbf{x}) &= \int_{\Omega} \Phi(\mathbf{x}, \mathbf{x}-\mathbf{s}) u(\mathbf{s}) \mathrm{d}\mathbf{s}, \\
\Phi(\mathbf{x}, \mathbf{x}-\mathbf{s}) &= \phi_a(\mathbf{x}-\mathbf{s}) \mathbf{P}^{\mathrm{T}}(\mathbf{x}-\mathbf{s}) \mathbf{M}^{-1}(\mathbf{x}) \mathbf{P}(\mathbf{x}-\mathbf{s}), \\
\mathbf{M}(\mathbf{x}) &= \int_{\Omega} \mathbf{P}(\mathbf{x}-\mathbf{s}) \mathbf{P}^{\mathrm{T}}(\mathbf{x}-\mathbf{s}) \mathrm{d}\mathbf{s},
\end{aligned}
\tag{17}
$$

where $\mathbf{M}(\mathbf{x})$ is the moment matrix; the term comes from the vanishing moments of the Taylor expansion of $u(\mathbf{s})$.

In practice, numerical integration must be employed in order to form an approximation, which can be carried out as:

$$
\begin{aligned}
u^h(\mathbf{x}) &= \sum_{I \in G_{\mathbf{x}}} \Phi(\mathbf{x}, \mathbf{x}-\mathbf{x}_I) u_I \Delta V_I \equiv \sum_{I \in G_{\mathbf{x}}} \Psi_I(\mathbf{x}) u_I, \\
\Phi(\mathbf{x}, \mathbf{x}-\mathbf{x}_I) &= \phi_a(\mathbf{x}-\mathbf{x}_I) \mathbf{P}^{\mathrm{T}}(\mathbf{x}-\mathbf{x}_I) \mathbf{M}^{-1}(\mathbf{x}) \mathbf{P}(\mathbf{x}-\mathbf{x}_I), \\
\mathbf{M}(\mathbf{x}) &= \sum_{I \in G_{\mathbf{x}}} \mathbf{P}(\mathbf{x}-\mathbf{x}_I) \mathbf{P}^{\mathrm{T}}(\mathbf{x}-\mathbf{x}_I) \Delta V_I.
\end{aligned}
\tag{18}
$$

The shape functions in (18) and their summation are shown in Figure 3 for n=1 for illustration, where the same kernel as the KE is employed, demonstrating that the correction corrects incompleteness in the KE approximation near boundaries in uniform discretizations. The KE and corresponding RK shape functions and their summation is shown in Figure 4 for a non-uniform discretization, which demonstrates that the RK approximation also corrects for incompleteness in the KE in non-uniform node distributions as well. The RK approximation can also provide arbitrarily higher order completeness if desired.

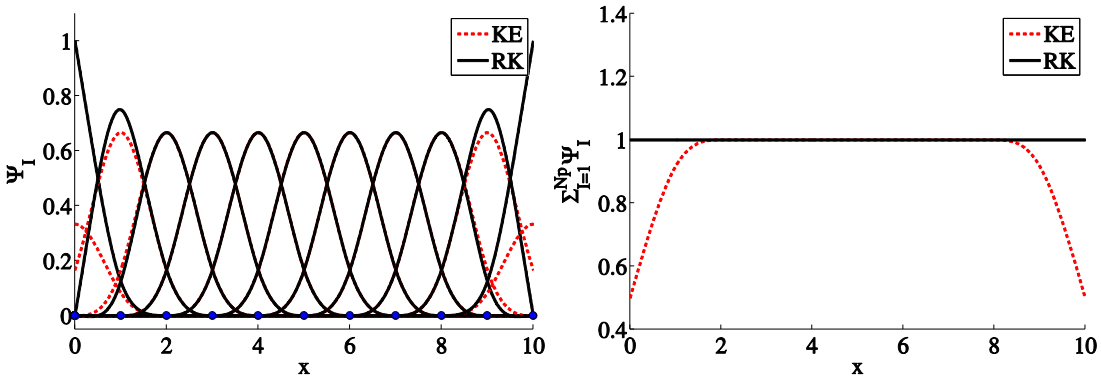

(a) (b)

Figure 3. KE and RK approximations in a uniform discretization: (a) shape functions, and (b) partition of unity check ($\sum_{I \in G_{\mathbf{x}}} \Psi_I(\mathbf{x}) = 1$).

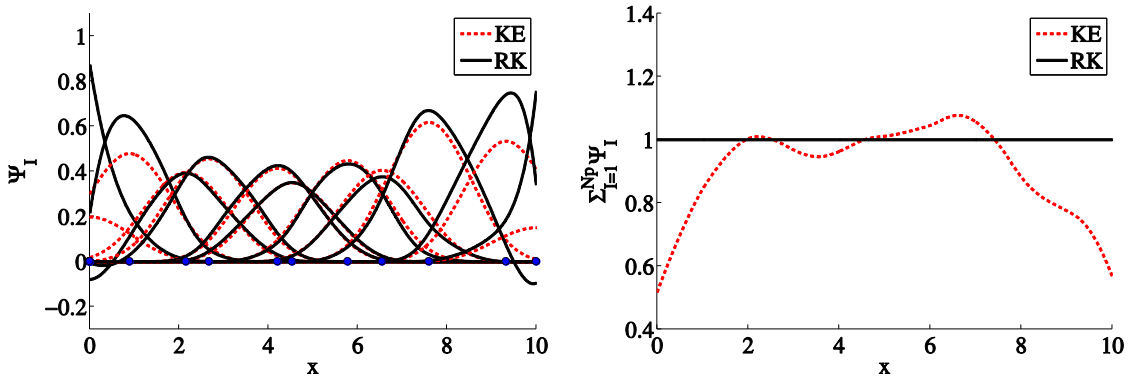

(a) (b)

Figure 4. KE and RK approximations in a non-uniform discretization: (a) shape functions, and (b) parstition of unity check ($\sum_{I\in G_{\mathbf{x}}}\Psi_I(\mathbf{x})=1$).

Chen et al. [24] showed that the numerical integration of the moment matrix and the RK approximation in (17) must be evaluated in a consistent manner (i.e., using the same quadrature weights ΔV_I in (18)) in order to preserve the consistency of the approximation. A discrete reproducing kernel approximation was then introduced in [83] which satisfies the reproducing conditions while omitting the quadrature weights:

$$\begin{aligned} u^h(\mathbf{x}) &= \sum_{I\in G_{\mathbf{x}}}\Psi_I(\mathbf{x})u_I, \\ \Psi_I(\mathbf{x}) &= \mathbf{p}^{\mathrm{T}}(\mathbf{x}-\mathbf{x}_I)\mathbf{c}(\mathbf{x})\phi_a(\mathbf{x}-\mathbf{x}_I). \end{aligned} \tag{19}$$

Under the discrete framework, $\phi_a(\mathbf{x}-\mathbf{x}_I)$ plays the same role as the weight function $w_a(\mathbf{x}-\mathbf{x}_I)$ in MLS. The coefficient vector $\mathbf{c}(\mathbf{x})$ is obtained by enforcing the exact reproduction of the bases, that is, if $u_I = p_i(\mathbf{x}_I)$, then $u^h(\mathbf{x}) = p_i(\mathbf{x})$:

$$\sum_{I\in G_{\mathbf{x}}}\Psi_I(\mathbf{x})\mathbf{p}(\mathbf{x}_I)=\mathbf{p}(\mathbf{x}). \tag{20}$$

When $\{p_i(\mathbf{x})\}_{i=1}^n$ is a set of complete monomials, obtaining $\mathbf{c}(\mathbf{x})$ from (20) yields the same approximation as MLS in (5), and the remarks in Section 2.1 apply. On the other hand, if non-monomial bases are used as $\{p_i(\mathbf{x})\}_{i=1}^n$, solving $\mathbf{c}(\mathbf{x})$ from (20) yields a different approximation than MLS. Further, the RK approximation can be extended to achieve synchronized convergence [91–93] and implicit gradient approximations [191], which deviate from the MLS approximation as will be discussed in Section 2.6. Detail discussions of RK approximation properties can be found in [85,192,193]. The RK approximation is the basis of the reproducing kernel particle method (RKPM) [23,24], the reproducing kernel collocation method (RKCM) [44], among others (see Tables 1 and 2).

2.4 Construction of Weight Functions and Kernel Functions for MLS and RK

Hereafter we use the terms kernel and weights interchangably, as they play the exact same role in the least squares (1)-(2) and discrete RK (19)-(20) approximations. Typically kernel functions are chosen as smooth, compactly supported functions. To take an example, the cubic B-spline kernel function shown in Figure 5 is:

$$\phi_a(x-s) =: \phi_a(z) = \begin{cases} \frac{2}{3} - 4z^2 + 4z^3 & for\ 0 \le z \le \frac{1}{2} \\ \frac{4}{3} - 4z + 4z^2 - \frac{4}{3}z^3 & for\ \frac{1}{2} \le z \le 1 \\ 0 & for\ z > 1 \end{cases}, \quad z = \frac{|x-s|}{a}. \tag{21}$$

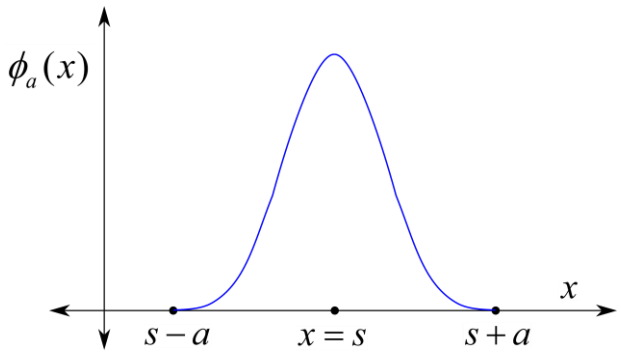

Figure 5. Kernel function $\phi_a(x-s)$.

A multi-dimensional kernel function $\phi_a(\mathbf{x}-\mathbf{x}_I)$ can be constructed by using the kernel function in one-dimension with box support as:

$$\phi_a(\mathbf{x}-\mathbf{x}_I) = \prod_{i=1}^{d} \phi_{a_i}(x_i - x_{iI}). \tag{22}$$

Alternatively, one can construct a multidimensional kernel with spherical support from the one-dimensional kernel as

$$\phi_a(\mathbf{x}-\mathbf{s}) = \phi_a(z), z = \frac{\|\mathbf{x}-\mathbf{s}\|}{a}. \tag{23}$$

The box support in (22) and spherical support in (23) are illustrated in Figure 6.

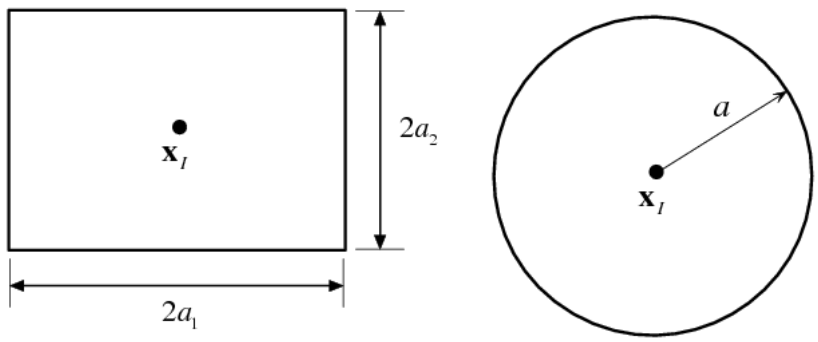

(a) (b)

Figure 6. (a) Rectangular and (b) circular supports of the 2-dimensional kernel function $\phi_a(\mathbf{x}-\mathbf{s})$.

2.5 Partition of Unity Methods

The *hp* clouds (HPC) [33,34] and the generalized finite element method (GFEM) [27,194] were developed based on the general framework of the partition of unity [31,32]. The partition of unity property is essential for convergence in Galerkin approximation of PDEs [32]. Let a domain be covered by overlapping patches ω_I, $\bar{\Omega} \subset \cup_{I \in Z} \omega_I$, each of which is associated with a function which is nonzero only in ω_I, and has the following property

$$\sum_{I \in G_{\mathbf{x}}} \Psi_I^0(\mathbf{x}) = 1. \tag{24}$$

An example of a partition of unity function is the Shepard function. The partition of unity can be used as a paradigm for construction of approximation functions with desired order of completeness or with enrichment of special bases representing characteristics of the PDEs. An example of PU is the following approximation [32]:

$$u^h(\mathbf{x}) = \sum_{I \in G_{\mathbf{x}}} \Psi_I^0(\mathbf{x}) \left(\sum_{i=1}^{k} a_{iI} P_i(\mathbf{x}) + \sum_{i=1}^{l} q_{iI} g_i(\mathbf{x}) \right), \tag{25}$$

where $\{P_i(\mathbf{x})\}_{i=1}^k$ are monomial bases used to impose completeness, and $\{q_{iI}(\mathbf{x})\}_{i=1}^l$ are other enhancement functions. Equation (25) is called an *extrinsic* adaptivity.

MLS and RK with constant basis yields a PU function $\Psi_I^0(\mathbf{x})$, and MLS and RK with complete monomials of degree k, denoted as $\Psi_I^k(\mathbf{x})$, can be viewed as PU with *intrinsic* enrichment (adding functions to the bases) [195]. Duarte and Oden [33] extended PU with extrinsic refinement as follows:

$$u^h(\mathbf{x}) = \sum_{I \in G_{\mathbf{x}}} \Psi_I^k(\mathbf{x})(u_I + \sum_{i=1}^{l} b_{il} q_i(\mathbf{x})) \ , \tag{26}$$

where $q_i(\mathbf{x})$ is the extrinsic basis which can be a monomial basis of any order greater than *k* or a special enhancement function. The extrinsic adaptivity allows the basis to vary from node to node, whereas intrinsic basis in MLS and RK cannot be changed without introducing a discontinuity. A good overview and comparison of the meshfree approximations discussed can be found in [189,195,196]. A reproducing kernel element method (RKEM) which uses finite element shape functions as the PU function with enriched bases has been proposed in [197] to achieve combined advantages of FEM (Kronecker-delta property) and polynomial reproducibility.

2.6 Derivative Approximations in Meshfree Methods

Several techniques have been employed for approximating derivatives in meshfree methods. Remarkably, though several researchers independently arrived at various approximations that seem unique, all of the approximations discussed herein are very closely related, and in most cases equivalent. The derivations of these methods can be unified and made clear under the discrete RK/MLS approximation with non-shifted monomial basis (5).

i). Direct Derivatives

The simplest way to obtain an approximation of derivatives is to directly differentiate an approximation of the primary variable. In this way, the derivatives in the solution of PDEs are consistent with the approximation. This was first introduced in the EFG method [12] for solving the PDEs with MLS. If we consider using the MLS approximation (5), an approximation for the derivative can be obtained by differentiating the approximation of the primary variable:

$$\begin{aligned}
&\partial^\alpha u(\mathbf{x}) \simeq \partial^\alpha u^h(\mathbf{x}) = \sum_{I \in G_{\mathbf{x}}} \partial^\alpha \Psi_I(\mathbf{x}) u_I, \\
&\partial^\alpha \Psi_I(\mathbf{x}) = \partial^\alpha \mathbf{p}(\mathbf{x})^{\mathrm{T}} \mathbf{A}(\mathbf{x})^{-1} \mathbf{p}(\mathbf{x}_I) w_a(\mathbf{x}-\mathbf{x}_I) \\
&\qquad + \mathbf{p}(\mathbf{x})^{\mathrm{T}} \partial^\alpha \mathbf{A}(\mathbf{x})^{-1} \mathbf{p}(\mathbf{x}_I) w_a(\mathbf{x}-\mathbf{x}_I) \\
&\qquad + \mathbf{p}(\mathbf{x})^{\mathrm{T}} \mathbf{A}(\mathbf{x})^{-1} \mathbf{p}(\mathbf{x}_I) \partial^\alpha w_a(\mathbf{x}-\mathbf{x}_I),
\end{aligned} \tag{27}$$

where α is a multi-index. The cost of computing the above is generally high, since the cost in computing MLS/RK shape functions is mostly comprised of matrix operations (see [198]). Thus, differentiation of $\mathbf{A}(\mathbf{x})^{-1}$, and the many matrix operations involved makes this type of derivative computationally expensive. On the other hand, using these definitions, one is able to obtain higher accuracy in the solution of PDEs than diffuse derivatives used in DEM [12]. The direct derivative is employed in most Galerkin and Collocation methods.

ii). Diffuse Derivatives

In the diffuse element method [11], derivatives in the Galerkin equation are approximated by "diffuse" derivatives of $u^h(\mathbf{x})$. In this method, when differentiating the MLS approximation, the derivatives of the coefficients of the bases in (1) are neglected, which actually vary due to the moving nature of the approximation ($\bar{\mathbf{x}} \to \mathbf{x}$). To make this clear, examining (1) and (5) we have for the MLS approximation:

$$u^h(\mathbf{x}) = \mathbf{p}(\mathbf{x})^{\mathrm{T}} \underbrace{\mathbf{A}(\mathbf{x})^{-1} \sum_{I \in G_{\mathbf{x}}} \mathbf{p}(\mathbf{x}_I) w_a(\mathbf{x} - \mathbf{x}_I) u_I}_{\mathbf{b}(\mathbf{x})}. \tag{28}$$

In the diffuse derivatives, the derivatives of $u(\mathbf{x})$ are approximated as:

$$\begin{aligned} \partial^\alpha u(\mathbf{x}) &\simeq \partial^\alpha \mathbf{p}(\mathbf{x})^{\mathrm{T}} \mathbf{b}(\mathbf{x}) \\ &= \partial^\alpha \mathbf{p}(\mathbf{x})^{\mathrm{T}} \mathbf{A}(\mathbf{x})^{-1} \sum_{I \in G_{\mathbf{x}}} \mathbf{p}(\mathbf{x}_I) w_a(\mathbf{x} - \mathbf{x}_I) u_I \\ &\equiv \sum_{I \in G_{\mathbf{x}}} \Psi_I^\alpha(\mathbf{x}) u_I . \end{aligned} \tag{29}$$

By employing (29) the approximation to $\partial^\alpha u(\mathbf{x})$ is just as smooth as the approximation to $u(\mathbf{x})$, and it retains the completeness properties of the true derivative $\partial^\alpha u^h(\mathbf{x})$ [11]. One other advantage of this method is that taking derivatives of $\mathbf{A}(\mathbf{x})^{-1}$ is circumvented, although at the cost of accuracy in the solution of PDEs as mentioned previously.

The diffuse derivative can be derived as follows. Rather than differentiating the approximation of the primary variable to obtain an approximation of derivatives, one can consider constructing an approximation to the derivative directly. First, at a given fixed point $\bar{\mathbf{x}}$, one can construct a weighted least-squares approximation (4). Then, an approximation to $\partial^\alpha u(\mathbf{x})$ at $\bar{\mathbf{x}}$, can be obtained by differentiation of that approximation with respect to the moving variable $\mathbf{x}$:

$$\begin{aligned} &\partial^\alpha u(\mathbf{x}) \simeq \partial^\alpha u_{\bar{\mathbf{x}}}^h(\mathbf{x}) = \sum_{I \in G_{\bar{\mathbf{x}}}} \partial^\alpha \Psi_I(\mathbf{x}, \bar{\mathbf{x}}) u_I , \\ &\partial^\alpha \Psi_I(\mathbf{x}, \bar{\mathbf{x}}) = \partial^\alpha \mathbf{p}(\mathbf{x})^{\mathrm{T}} \mathbf{A}(\bar{\mathbf{x}})^{-1} \mathbf{p}(\mathbf{x}_I) w_a(\bar{\mathbf{x}} - \mathbf{x}_I), \\ &\mathbf{A}(\bar{\mathbf{x}}) = \sum_{I \in G_{\bar{\mathbf{x}}}} \mathbf{p}(\mathbf{x}_I) \mathbf{p}^{\mathrm{T}}(\mathbf{x}_I) w_a(\bar{\mathbf{x}} - \mathbf{x}_I). \end{aligned} \tag{30}$$

Finally, the approximation is made global by taking $\bar{\mathbf{x}} \to \mathbf{x}$ as in the MLS approximation:

$$\partial^\alpha u(\mathbf{x}) \simeq \left[\partial^\alpha u_{\bar{\mathbf{x}}}^h(\mathbf{x}) \right]_{\bar{\mathbf{x}} \to \mathbf{x}} = \sum_{I \in G_{\mathbf{x}}} \Psi_I^\alpha(\mathbf{x}) u_I , \tag{31}$$

where Ψ_I^α is the diffuse derivative shape function in (29).

iii). Implicit Gradients and Synchronized Derivatives

The implicit gradient was introduced as a regularization in strain localization problems without taking direct derivatives [191], where the idea came directly from the synchronized RK approximation [91–93] as a way to approximate derivatives. In the implicit gradient method, derivative approximations are constructed directly by employing the same form as the RK shape function (19):

$$\Psi_I^\alpha(\mathbf{x}) = \mathbf{c}^\alpha(\mathbf{x})\mathbf{p}(\mathbf{x}-\mathbf{x}_I)\phi_a(\mathbf{x}-\mathbf{x}_I). \tag{32}$$

The coefficients $\mathbf{c}^\alpha(\mathbf{x})$ are obtained from the following gradient reproducing conditions, analogous to (20):

$$\sum_{I\in G_\mathbf{x}} \Psi_I^\alpha(\mathbf{x})\mathbf{p}(\mathbf{x}) = \partial^\alpha \mathbf{p}(\mathbf{x}). \tag{33}$$

Following the usual procedures in RK approximations, the implicit gradient RK approximation is:

$$\begin{aligned}
&\partial^\alpha u(\mathbf{x}) \simeq \sum_{I\in G_\mathbf{x}} \Psi_I^\alpha(\mathbf{x}) u_I,\\
&\Psi_I^\alpha(\mathbf{x}) = \partial^\alpha \mathbf{p}(\mathbf{x})^{\mathrm{T}} \mathbf{M}(\mathbf{x})^{-1} \mathbf{p}(\mathbf{x}_I) w_a(\mathbf{x}-\mathbf{x}_I),\\
&\mathbf{M}(\mathbf{x}) = \sum_{I\in G_\mathbf{x}} \mathbf{p}(\mathbf{x}_I)\mathbf{p}^{\mathrm{T}}(\mathbf{x}_I) w_a(\mathbf{x}-\mathbf{x}_I).
\end{aligned} \tag{34}$$

Comparing (34) to (29), we see that implicit gradient are indeed diffuse derivatives. Implicit gradients have been employed for regularization in strain localization problems [191] to avoid the need of ambiguous boundary conditions associated with the standard gradient-type regularization methods, and easing the computational cost of meshfree collocation methods [45]. The idea has also been introduced as a stabilization of meshfree solutions of convection dominated problems without the need for high order differentiation of the test function [199].

In [191], it was shown that (34) is equivalent to:

$$\begin{aligned}
&\Psi_I^\alpha(\mathbf{x}) = \mathbf{p}^{\alpha\mathrm{T}} \mathbf{M}(\mathbf{x})^{-1} \mathbf{p}(\mathbf{x}-\mathbf{x}_I) w_a(\mathbf{x}-\mathbf{x}_I),\\
&\mathbf{M}(\mathbf{x}) = \sum_{I\in G_\mathbf{x}} \mathbf{p}(\mathbf{x}-\mathbf{x}_I)\mathbf{p}^{\mathrm{T}}(\mathbf{x}-\mathbf{x}_I) w_a(\mathbf{x}-\mathbf{x}_I),\\
&\mathbf{p}^\alpha = \underset{\uparrow}{[0,\ \ldots,\ 0,\ \alpha!(-1)^{|\alpha|},\ 0,\ \ldots,\ 0]^{\mathrm{T}}},\\
&\qquad\qquad\quad \alpha \text{ entry}
\end{aligned} \tag{35}$$

which is the same expression as the synchronized derivatives proposed in [91–93], scaled by $\alpha!$, with the difference in sign emanating from the convention in shifting the bases. In this form the reproduction of derivative terms can be seen by examining alternative vanishing moment conditions in (14) and (15). Using this idea, in [91] it was shown that employing certain linear combinations of synchronized derivatives and the RK approximation, synchronized convergence can be obtained in the L^2 norm and H^k norms up to some order k with the proper selection of coefficients C^α in the following:

$$\tilde{\Psi}_I(\mathbf{x}) = \Psi_I(\mathbf{x}) + \sum_{|\alpha|=1}^{n} C^\alpha \Psi_I^\alpha(\mathbf{x}). \tag{36}$$

Since the additional terms in the above satisfy partition of nullity, they termed the resulting approximation (36) a hierarchical partition of unity [92,93].

iv). Generalized Finite Difference Methods

In the finite difference work by Liszka and Orkisz [5,6], derivative approximations were constructed directly by satisfaction of truncated Taylor expansions. Here we begin with this method, as it is a generalization of previous similar methods. In [6], the generalized finite difference method started with the Taylor expansion of function $u(\mathbf{x})$ about at point $u(\mathbf{x}_I)$ truncated to a given order n:

$$u(\mathbf{x}_I) = \sum_{|\alpha|=0}^{n} \frac{(-1)^\alpha}{\alpha!} (\mathbf{x} - \mathbf{x}_I)^\alpha \partial^\alpha u(\mathbf{x}). \tag{37}$$

In order to solve for approximations of the derivatives, and the approximation of $u(\mathbf{x})$, the above can be evaluated at m points in a stencil (or "star" in GFD terminology) surrounding $\mathbf{x}$, and one obtains the system

$$\mathbf{u} = \mathbf{R}(\mathbf{x})\mathbf{J}\mathbf{u}^h(\mathbf{x}) \equiv \mathbf{R}(\mathbf{x})\mathbf{u}_\mathbf{J}^h(\mathbf{x}), \tag{38}$$

where $\mathbf{u}^h(\mathbf{x}) \simeq \{u(\mathbf{x}), \ldots, \partial^\alpha u(\mathbf{x}), \ldots, \partial^{|\alpha|=n} u(\mathbf{x})\}^{\mathrm{T}}$ is the vector of unknowns, $\mathbf{J}$ is a diagonal matrix of $\{(-1)^\alpha / \alpha!\}_{|\alpha|=0}^{n}$ and

$$\mathbf{u} = \left\{u(\mathbf{x}_1), \ldots, u(\mathbf{x}_I), \ldots, u(\mathbf{x}_m)\right\}^{\mathrm{T}}, \tag{39}$$

$$\mathbf{R}(\mathbf{x}) = \begin{Bmatrix} 1 & x-x_1 & \dots & (\mathbf{x}-\mathbf{x}_1)^\alpha \\ \vdots & \vdots & & \vdots \\ 1 & x-x_I & \dots & (\mathbf{x}-\mathbf{x}_I)^\alpha \\ \vdots & \vdots & & \vdots \\ 1 & x-x_m & \dots & (\mathbf{x}-\mathbf{x}_m)^\alpha \end{Bmatrix} = \begin{Bmatrix} \mathbf{p}^{\mathrm{T}}(\mathbf{x}-\mathbf{x}_1) \\ \vdots \\ \mathbf{p}^{\mathrm{T}}(\mathbf{x}-\mathbf{x}_I) \\ \vdots \\ \mathbf{p}^{\mathrm{T}}(\mathbf{x}-\mathbf{x}_m) \end{Bmatrix}, \tag{40}$$

where I=1,…,m is a local node numbering. Now, if the number of points in the "star" (stencil) is equal to the number of unknowns, then a solution to the system can be obtained by solving (38) directly, which is the method proposed by Jensen [78]. Selecting a suitable star such that the resulting system is not linearly dependent was one of the essential troubles of the early GFD methods, as the number of points in the star was fixed, and each point in the star had to be of sufficient "quality" to avoid linear dependence, leading to a difficult situation. While effort was made at the time for better star selection, Liszka and Orkisz [5,6] greatly improved upon the method by considering that a larger number of points in the star could be used, and the resulting over-determined system could be solved by least squares, or weighted least squares:

$$\mathbf{T}(\mathbf{x})\mathbf{u}_{\mathbf{J}}^h(\mathbf{x}) = \mathbf{R}^{\mathrm{T}}(\mathbf{x})\mathbf{W}(\mathbf{x})\mathbf{u}\,, \tag{41}$$

where $\mathbf{W}(\mathbf{x})$ is a matrix of weights, and with the proper selection of $\mathbf{W}(\mathbf{x})$:

$$\mathbf{W}(\mathbf{x}) = \begin{bmatrix} w_a(\mathbf{x}-\mathbf{x}_1) & \cdots & 0 & \cdots & 0 \\ \vdots & \ddots & & & \vdots \\ 0 & & w_a(\mathbf{x}-\mathbf{x}_I) & & 0 \\ \vdots & & & \ddots & \vdots \\ 0 & \cdots & 0 & \cdots & w_a(\mathbf{x}-\mathbf{x}_m) \end{bmatrix}, \tag{42}$$

$\mathbf{T}(\mathbf{x}) = \mathbf{R}^{\mathrm{T}}(\mathbf{x})\mathbf{W}(\mathbf{x})\mathbf{R}(\mathbf{x})$ is exactly the matrix $\mathbf{A}(\mathbf{x})$ for MLS, and the moment matrix $\mathbf{M}(\mathbf{x})$ in the discrete RK approximation with monomials.

Solving the system (41), we then have

$$\mathbf{u}^h(\mathbf{x}) = \sum_{I\in G_{\mathbf{x}}} \mathbf{J}^{-1}\mathbf{M}^{-1}(\mathbf{x})\mathbf{P}(\mathbf{x}-\mathbf{x}_I)w_a(\mathbf{x}-\mathbf{x}_I)u_I\,. \tag{43}$$

Then, to obtain the approximation for $u(\mathbf{x})$, we can pre-multiply the right hand side of (43) by $\mathbf{P}(\mathbf{0})$ to obtain the first row of the vector $\mathbf{u}^h$ on the left hand side of (43), and as the first entry of $\mathbf{J}^{-1}$ is unity, immediately the MLS approximation is obtained. One can also identify a row in the left hand side of (43) corresponding to the approximation of $\partial^\alpha u(\mathbf{x})$, as the premultiplication of right hand side of (43) by $\mathbf{p}^\alpha$ in (35), and we see immediately that the generalized finite differences are also indeed the diffuse derivative approximations.

Remark 2.2

Comparing the GFD and synchronized derivatives to the RK approximation, one can observe that the moment matrix contains information on how to approximate the primary variable as well as derivatives.

v). Savitzky–Golay Filters and Peridynamics

Very recently, Bessa et al. [62] made the connection between synchronized derivatives, Savitzky-Golay filters [186], and Peridynamics. They showed that under uniform discretizations, the deformation gradient in nodally collocated state-based Peridynamics [59] is equivalent to employing Savitzky-Golay filters for constructing the deformation gradient. In addition, they showed that this approximation was a special case of diffuse derivatives with quadratic basis and flat kernels. They suggested that this was likely also true in the non-uniform case, as the procedures described herein to generate diffuse derivatives could be considered as a generalization of Savitzky-Golay filters. The precise connection between meshfree approximations and Peridynamics under general non-uniform discretizations will be discussed in a forthcoming paper.

3. Galerkin Based Meshfree Method

The meshfree approximation functions discussed in the previous sections can be used to form finite dimensional spaces for the numerical solution of PDEs under either the Galerkin framework (this section) or the strong form collocation framework (Section 4). For demonstration purposes, consider the following elasticity problem:

$$\nabla \cdot \boldsymbol{\sigma} + \mathbf{b} = \mathbf{0} \quad \text{in } \Omega, \tag{44}$$

$$\mathbf{n} \cdot \boldsymbol{\sigma} = \mathbf{h} \qquad \text{on } \partial\Omega_h, \tag{45}$$

$$\mathbf{u} = \mathbf{g}, \qquad \text{on } \partial\Omega_g, \tag{46}$$

where $\mathbf{u}$ is the displacement vector, $\boldsymbol{\sigma} = \mathbf{C} : \boldsymbol{\varepsilon}(\mathbf{u})$ is the Cauchy stress tensor, $\mathbf{C}$ is the elasticity tensor, $\boldsymbol{\varepsilon}(\mathbf{u}) = \nabla^s \mathbf{u} \equiv 1/2(\nabla \otimes \mathbf{u} + \mathbf{u} \otimes \nabla)$ is the strain tensor, $\mathbf{n}$ is the surface normal on $\partial\Omega$, $\mathbf{b}$ is the body force, $\mathbf{h}$ is the prescribed traction on $\partial\Omega_h$, $\mathbf{g}$ is the prescribed displacement on $\partial\Omega_g$, $\partial\Omega_g \cup \partial\Omega_h = \partial\Omega$, and $\partial\Omega_g \cap \partial\Omega_h = \varnothing$.

In the Galerkin statement of the problem, for generality we consider the solution $\mathbf{u}$ and its variation $\mathbf{v}$ approximated with meshfree shape functions by $\mathbf{u}^h$ and $\mathbf{v}^h$, respectively, as

$$\mathbf{u}^h(\mathbf{x}) = \sum_{I \in G_{\mathbf{x}}} \Psi_I(\mathbf{x})\mathbf{u}_I,$$
$$\mathbf{v}^h(\mathbf{x}) = \sum_{I \in G_{\mathbf{x}}} \hat{\Psi}_I(\mathbf{x})\mathbf{v}_I, \tag{47}$$

where Ψ_I and $\hat{\Psi}_I$ are meshfree shape functions, possibly different from each other, and $\{\mathbf{u}_I\}_{I=1}^{Np}$ is the set of unknowns. Note that in the Bubnov-Galerkin case $\hat{\Psi}_I(\mathbf{x}) = \Psi_I(\mathbf{x})$.

3.1 Enforcement of Essential Boundary Conditions

Essential boundary condition enforcement in the traditional finite element method is generally straightforward due to the property that nodal coefficients in the approximation coincide with the values at the nodes, and therefore, kinematic constraints can be imposed directly on the nodal coefficients. Most meshfree methods on the other hand, do not enjoy this property, and special attention must be paid to enforcing essential (Dirichlet) boundary conditions. The enforcement of essential boundary conditions in meshfree methods can generally be classified into two types of enforcement: (1) Strong enforcement at nodes, i.e., collocation of the essential boundary condition at nodes on the essential boundary, and (2) weak enforcement of conditions along the essential boundary. We do note a few exceptions to these cases later in the text. The Galerkin approximation of (44)-(46) has been formulated with the methods to be discussed as follows.

i). Strong Enforcement of Essential Boundary Conditions

One way to strongly enforce essential boundary conditions at nodes is to utilize the relationship between nodal coefficients and field values at the nodes [24,201–205], called the *transformation method* or *collocation method*. It appears that several researchers had arrived at this formulation independently around the same time. These relationships yield matrix equations that operate on nodal values, and thus kinematic constraints can be imposed directly with static condensation. This transformation can be constructed such that inverting a transformation matrix only related to the constrained degrees of freedom is necessary [201,204,205]. One can note that in essence, this method is a special case of the Lagrange multiplier method where the approximation of the multiplier is a delta function [205].

Modification to the standard meshfree approximation functions has been proposed so that that nodal degrees of freedom coincide with field variables [87,205–207]. Some of these special constructions of shape functions are introduced at constrained nodes only, such as the use of a singular weight function [205,207], as first suggested by Shepard, as well as Lankaster and Sulkus [80,113]. A scheme was proposed in [87] where an MLS-based method which has interpolation property. Coupling with FEM shape functions in the discretization on the boundary has also been proposed, to take advantage of the finite element method's ability to easily impose boundary conditions (see, e.g., [208,209]).

Methods which impose boundary conditions strongly offer very simple implementation of enforcement of essential boundary conditions. In addition, compared to other methods mentioned later in the text, no additional degrees of freedom, special matrix terms with boundary integration, or parameters to choose are present. With these approaches, a kinematically admissible finite dimensional space can be constructed, and the Galerkin approximation of (44)-(46) can be formulated as seeking $\mathbf{u}^h \in U^h \subset [H_g^1]^d$ such that $\forall \mathbf{v}^h \in V^h \subset [H_0^1]^d$:

$$\int_\Omega \boldsymbol{\varepsilon}(\mathbf{v}^h) : \mathbf{C} : \boldsymbol{\varepsilon}(\mathbf{u}^h) \mathrm{d}\Omega = \int_\Omega \mathbf{v}^h \cdot \mathbf{b} \mathrm{d}\Omega + \int_{\partial\Omega_h} \mathbf{v}^h \cdot \mathbf{h} \mathrm{d}\Gamma \,. \tag{48}$$

ii). Weak Enforcement of Essential Boundary Conditions

In the seminal work on EFG by Belytschko et al. [12], Lagrange multipliers were employed to weakly enforce boundary conditions. In this approach, the Galerkin approximation seeks $(\mathbf{u}^h, \boldsymbol{\lambda}^h) \in U^h \times \Lambda^h$ such that $\forall (\mathbf{v}^h, \boldsymbol{\gamma}^h) \in V^h \times \Gamma^h$, with $U^h \subset U$, $V^h \subset V$, $\Gamma \subset \Gamma^h$, and $\Lambda \subset \Lambda^h$, the following equation holds:

$$\begin{aligned} \int_\Omega \boldsymbol{\varepsilon}(\mathbf{v}^h) : \mathbf{C} : \boldsymbol{\varepsilon}(\mathbf{u}^h) \mathrm{d}\Omega + \int_{\partial\Omega_g} \boldsymbol{\gamma}^h \cdot \mathbf{u}^h \mathrm{d}\Gamma = \int_\Omega \mathbf{v}^h \cdot \mathbf{b} \mathrm{d}\Omega + \int_{\partial\Omega_h} \mathbf{v}^h \cdot \mathbf{h} \mathrm{d}\Gamma \\ + \int_{\partial\Omega_g} \mathbf{v}^h \cdot \boldsymbol{\lambda}^h \mathrm{d}\Gamma - \int_{\partial\Omega_g} \boldsymbol{\gamma}^h \cdot \mathbf{g} \mathrm{d}\Gamma \end{aligned}, \tag{49}$$

where $U = V = [H^1(\Omega)]^d$, $\Lambda = \Gamma = [L^2(\partial\Omega_g)]^d$; and $\boldsymbol{\lambda}^h$ and $\boldsymbol{\gamma}^h$ are approximations of the Lagrange multiplier $\boldsymbol{\lambda}$ and its variation $\boldsymbol{\gamma}$, respectively:

$$\begin{aligned} \boldsymbol{\lambda}^h(\mathbf{x}) &= \sum_{I \in G_{\mathbf{x}}^B} \varphi_I(\mathbf{x}) \boldsymbol{\lambda}_I \,, \\ \boldsymbol{\gamma}^h(\mathbf{x}) &= \sum_{I \in G_{\mathbf{x}}^B} \hat{\varphi}_I(\mathbf{x}) \boldsymbol{\gamma}_I \,, \end{aligned} \tag{50}$$

where φ_I and $\hat{\varphi}_I$ are shape functions, $G_{\mathbf{x}}^B$ is the set of nodes associated with the enforcing the essential boundary conditions which cover $\mathbf{x}$, and $\{\boldsymbol{\lambda}_I\}_{I=1}^{Np}$ is a set of additional unknowns, representing tractions on the essential boundary.

While straightforward, this method results in a positive semi-definite matrix and also adds degrees of freedom to the system. In addition, to ensure numerical stability, the choice of the finite dimensional spaces are subject to the *Babuška-Brezzi stability condition.* The work in [14] proposes an alternative approach called the modified variational principle, where the Lagrange multiplier is replaced by its physical counterpart (e.g., the traction in elasticity) as constructed by the primary approximation space, and does not suffer from these issues. It can be noted that this approach is a

special case of Nitche's method [210] with penalty parameter of zero, which in this case the bilinear form is not guaranteed to be coercive [127].

Imposing essential boundary conditions weakly using the penalty method has been employed in meshfree formulations (cf. [38,201]), and is an attractive choice due to its simplicity. It does not add degrees of freedom, and it is simple to implement. However, using this approach, the solution may not converge optimally [209]. In addition, the solution error is sensitive to the choice of penalty parameter employed, as large parameters can cause ill-conditioning of the system, while smaller parameters do not enforce boundary conditions well [209]. It is also noted that with the penalty method, the weak form does not attest to the strong form.

Nitche's method [210] can also be employed, which is essentially a combination of the penalty method and the modified variational principle. This method attests to the strong form, and also relaxes the strong dependence of the solution accuracy on the choice of the penalty parameter, thus addressing the issues with the penalty method. Using this technique, the solution is stable and convergent with the proper selection of the penalty parameter [127,209,210]. In [209] they showed that for two-dimensional problems, if the penalty parameter is of order h^{-2} optimal convergence could be achieved. In [127], it was demonstrated that one can estimate a parameter that gives optimal convergence by using an eigenvalue problem. Using this approach, the Galerkin problem is to find $\mathbf{u}^h \in U^h$ such that $\forall \mathbf{v}^h \in U^h$ the following equation holds:

$$\begin{aligned}&\int_\Omega \boldsymbol{\varepsilon}(\mathbf{v}^h) : \mathbf{C} : \boldsymbol{\varepsilon}(\mathbf{u}^h) \mathrm{d}\Omega - \int_{\partial\Omega_g} \mathbf{n} \cdot \left(\mathbf{C} : \boldsymbol{\varepsilon}(\mathbf{v}^h)\right) \cdot \mathbf{u}^h \mathrm{d}\Gamma - \int_{\partial\Omega_g} \mathbf{v}^h \cdot \mathbf{n} \cdot \left(\mathbf{C} : \boldsymbol{\varepsilon}(\mathbf{u}^h)\right) \mathrm{d}\Gamma \\ &+ \beta \int_{\partial\Omega_g} \mathbf{v}^h \cdot \mathbf{u}^h \mathrm{d}\Gamma = \int_\Omega \mathbf{v}^h \cdot \mathbf{b} \mathrm{d}\Omega + \int_{\partial\Omega_h} \mathbf{v}^h \cdot \mathbf{h} \mathrm{d}\Gamma + \int_{\partial\Omega_g} \mathbf{n} \cdot \left(\mathbf{C} : \boldsymbol{\varepsilon}(\mathbf{v}^h)\right) \cdot \mathbf{g} \mathrm{d}\Gamma + \beta \int_{\partial\Omega_g} \mathbf{v}^h \cdot \mathbf{g} \mathrm{d}\Gamma\end{aligned}, \quad (51)$$

where β is a penalty parameter, and $U^h \subset [H^1]^d$. It is worth mentioning a few other approaches which do not strictly fall into any one of the two categories. In [202], the D'Alembert's principle was utilized to enforce constraints. A novel way to impose boundary conditions strongly using only one layer of FEM elements was proposed in [211].

To summarize, due to the lack of Kronecker delta property, imposing boundary conditions in meshfree methods is not as straightforward as in finite elements. However, substantial effort has been made to address this issue, and many methods offer ease of implementation as well as other attractive features. In particular, Nitche's method is straightforward to implement, efficient, and optimally convergent and stable given the proper selection of the penalty parameter [127]. Another attractive option is modifying the approximation space near the boundary [87,205,207], where no matrix construction and operations are involved as in transformation methods [24,201–205]. In this approach, there is also no stability condition, nor selection of any parameters. The method is simple to implement, efficient, and it can be easily introduced into existing finite element codes which implicitly operate on generalized displacements.

Lastly, several meshfree methods do not require special treatment of boundary conditions such as the Maximum Entropy method [54,55] which enjoys the weak Kronecker delta property. An interesting recent development is the introduction of a generalization of MLS, RK and ME approximations in [141,144], where consistency, convexity, and the weak Kronecker delta property, can be obtained in various combinations such as MLS with weak Kronecker delta at the boundary, and higher order convex approximations.

3.2 Convergence of the Meshfree Method in PDEs

The convergence of the Galerkin meshfree method using MLS/RK/PU approximation with p^{th} order completeness has been shown to be [84–87]:

$$\left\| u - u^h \right\|_{\ell,\Omega} \le C a^{p+1-\ell} \left| u \right|_{p+1,\Omega}, \quad \ell \ge 0, \tag{52}$$

where a is the maximum support dimension of the approximation functions and C is independent of a and p. While the convergence rate in meshfree approximations with p^{th} order completeness yields the same rate of convergence compared to that of p-order finite elements, the constant C can be made smaller in meshfree methods with proper selection of smoothness in the meshfree approximation. Consider a Poisson problem on $\Omega : (0,1)\times(0,1)$ with a high order solution:

$$\begin{aligned} &\nabla^2 u = (x^2 + y^2) e^{xy} && \text{in } \Omega \\ &u = e^{xy} && \text{on } \partial\Omega \end{aligned}. \tag{53}$$

The problem above is solved with linear finite elements (p=1, C^0 continuity) and linear RKPM with quintic B-spline kernels with normalized support of 2.5 (p=1, C^4 continuity), both with uniform discretizations of 81, 289, 1089, and 4225 nodes. As seen in Figure 7, both methods yield similar rates of convergence, yet the error is much lower for RKPM. The final ratio between the errors in this case is roughly 1/8 for the L_2 norm and 1/6 for the H_1 semi-norm.

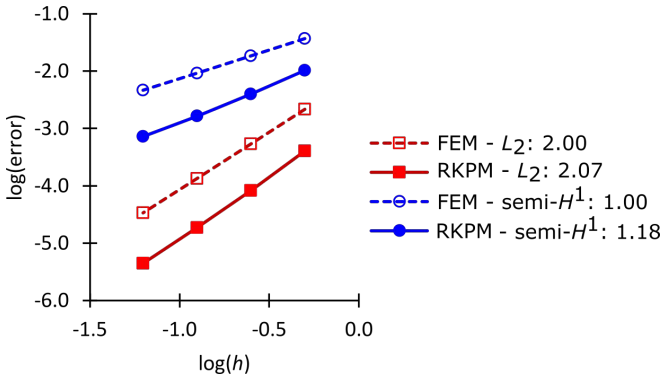

Figure 7. Convergence of linear FEM and linear RKPM in a second order PDE with a smooth solution. Rates are indicated in the legend.

3.3 Domain Integration

A key issue in weak form-based Galerkin methods is the choice of a quadrature scheme to perform domain integration. The problems at hand can be generally categorized as: (1) influence of domain integration error on solution error and convergence rates; and (2) rank instability in the solution with the choice of particular quadrature schemes such as nodal integration.

i). Quadrature Schemes for Efficient and Convergent Meshfree Solutions

In the early development of meshfree methods, Gauss integration using background cells, as shown in Figure 8, was commonly employed [12,24,190,195]. However, difficulty in obtaining accuracy in domain integration can be encountered when shape functions are rational, as they often are in meshfree methods (see Table 1), and Gauss integration cannot always accurately evaluate integrals in the Galerkin equation. Another major source of quadrature error is the misalignment of integration cells and shape function supports [109], which is typically the case in a general setting, as shown in Figure 8. As a result of these difficulties, large error can be introduced into the solution if careful attention is not paid to domain integration, and optimal convergence rates can be lost. In particular, the solutions under uniform discretizations generally do not suffer from integration issues, while the solutions under non-uniform discretizations are sensitive to the choice of domain integration [61].

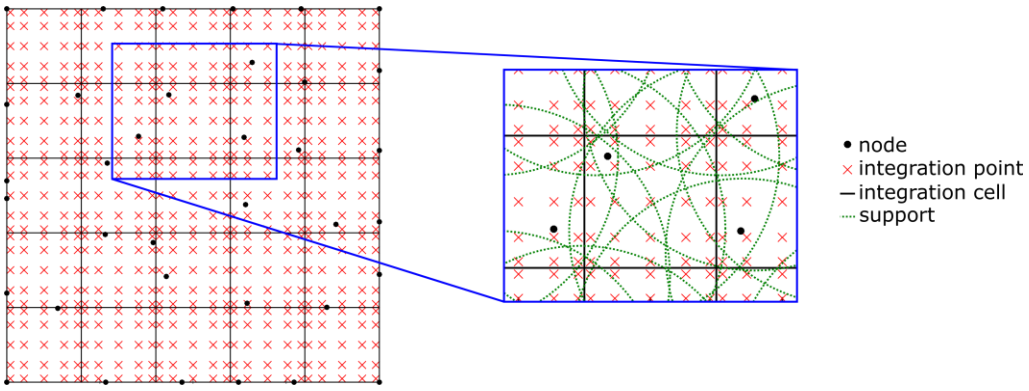

Figure 8. Gauss integration with a zoom-in showing nodal supports.

For illustration, various orders of quadrature are employed in background Gauss cells for RKPM with linear basis, for solving (53) with the non-uniform discretizations shown in Figure 9. As seen in Figure 10, 5×5 Gauss integration is needed to attain optimal convergence rates (at least a rate of two and one in the L_2 norm H_1 semi-norm, respectively).

It has been recognized by many researchers that high order quadrature is necessary in order to ensure acceptable convergence rates and accuracy in the solution [46,61,109,212]; this is prohibitively expensive in any practical problem. Because of this difficulty, many approaches have been developed to circumvent this issue.

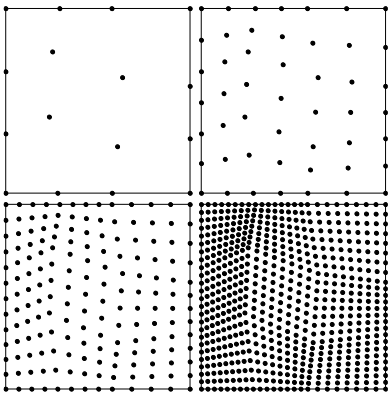

Figure 9. Non-uniform discretizations used in the convergence study.

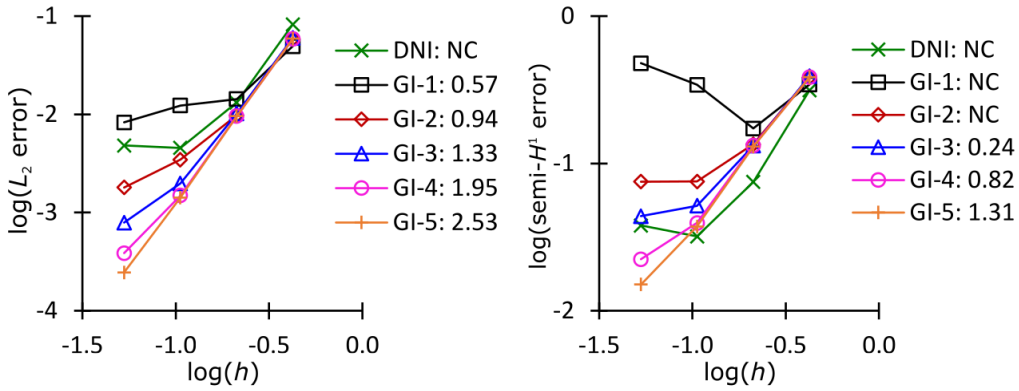

Figure 10. Convergence of RKPM with linear basis with various integration methods. Convergence rates are indicated in the legend, where "NC" denotes no convergence.

The solution error due to misalignment of meshfree supports and integration cells has motivated several algorithms. In [109] cells were constructed that aligned with the supports which significantly reduced the solution error due to numerical integration. Procedures were proposed in [124] to construct integration cells based on the structure of overlapping compact supports. In a similar spirit, a support integration scheme has also been developed in [213].

One condition leveraged in meshfree literature is the divergence constraint (often termed the *integration constraint*) on the test function space and numerical integration, necessary for satisfying the linear patch test [46,77,214]:

$$\hat{\int_{\Omega}} \nabla \Psi_I \mathrm{d}\Omega = \hat{\int_{\partial\Omega}} \Psi_I \mathbf{n} \mathrm{d}\Gamma \,, \tag{54}$$

where "^" over the integral symbol denotes numerical integration. In [77], an iterative technique to satisfy this condition via modification of approximation functions was proposed.

One particularly effective approach to achieve (54) is the stabilized conforming nodal integration (SCNI) by Chen et al. [46], which employs nodal integration with gradients smoothed over conforming representative nodal domains, as shown in Figure 11(b), converted to boundary integration using the divergence theorem:

$$\tilde{\nabla} \Psi_I(\mathbf{x}_L) = \frac{1}{W_L} \int_{\Omega_L} \nabla \Psi_I \mathrm{d}\Omega = \frac{1}{W_L} \int_{\partial\Omega_L} \Psi_I \mathbf{n} \mathrm{d}\Gamma \,, \tag{55}$$

where W_L is the integration weight associated with node L, and $\tilde{\nabla}$ denotes the smoothed gradient operator. In this method, smoothed gradients are employed for both test and trial functions, as the approximation (55) enjoys first order completeness [61]. If the smoothing domains $\{\Omega_L\}_{L=1}^{NP}$ are conforming, nodal integration with smoothed gradients $\tilde{\nabla}$ meets the condition (54) [46]. The smoothed gradient at the nodal point in (24) is then introduced in the weak form and integrated with nodal integration to form the stiffness matrix, see [46] for details. This approach has also been applied to large deformation problems with strain smoothing applied to the nodal evaluation of the deformation gradient [47].

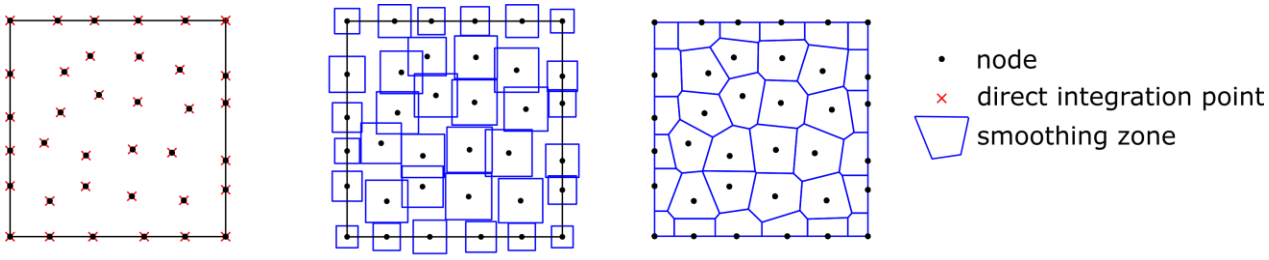

(a) (b) (c)

Figure 11. Nodal integration schemes in meshfree methods: (a) direct nodal integration, (b) stabilized conforming nodal integration, and (c) stabilized non-conforming nodal integration.

This method yields optimal convergence for linear approximation spaces, as shown in Figure 12, and provides a far more effective approach than Gauss integration. In addition, the method can serve as a correction to direct nodal integration (DNI), as shown in Figure 11(a), which suffers from significant convergence problems, as seen in Figure 10. For fragment-impact problems where maintaining conforming cells is cumbersome, a non-conforming version of SCNI has been

proposed in [215,216], termed stabilized non-conforming nodal integration (SNNI); this scheme is depicted in Figure 11(c). The relaxation of the conforming condition sacrifices optimal convergence, as seen in Figure 10, but is still efficient, and maintains superior stability over DNI. The reduced accuracy in SNNI compared to SCNI can be corrected to recover optimal convergence by variationally consistent integration [61], to be discussed in later in the text.

The SCNI method has been extended to many methods and problems: non-linear solid mechanics problems [47], the natural element method [48], the Schrödinger equation [217], plate and shell problems [218–220], and more recently, convection dominated problems [199] and coupled analysis of fluid-saturated porous media [221].

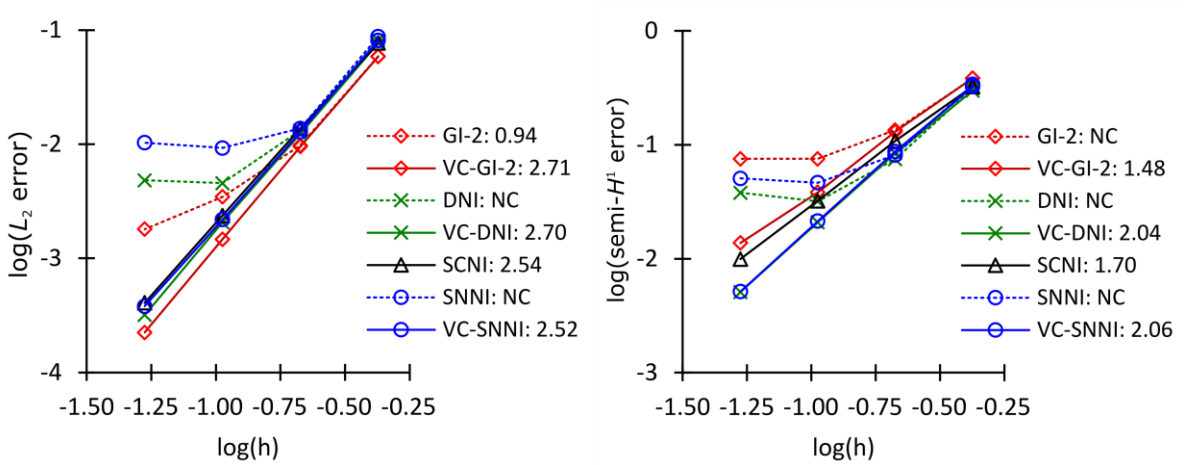

Figure 12. Convergence of RKPM with linear basis with various integration methods with and without variational consistency. Variationally consistent methods are denoted with the prefix "VC-"; *q* order of Gauss integration (GI) is denoted with the suffix "-q". Convergence rates are indicated in the legend.

The concept of strain smoothing in SCNI has also been applied to the finite element methods. The Ph.D. thesis of Guan [222] first introduced the strain smoothing in SCNI to finite elements as the basis for coupling FEM and RKPM with unified discretization and domain integration. Various nodal and element strain smoothing techniques have been proposed by Liu et al. for finite elements, and are termed the smoothed finite element methods [2,223,224]. The SCNI method has been shown to be grounded in variational principles [225].

In a recent development, a framework of variationally consistent integration (VCI) has been proposed by Chen, Hillman, and Rüter [61], where a generalization of the integration constraints in SCNI to arbitrary order revealed that the divergence condition in (54) is a special case of an integration by parts constraint necessary in order to obtain n^{th} order Galerkin exactness in the solution:

$$\int_{\Omega}^{\wedge} \nabla \hat{\Psi}_I \cdot \boldsymbol{\varepsilon}(\mathbf{u}^{\alpha}) \mathrm{d}\Omega = -\int_{\Omega}^{\wedge} \hat{\Psi}_I \nabla \cdot \boldsymbol{\varepsilon}(\mathbf{u}^{\alpha}) \mathrm{d}\Omega + \int_{\Gamma}^{\wedge} \hat{\Psi}_I \mathbf{n} \cdot \boldsymbol{\varepsilon}(\mathbf{u}^{\alpha}) \mathrm{d}\Gamma \quad \forall I, \quad |\alpha| = 0,1,\ldots,n, \quad (56)$$

where $\mathbf{u}^{\alpha} = \mathbf{c}_{\alpha}\mathbf{x}^{\alpha}$, and here we have included the possibility of different test and trial functions. One significant result is that with the satisfaction of these constraints, Galerkin orthogonality is restored up to order n [226]. Approximation spaces compatible with numerical integration in the form of the above have been termed VCI methods. Using this technique, optimal convergence can be attained using far lower-order quadrature than would otherwise be required [61]. For VC conditions for other mechanics problems, consult reference [61].

A Petrov-Galerkin method with enriched test functions has been proposed in [61] to satisfy the constraints, by leveraging the fact that (56) involves the test functions, while the trial functions are constructed to be n^{th} order complete. This method can be employed to correct any integration method at hand (as well as any approximation space cf. [227]), such as nodal integration. As seen in Figure 12, optimal convergence rates can be attained using various low order quadrature schemes (including DNI and SNNI) using the variationally consistent methods. In [110], a method called QC3 was proposed that satisfies the second order constraints, which was shown to be a generalization of the SCNI technique to second order. Very recently, a two-level smoothing technique has been proposed in [228] that is second-order exact, and was shown to provide even further efficiency over QC3. Mathematical analysis of the effect of the accuracy of domain integration has been provided Babuška and colleagues in [229,230], where a zero-row sum condition and corrected quadrature scheme to achieve VC conditions were proposed.

ii). Stabilization of Nodal Integration

Several of the methods discussed in the previous text offer viable quadrature techniques to yield efficient and convergent solutions in the Galerkin meshfree method. However, nodal integration such as the direct nodal integration scheme shown in Figure 11(a), is often desired so that stress and state variables "live" at the nodes, and also because it offers a technique devoid of meshes. Another reason this method is often pursued is its simplicity and efficiency. While the inaccuracy and non-convergent properties of nodal integration (see [46,61,111] for additional examples) can be addressed by methods mentioned in the previous text, as seen in Figure 10, the instability in the solution due to nodal integration type methods is widely recognized [46,74,111].

The instability resulting from nodal integration can be attributed to vanishing derivatives of short-wavelength (two times the nodal spacing) modes, and thus have little or no energy, and can grow unbounded in the solution [46,74,111]. In essence, the strain energy density is severely underestimated for this mode.

One way to circumvent this instability is to employ methods which minimize the least-squares residual [77,111,231,232]. These methods however, involve second-order derivatives of approximation functions, and typically a stabilization parameter. Another way to circumvent this difficulty is to calculate gradients in locations other than the nodes, often called the stress point method [75,233,234], which gives more reasonable strain energy at the stress points. This method does however require additional techniques such as residual-based stabilization in order to ensure convergent and stable solutions in all situations [231].

Utilizing Taylor expansions also allows one to obtain "extra" information around the integration points, and thus stabilize modes which have zero or near-zero energy associated with them. The origin of these methods is the unification of stabilization in finite elements [235]. The technique has been utilized to stabilize nodal integration in [236,237], and also other types of low order quadrature [96,193]. While stable, the drawbacks of this technique are that it requires calculation of high order derivatives and generally employs background cells.

Part of the dual motivation for the SCNI technique was that it also stabilizes zero energy modes in direct nodal integration by avoiding evaluating derivatives directly at nodal points [46,47]. In this method, the order of differentiation for constructing a stable method is actually reduced, also leading to enhanced efficiency. However, the smoothed integrations SCNI and SNNI are subject to spurious, oscillatory low-energy modes which can show up when the surface to volume ratio is sufficiently small, or in sufficiently fine discretizations [238]. An example of this mode for the SNNI method, obtained by eigenvalue analysis, is shown in Figure 13.

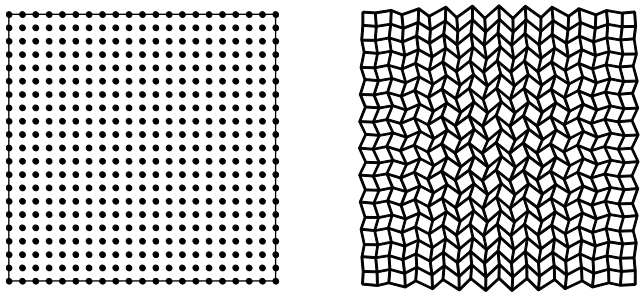

(a) (b)

Figure 13. (a) Discretization, and (b) lowest energy mode of SNNI.

Stabilization of these modes for SCNI and SNNI has been proposed in [238], where these modes are penalized throughout the smoothing domain, resulting in modified SCNI (MSCNI) and modified SNNI (MSNNI) in the strain energy:

$$a_{MS}\langle \mathbf{v}^h, \mathbf{u}^h \rangle = a_S \langle \mathbf{v}^h, \mathbf{u}^h \rangle + a_M \langle \mathbf{v}^h, \mathbf{u}^h \rangle, \tag{57}$$

where $a_S\langle\cdot,\cdot\rangle$ is the strain energy with strain smoothing:

$$a_S\langle \mathbf{v}^h, \mathbf{u}^h\rangle = \sum_{L=1}^{NP} \tilde{\boldsymbol{\varepsilon}}_L(\mathbf{v}^h) : \mathbf{C} : \tilde{\boldsymbol{\varepsilon}}_L(\mathbf{u}^h) W_L \ . \tag{58}$$

Here $\tilde{\boldsymbol{\varepsilon}}_L(\mathbf{u}^h) = 1/2(\tilde{\nabla} \otimes \mathbf{u}(\mathbf{x}_L) + \mathbf{u}(\mathbf{x}_L) \otimes \tilde{\nabla})$ is the smoothed strain, and

$$a_M\langle \mathbf{v}^h, \mathbf{u}^h\rangle = \sum_{L=1}^{NP}\sum_{K=1}^{NS} \beta\left[\left(\tilde{\boldsymbol{\varepsilon}}_L(\mathbf{v}^h) - \boldsymbol{\varepsilon}_L^K(\mathbf{v}^h)\right) : \mathbf{C} : \left(\tilde{\boldsymbol{\varepsilon}}_L(\mathbf{u}^h) - \boldsymbol{\varepsilon}_L^K(\mathbf{u}^h)\right) W_L^K\right] \tag{59}$$

is the additional stabilization where $0.0 \le \beta \le 1.0$, $\boldsymbol{\varepsilon}_L^K(\mathbf{u}^h) = \boldsymbol{\varepsilon}(\mathbf{u}^h(\mathbf{x}_L^K))$ is the strain evaluated at the centroid of sub-cells $\mathbf{x}_L^K$, and W_L^K is the weight of the sub-cell calculated from the weight W_L . It is clear from (59) that for $\beta > 0.0$ additional coercivity is added to the solution. The key to the success of this method in SCNI is that the additional stabilization maintains linear exactness of SCNI. The stabilized mode corresponding to the previous example is shown for SNNI in Figure 14(a).

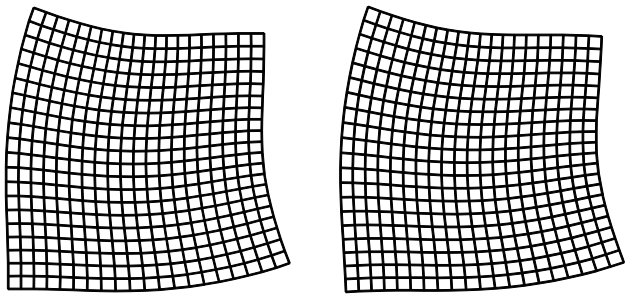

(a) (b)

Figure 14. Lowest energy modes of (a) modified SNNI and (b) NSNI.

An implicit gradient expansion has been proposed [239] which employs implicit gradients [45,191] (see Section 2.6) in a Taylor expansion to yield stabilization without explicit computation of higher order derivatives. In this approach, the implicit gradient expansion of the strain around a node $\mathbf{x}_L$ is defined as, in two dimensions:

$$\boldsymbol{\varepsilon}(\mathbf{u}^h(\mathbf{x})) \approx \boldsymbol{\varepsilon}_L(\mathbf{u}^h) + (x - x_L)\boldsymbol{\varepsilon}_L(\hat{\mathbf{u}}_x^h) + (y - y_L)\boldsymbol{\varepsilon}_L(\hat{\mathbf{u}}_y^h), \tag{60}$$

where $\boldsymbol{\varepsilon}_L(\hat{\mathbf{u}}_x^h) \equiv \boldsymbol{\varepsilon}(\hat{\mathbf{u}}_x^h(\mathbf{x}_L))$, $\boldsymbol{\varepsilon}_L(\hat{\mathbf{u}}_y^h) \equiv \boldsymbol{\varepsilon}(\hat{\mathbf{u}}_y^h(\mathbf{x}_L))$, and first order implicit gradients $\{\Psi_I^\alpha(\mathbf{x})\}_{|\alpha|=1}$ are

used to approximate the terms in the expansion:

$$\hat{\mathbf{u}}_x^h(\mathbf{x}_L) = \sum_{I \in G_{\mathbf{x}_L}} \Psi_I^{(1,0)}(\mathbf{x}_L)\mathbf{u}_I,$$
$$\hat{\mathbf{u}}_y^h(\mathbf{x}_L) = \sum_{I \in G_{\mathbf{x}_L}} \Psi_I^{(0,1)}(\mathbf{x}_L)\mathbf{u}_I, \tag{61}$$

where $\Psi_I^{\alpha}(\mathbf{x})$ is the implicit gradient shape function in (35). Substituting (60) for the strains near each node, following [239], one obtains a stabilized strain energy $a_{ND}\langle\cdot,\cdot\rangle$:

$$a_{ND}\langle \mathbf{v}^h, \mathbf{u}^h\rangle = a_D\langle \mathbf{v}^h, \mathbf{u}^h\rangle + a_N\langle \mathbf{v}^h, \mathbf{u}^h\rangle, \tag{62}$$

where $a_D\langle\cdot,\cdot\rangle$ is the quadrature version of the nodally integrated strain energy

$$a_D\langle \mathbf{v}^h, \mathbf{u}^h\rangle = \sum_{L=1}^{NP} \boldsymbol{\varepsilon}_L(\mathbf{v}^h) : \mathbf{C} : \boldsymbol{\varepsilon}_L(\mathbf{u}^h) W_L, \tag{63}$$

where $\boldsymbol{\varepsilon}_L(\mathbf{u}^h) = \boldsymbol{\varepsilon}(\mathbf{u}^h(\mathbf{x}_L))$ is the nodal strain; and

$$a_N\langle \mathbf{v}^h, \mathbf{u}^h\rangle = \sum_{L=1}^{NP} \left\{ \boldsymbol{\varepsilon}_L(\hat{\mathbf{v}}_x^h) : \mathbf{C} : \boldsymbol{\varepsilon}_L(\hat{\mathbf{u}}_x^h) M_{Lx} + \boldsymbol{\varepsilon}_L(\hat{\mathbf{v}}_y^h) : \mathbf{C} : \boldsymbol{\varepsilon}_L(\hat{\mathbf{u}}_y^h) M_{Ly} + \boldsymbol{\varepsilon}_L(\hat{\mathbf{v}}_z^h) : \mathbf{C} : \boldsymbol{\varepsilon}_L(\hat{\mathbf{u}}_z^h) M_{Lz} \right\} \tag{64}$$

is the additional stabilization, where M_{Lx}, M_{Ly}, and M_{Lz} are the second moments of inertia of the nodal domains about node L. Clearly, for coercive forms of $a(\cdot,\cdot)$, (64) adds additional stabilization for the strain energy. The stabilized nodal integration in (62)-(64) has been termed naturally stabilized nodal integration (NSNI) since the constants in the stabilization come naturally from the discretization. Performing an eigenvalue analysis of the associated stiffness matrix, the first non-zero energy mode is stable, as shown in Figure 14(b). In [239] it was demonstrated through complexity analysis that speed-up factors of up to twenty times could be achieved over methods such as MSCNI and MSNNI that involve additional sampling points.

Another form of stabilization considers a displacement smoothing and Taylor expansion [89,161]. This method has been shown to be a very effective approach to give a stable solution by nodal integration, without the use of numerical parameters or background cells. Integration techniques based on the partition of unity have been developed in [240,241] which do not require a mesh and is applied as a nodal sub-domain integration technique. Note that nodal integrations with corrective VCI procedures and stabilization can be formulated such that they do not detract from the "meshfree character" of the method [61,144,226,238,242,243].

To conclude, careful attention must be paid to domain integration in meshfree methods. If one "does nothing" and employs Gauss integration, prohibitively expensive high order quadrature is required to ensure accuracy and optimal convergence in all discretizations. On the other hand, without special treatment, nodal integration yeilds both inaccurate and unstable solutions. Dispite this fact, several effective methods have been developed over the past two decades to adress these issues of accuracy, efficiency, and stability. The SCNI method [46] has proven to be a robust method in a variety of settings [46,47,199,218–221], and is effective in terms of high accuracy and low CPU time [46]. While this method necessitates additional stabilization (57)-(59), this can be accomplished straightforwardly (see [199,238,244,245] for more details and variations on implementation). A few new promising recent developments are (a) corrections to achieve arbitrary order Galerkin exactness in any given integration method, which can achieve optimal convergence with low order quadarture [61], and can correct nodal integration methods for optimal convergence; (b) extensions of SCNI to achieve higher order Galerkin exactness [110,228]; and (c) accelerated stabilization (60)-(64) (see [239] for details) which can avoid many issues associated with stabilized nodal integration proposed in the past. Although quadrature for meshfree methods is still an active research, it apears that many of the problems with domain integration are being resolved.

4. Strong Form Collocation Based Meshfree Method

4.1 The Meshfree Collocation Method

An alternative approach to address domain integration issues in meshfree methods is by collocation of strong forms, such as the finite point method [35], the radial basis collocation methods [7,8] and the reproducing kernel collocation method [43,44]. For demonstration, consider the application of strong form collocation to the boundary value problem for elasticity in (44)-(46). Introducing the approximation $\mathbf{u}^h(\mathbf{x})$ into (44)-(46) and enforcing the residuals to be zero at N_C collocation points $\{\boldsymbol{\xi}_J\}_{J=1}^{N_C} \in \bar{\Omega} \equiv \Omega \cup \partial\Omega$, we have

$$\begin{aligned} &\nabla \cdot \boldsymbol{\sigma}\left(\mathbf{u}^h(\boldsymbol{\xi}_J)\right) = -\mathbf{b}(\boldsymbol{\xi}_J) && \forall \boldsymbol{\xi}_J \in \Omega, \\ &\mathbf{n} \cdot \boldsymbol{\sigma}\left(\mathbf{u}^h(\boldsymbol{\xi}_J)\right) = \mathbf{h}(\boldsymbol{\xi}_J) && \forall \boldsymbol{\xi}_J \in \partial\Omega_h, \\ &\mathbf{u}^h(\boldsymbol{\xi}_J) = \mathbf{g}(\boldsymbol{\xi}_J) && \forall \boldsymbol{\xi}_J \in \partial\Omega_g. \end{aligned} \tag{65}$$

The collocation in equation (65) is equivalent to the weighted residual of (44)-(46) as seeking $\mathbf{u}^h \in [H^2]^d$ such that $\forall \mathbf{w}, \mathbf{w}_h, \mathbf{w}_g \in [L^2]^d$:

$$\begin{aligned} &\int_\Omega \mathbf{w}(\mathbf{x}) \cdot \left(\nabla \cdot \boldsymbol{\sigma}\left(\mathbf{u}^h(\mathbf{x})\right) + \mathbf{b}(\mathbf{x})\right) d\Omega, \\ &+ \int_{\partial\Omega_h} \mathbf{w}_h(\mathbf{x}) \cdot \left(\mathbf{n} \cdot \boldsymbol{\sigma}\left(\mathbf{u}^h(\mathbf{x})\right) - \mathbf{h}(\mathbf{x})\right) d\Gamma + \int_{\partial\Omega_g} \mathbf{w}_g(\mathbf{x}) \cdot \left(\mathbf{u}^h(\mathbf{x}) - \mathbf{g}(\mathbf{x})\right) d\Gamma = 0. \end{aligned} \tag{66}$$

The weighted residual (66) leads to (65) when $\mathbf{w} = \mathbf{w}_h = \mathbf{w}_g = \sum_{J=1}^{N_C} \delta(\mathbf{x} - \boldsymbol{\xi}_J)\bar{\mathbf{w}}_J$ where $\delta(\cdot)$ is the Dirac Delta function in the *d*-dimensional space and $\bar{\mathbf{w}}_J$ is the associated arbitrary coefficient. Note that in this approach the admissible approximation $\mathbf{u}^h$ is required to be in $[H^2]^d$, which is difficult for the conventional FEM approximation to achieve. However, for the general meshfree approximations discussed in Section 2, the regularity requirement can be readily met.

Let the approximation of **u** be

$$\mathbf{u}^h(\mathbf{x}) = \sum_{I \in G_{\mathbf{x}}} g_I(\mathbf{x})\mathbf{u}_I \,, \tag{67}$$

where g_I is the meshfree shape function associated with $\mathbf{x}_I$, and $\mathbf{u}_I$ is the corresponding coefficient. To use the terminology of collocation methods, herein when discussing collocation we call the nodes in the set *Z source points*, and we denote the number of source points in the set by *Ns*. In matrix form, (65) can be rewritten as:

$$\begin{aligned}
&\sum_{I \in G_{\boldsymbol{\xi}_J}} \mathbf{L} g_I(\boldsymbol{\xi}_J)\mathbf{u}_I = -\mathbf{b}(\boldsymbol{\xi}_J) \quad \forall \boldsymbol{\xi}_J \in \Omega, \\
&\sum_{I \in G_{\boldsymbol{\xi}_J}} \mathbf{B}_h g_I(\boldsymbol{\xi}_J)\mathbf{u}_I = \mathbf{h}(\boldsymbol{\xi}_J) \quad \forall \boldsymbol{\xi}_J \in \partial\Omega_h, \\
&\sum_{I \in G_{\boldsymbol{\xi}_J}} \mathbf{B}_g g_I(\boldsymbol{\xi}_J)\mathbf{u}_I = \mathbf{g}(\boldsymbol{\xi}_J) \quad \forall \boldsymbol{\xi}_J \in \partial\Omega_g,
\end{aligned} \tag{68}$$

where, for two dimensions

$$\begin{aligned}
\mathbf{L} &= \begin{bmatrix} (\lambda+2\mu)\dfrac{\partial^2}{\partial x^2} + \mu\dfrac{\partial^2}{\partial y^2} & (\lambda+\mu)\dfrac{\partial}{\partial x \partial y} \\ (\lambda+\mu)\dfrac{\partial}{\partial x \partial y} & \mu\dfrac{\partial^2}{\partial x^2} + (\lambda+2\mu)\dfrac{\partial^2}{\partial y^2} \end{bmatrix}, \\
\mathbf{B}_h &= \begin{bmatrix} (\lambda+2\mu)n_x\dfrac{\partial}{\partial x} + \mu n_y\dfrac{\partial}{\partial y} & \mu n_y\dfrac{\partial}{\partial x} + \lambda n_x\dfrac{\partial}{\partial y} \\ \lambda n_y\dfrac{\partial}{\partial x} + \mu n_x\dfrac{\partial}{\partial y} & \mu n_x\dfrac{\partial}{\partial x} + (\lambda+2\mu)n_y\dfrac{\partial}{\partial y} \end{bmatrix}, \\
\mathbf{B}_g &= \begin{bmatrix} 1 & 0 \\ 0 & 1 \end{bmatrix}.
\end{aligned} \tag{69}$$

If $N_c = N_s$, the approach is termed as the direct collocation method [10]. When $N_c > N_s$, (68) leads to an overdetermined system and its solution can be obtained using a least-squares method. The

solution from an overdetermined system usually offers better accuracy and is less sensitive to the nodal distribution; however, to achieve optimal accuracy, the least-squares system needs to be properly weighted, which is referred to as the weighted collocation method. The details will be discussed in Section 4.3.

4.2 Approximation Functions and Convergence for Strong Form Collocation

i). Radial Basis Functions

Although any approximation in the $[H^2]^d$ space can be used in the collocation methods, the radial basis functions (RBFs) are popular for collocation solutions of PDEs, tracing back to the seminal work of Kansa [7,8]. RBFs have been used in many applications, such as surface fitting, turbulence analysis, neural networks, meteorology, and so forth. Hardy [155] first investigated multiquadric RBFs for interpolation problems, and Franke and Schaback [160] showed good performance in scattered data interpolation using multiquatric and thin-plate spline radial basis functions. Since then, the advances in applying RBFs to various problems has progressed constantly. A few commonly used radial basis functions are given below:

Multiquadrics (MQ): $$g_I(\mathbf{x}) = \left(r_I^2 + c^2\right)^{n-\frac{3}{2}} \tag{70}$$

Gaussian: $$g_I(\mathbf{x}) = \begin{cases} \exp\left(-\dfrac{r_I^2}{c^2}\right) \\ \left(r_I^2 + c^2\right)^{n-\frac{3}{2}} \exp\left(-\dfrac{r_I^2}{a^2}\right) \end{cases} \tag{71}$$

Thin plate splines: $$g_I(\mathbf{x}) = \begin{cases} r_I^{2n} \ln r_I \\ r_I^{2n-1} \end{cases} \tag{72}$$

Logarithmic: $$g_I(\mathbf{x}) = r_I^n \ln r_I \tag{73}$$

where, $r_I = \|\mathbf{x} - \mathbf{x}_I\|$ with $\|\cdot\|$ the Euclidean norm, and $\mathbf{x}_I$ is the source point of the RBF. The constant *c* involved in (70) and (71) is called the *shape parameter* of RBF. The MQ RBF in (70)function is the most popular function used in the solution of PDEs; the function is called reciprocal MQ RBF if *n*=1, linear MQ RBF if *n*=2, cubic MQ RBF if *n*=3, and so on. Madych [246] established several types of error bounds for MQ, Wu and Schaback [247] investigated local errors of scattered data interpolation by RBFs in suitable variational formulations, and Yoon [248] showed the convergence of RBFs in Sobolev spaces. All of these studies show that there exists an exponential

convergence rate in RBFs. Buhmann and Micchelli [157] showed that the convergence rate is accelerated for monotonically ordered *c*.

For a smooth function $u(\mathbf{x})$, the approximation, denoted by $u^h(\mathbf{x})$, is expressed by (67). There exists an exponential convergence rate of RBFs given by Madych [246]:

$$\left\| u - u^h \right\|_\ell \le C_\nu \eta^{c/H} \left\| u \right\|_t , \tag{74}$$

where $0 < \eta < 1$ is a real number, C_ν is a generic constant with the subscript ν denoting that it is dependent on the Poisson's ratio ν, $\|\cdot\|_\ell$ is the Sobolev ℓ-norm, and $\|\cdot\|_t$ is induced from the regularity requirements of the approximated function *u* and RBFs, see [159,246], *H* is the radial distance defined as $H := H(\Omega, \mathbf{S}) = \sup_{\mathbf{x}\in\Omega} \min_{\mathbf{x}_I \in Z} \|\mathbf{x} - \mathbf{x}_I\|$, and $\eta = \exp(-\theta)$ with $\theta > 0$. The accuracy and rate of convergence of MQ-RBF approximations is determined by the number of basis functions (the number of source points) N_S and the shape parameter *c*. The application of RBFs to partial differential equations is natural as the RBFs are infinitely differentiable ($g_I(\mathbf{x}) \in C^\infty$).

ii). Moving Least Squares and Reproducing Kernel

The MLS/RK approximations described in Section 2 can be adopted in the collocation methods, e.g. the reproducing kernel collocation method (RKCM) [43,44,198], and the gradient reproducing kernel collocation method (G-RKCM) [45]. In addition to first derivatives, higher order derivatives of MLS/RK approximations are mandatory when using strong form collocation. They can be obtained by direct differentiation of the MLS/RK approximations or by implicit gradients [92,93,191], as discussed in Section 2.6.

Note that although the employment of the C^2 continuous kernel (21) in MLS/RK would satisfy the regularity requirements of strong form collocation, higher-order continuous kernels offers better numerical stability, especially when the point density is high. Therefore, a quintic B-spline is often adopted in RKCM:

$$\phi_a(z) = \begin{cases} \frac{11}{20} - \frac{9}{2}z^2 + \frac{81}{4}z^4 - \frac{81}{4}z^5 & for\ 0 \le z \le \frac{1}{3} \\ \frac{17}{40} + \frac{15}{8}z - \frac{63}{4}z^2 + \frac{135}{4}z^3 - \frac{243}{8}z^4 + \frac{81}{8}z^5 & for\ \frac{1}{3} \le z \le \frac{2}{3} \\ \frac{81}{40} - \frac{81}{8}z + \frac{81}{4}z^2 - \frac{81}{4}z^3 + \frac{81}{8}z^4 - \frac{81}{40}z^5 & for\ \frac{2}{3} \le z \le 1 \\ 0 & for\ z > 1 \end{cases}. \tag{75}$$

For a smooth function $u(\mathbf{x})$, the approximation, denoted by $u^h(\mathbf{x})$, can be expressed by the linear combination of MLS/RK shape functions. Solving a PDE by collocation (57) with the MLS/RK approximation, there exists an algebraic convergence rate as shown by Hu et al. [198]:

$$\left\| u - u^h \right\|_E \le C \chi a^{p-1} |u|_{p+1,\Omega}, \tag{76}$$

where C is a generic constant, χ is the overlapping parameter, a is the support measure, p is the order of complete monomials in MLS/RK shape functions, and

$$\|v\|_E \equiv \left(\|v\|_{1,\Omega}^2 + \|\mathcal{L}v\|_{0,\Omega}^2 + \|\mathcal{B}_h v\|_{0,\partial\Omega_h}^2 + \|\mathcal{B}_g v\|_{0,\partial\Omega_g}^2 \right)^{\frac{1}{2}}, \tag{77}$$

where $\mathcal{L}$, $\mathcal{B}_h$, and $\mathcal{B}_g$ denote the differential operators associated with the domain, Neumann boundary, and Dirichlet boundary, respectively. From (76), it is important to note that the solution does not converge when $p = 1$ is used for solving a second order PDE. An order p of at least 2 is mandatory for convergence.

iii). Reproducing Kernel Enhanced Local Radial Basis

The commonly used RBF approximation function in the strong form collocation method offers exponential convergence, however the method suffers from large condition numbers due to its "nonlocal" approximation. The MLS/RK functions, on the other hand, provide polynomial reproducibility in a "local" approximation, and the corresponding discrete systems are relatively well conditioned. Nonetheless, RKCM produces only algebraic convergence [44]. An approach has been proposed to combine the advantages of RBF and RK functions to yield a local approximation that is better conditioned than that of the RBF, while at the same time offers a higher rate of convergence than that of RK (19):

$$u^h(\mathbf{x}) = \sum_{I \in G_{\mathbf{x}}} \left[\Psi_I(\mathbf{x}) \left(a_I + \sum_{J=1}^{M} g_I^J(\mathbf{x}) d_I^J \right) \right], \tag{78}$$

where $\Psi_I(\mathbf{x})$ is the RK function with compact support, and g_I^J is the RBF. Applying the approximation in (78) to the weighted strong form collocation as described in Section 4.3 is called the localized radial basis collocation method (L-RBCM).

The above approximation utilizes the compactly supported partition of unity to “patch” the global RBFs together. Error analysis shows that if the error of the RK approximation is sufficiently small, the proposed method maintains the exponential convergence of RBFs, while significantly improving the condition of the discrete system, and yields a banded matrix [172] as discussed below.

(1) Using the partition of unity properties of the RK localizing function, there exists the following error bound [172]:

$$\| u - u_I^h \|_{0,\Omega} \le \beta C \eta_0^{c/\delta} \| u \|_t, \tag{79}$$

where β is the maximum cover number for the RK localizing function. Other parameters are the same as defined earlier.

(2) The enhanced stability in the L-RBCM can be demonstrated by a perturbation analysis of the strong form collocation equations in (68) expressed in the following linear system:

$$\mathbf{Kd} = \mathbf{f} \,. \tag{80}$$

The stability of the above linear system can be measured by the condition number of **F**. The work in [172] obtained the following estimation of the condition number of L-RBCM:

$$Cond\left(\mathbf{K}\right) \approx O\left(a^{-3d/2}\right), \tag{81}$$

where *d* is the spatial dimension. In two-dimensional elasticity, we have the following comparison of condition numbers using RBCM with pure RBFs, RKPM with pure RK in (19), and L-RBCM with localized RBF in (78):

$$\begin{aligned} &\text{RBCM}: && Cond\left(\mathbf{K}\right) \approx O(h^{-8}), \\ &\text{RKPM}: && Cond\left(\mathbf{K}\right) \approx O(h^{-2}), \\ &\text{L}-\text{RBCM}: && Cond\left(\mathbf{K}\right) \approx O(h^{-3}). \end{aligned} \tag{82}$$

The L-RBCM approach offers a significant improvement on stability over RBCM. Although the discrete system of L-RBCM is slightly less well-conditioned than that of RKPM, it offers a higher convergence rate similar to that in RBCM.

4.3 Weighted collocation methods and optimal weights

When $N_C > N_S$, the collocation equations (68) recast in a matrix form as (80) leads to an overdetermined system, and a least-squares method can be applied for seeking the solution, equivalent to minimizing a weighted residual. The residual is defined as $e(\mathbf{d}) = 1/2(\mathbf{Kd}-\mathbf{f})^T\mathbf{W}(\mathbf{Kd}-\mathbf{f})$, where **W** a symmetric weighting matrix, Minimizing $e(\mathbf{d})$ yields

$$\mathbf{K}^T\mathbf{WKd} = \mathbf{K}^T\mathbf{Wf} \,. \tag{83}$$

It has been shown in [10] that solving strong form collocation equations by a least-squares method is equivalent to minimizing a least-squares functional with quadrature. It states to find $\mathbf{u}^h$ such that

$$E\left(\mathbf{u}^h\right) = \inf_{\mathbf{v}\in V} E\left(\mathbf{v}\right), \tag{84}$$

where *V* is an admissible finite dimensional space spanned by meshfree shape functions, and

$$E(\mathbf{v}) = \frac{1}{2}\hat{\int}_{\Omega}\left(\mathbf{L}\mathbf{v}+\mathbf{b}\right)^2 d\Omega + \frac{1}{2}\hat{\int}_{\partial\Omega_h}\left(\mathbf{B}_h\mathbf{v}-\mathbf{h}\right)^2 d\Gamma + \frac{1}{2}\hat{\int}_{\partial\Omega_g}\left(\mathbf{B}_g\mathbf{v}-\mathbf{g}\right)^2 d\Gamma . \qquad (85)$$

Recall that $\hat{\int}$ denotes integration with quadrature. It has been shown in [10] that the errors from the domain and boundary integrals in (85) are unbalanced. Therefore, a weighted least-squares functional can be introduced:

$$E(\mathbf{v}) = \frac{1}{2}\hat{\int}_{\Omega}\left(\mathbf{L}\mathbf{v}-\mathbf{f}\right)^2 d\Omega + \frac{\alpha^h}{2}\hat{\int}_{\partial\Omega_h}\left(\mathbf{B}_h\mathbf{v}-\mathbf{h}\right)^2 d\Gamma + \frac{\alpha^g}{2}\hat{\int}_{\partial\Omega_g}\left(\mathbf{B}_g\mathbf{v}-\mathbf{g}\right)^2 d\Gamma . \qquad (86)$$

Here the weights α^h and α^g are determined by considering error balancing of the weighted least-squares functional associated with the domain and boundary equations in [10]:

$$\sqrt{\alpha_h} \approx O(1), \sqrt{\alpha_g} \approx O(\kappa N_S), \qquad (87)$$

where $\kappa = \max(\lambda, \mu)$, or more generally, the maximum coefficient involved in the differential operator and boundary operator for the problem at hand. It is also noted that when dealing with nearly incompressible problems, $\kappa = \mu$ has been suggested in [167] as λ goes unbounded in the incompressible limit.

Minimizing (86) is equivalent to solving the following weighted collocation equations by a least squares method:

$$\begin{aligned}
\sum_{I\in G_{\boldsymbol{\xi}_J}} \mathbf{L}g_I(\boldsymbol{\xi}_J)\mathbf{u}_I &= -\mathbf{b}(\boldsymbol{\xi}_J) \qquad \forall \boldsymbol{\xi}_J \in \Omega, \\
\sqrt{\alpha_h}\sum_{I\in G_{\boldsymbol{\xi}_J}} \mathbf{B}_h g_I(\boldsymbol{\xi}_J)\mathbf{u}_I &= \sqrt{\alpha_h}\mathbf{h}(\boldsymbol{\xi}_J) \quad \forall \boldsymbol{\xi}_J \in \partial\Omega_h, \\
\sqrt{\alpha_g}\sum_{I\in G_{\boldsymbol{\xi}_J}} \mathbf{B}_g g_I(\boldsymbol{\xi}_J)\mathbf{u}_I &= \sqrt{\alpha_g}\mathbf{g}(\boldsymbol{\xi}_J) \quad \forall \boldsymbol{\xi}_J \in \partial\Omega_g .
\end{aligned} \qquad (88)$$

Example 4.1

An infinitely long (plane-strain) elastic tube is subjected to an internal pressure. The tube is made of an elastic material with Young's modulus $E = 3\times10^7$ Pa, and Poisson ratio υ=0.25. The inner and outer radii of the tube are 4 m and 10 m, respectively, and the inner surface of the tube is subjected to pressure $P = 100\text{N/m}^2$. Due to symmetry, only a quarter of the model, as shown in Figure 15(a), is discretized by the RBF collocation method with proper symmetric boundary conditions specified. The corresponding boundary value problem can be expressed as

$$\nabla \cdot \boldsymbol{\sigma} = \mathbf{0} \quad \text{in } \Omega \tag{89}$$

with boundary conditions:

$$\begin{aligned} h_i &= -Pn_i && \text{on } \Gamma_1 \\ h_1 &= 0, u_2 = 0 && \text{on } \Gamma_2 \\ h_i &= 0_i && \text{on } \Gamma_3 \\ h_2 &= 0, u_1 = 0 && \text{on } \Gamma_4 \end{aligned} \tag{90}$$

where $h_i = \sigma_{ij} n_j$.

In this problem, both source points and collocation points are non-uniformly distributed as shown in Figure 15(b). Three different discretizations, 7×7, 9×9, and 11×11 source points, are used, and the shape parameters *c* for the three discretizations are 10, 7.5 and 6 respectively. The number of corresponding collocation points is $(2N_1 - 1)(2N_2 - 1)$, where N_1 is the number of source points along the radial direction and N_2 is the number of source points along the angular direction.

The direct collocation method (DCM) and weighted collocation method (WCM) with MQ RBFs are used in the numerical test. For WCM, weights for Dirichlet collocation equations $\sqrt{\alpha_g} = 10$ and Neumann collocation equations $\sqrt{\alpha_h} = 1$ are selected based on (87). The convergence of the L^2 norm and H^1 semi-norm obtained by DCM and WCM are compared in Figure 16. As is shown in the numerical results, the direct collocation method with proper weights for Dirichlet and Neumann boundaries offer a much improved solution over DCM.

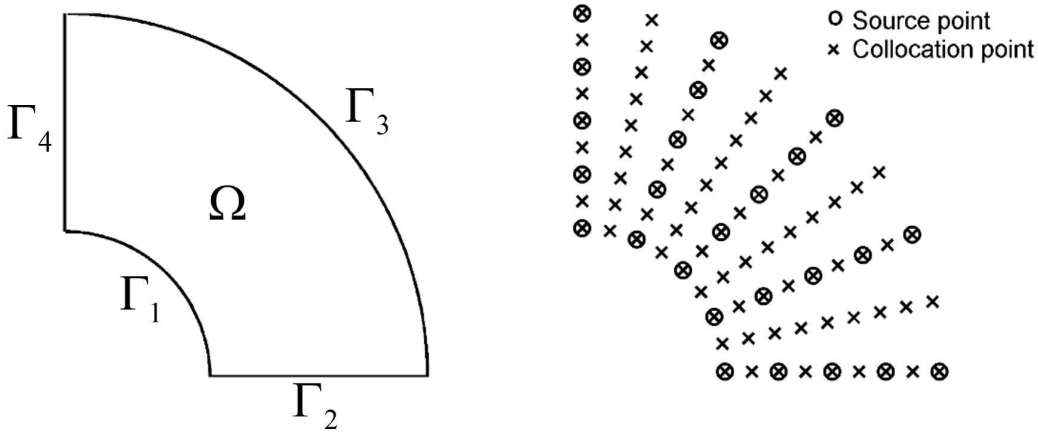

(a) (b)

Figure 15. Tube problem: (a) Quarter model, and (b) distribution of source points and collocation points.

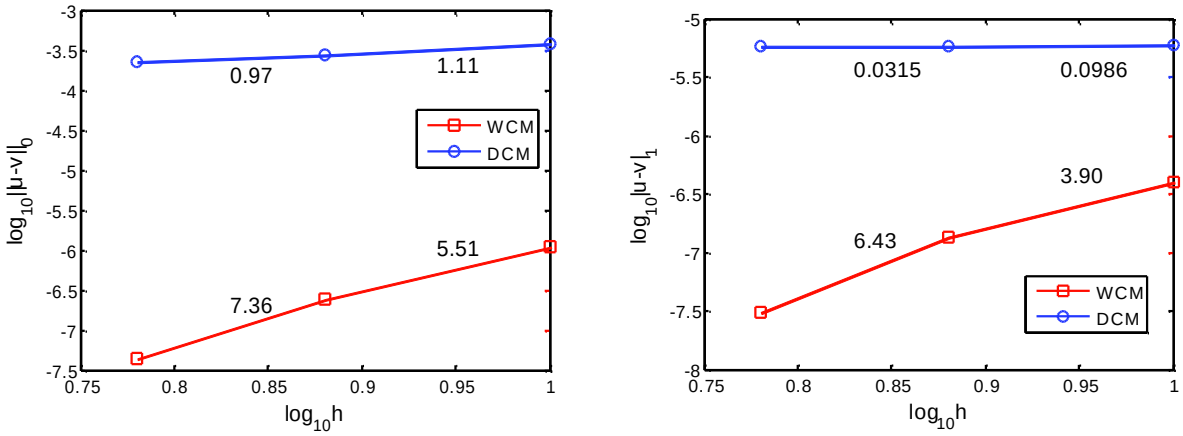

Figure 16. Convergence in the tube problem in the L^2 error norm, and the H^1 semi-norm.

4.4 Gradient Reproducing Kernel Collocation Method

While MLS/RK approximation functions can be arbitrarily smooth, taking derivatives of these functions is computationally costly. In particular, the high complexity in RKCM is caused by taking derivatives of the moment matrix inversion in the multi-dimensional MLS/RK shape functions(see the detailed complexity and error analysis of RKCM in [198]). Further, for optimal convergence in RKCM, using the number of collocation points much larger than the number of source points is needed, and this adds additional computational effort [44,198]. To enhance computational efficiency in RKCM, an implicit gradient approximation (see Section 2.6) has been introduced in [45] for solving second order PDEs with strong form collocation, which has been termed the gradient reproducing kernel collocation method (G-RKCM).

Consider the two-dimensional version of the elastic model problem in (44)-(46). The approximations of the derivatives $\mathbf{u}_{,x}$ and $\mathbf{u}_{,y}$ are constructed by employing first order implicit gradients $\{\Psi_I^{\alpha}(\mathbf{x})\}_{|\alpha|=1}$ where $\Psi_I^{\alpha}(\mathbf{x})$ is given in (35):

$$\begin{aligned}\mathbf{u}_{,x} &\approx \mathbf{u}_x^h = \sum_{I\in G_{\mathbf{x}}} \Psi_I^{(1,0)}(\mathbf{x})\mathbf{u}_I,\\ \mathbf{u}_{,y} &\approx \mathbf{u}_y^h = \sum_{I\in G_{\mathbf{x}}} \Psi_I^{(0,1)}(\mathbf{x})\mathbf{u}_I.\end{aligned} \tag{91}$$

The approximation of second order derivatives of $\mathbf{u}$ is obtained by taking direct derivatives of $\mathbf{u}_x^h$ and $\mathbf{u}_y^h$, e.g.,

$$\mathbf{u}_{,xx} \approx \mathbf{u}^h_{x,x} = \sum_{I \in G_{\mathbf{x}}} \Psi^{(1,0)}_{I,x}(\mathbf{x})\mathbf{u}_I,$$
$$\mathbf{u}_{,yy} \approx \mathbf{u}^h_{y,y} = \sum_{I \in G_{\mathbf{x}}} \Psi^{(0,1)}_{I,y}(\mathbf{x})\mathbf{u}_I. \tag{92}$$

Introducing (91) and (67) in the discretization in the strong form (44)-(46) leads to:

$$\begin{aligned} &\mathbf{L}^1_h \mathbf{u}^h_x + \mathbf{L}^2_h \mathbf{u}^h_y = -\mathbf{b} && \text{in } \Omega \\ &\mathbf{B}^1_h \mathbf{u}^h_x + \mathbf{B}^2_h \mathbf{u}^h_y = \mathbf{h} && \text{on } \partial\Omega_h \\ &\mathbf{B}_g \mathbf{u}^h = \mathbf{g} && \text{on } \partial\Omega_g \end{aligned} \tag{93}$$

where

$$\mathbf{L}^1_h = \begin{bmatrix} (\lambda+2\mu)\dfrac{\partial}{\partial x} & \mu\dfrac{\partial}{\partial y} \\ \lambda\dfrac{\partial}{\partial y} & \mu\dfrac{\partial}{\partial x} \end{bmatrix}, \quad \mathbf{L}^2_h = \begin{bmatrix} \mu\dfrac{\partial}{\partial y} & \lambda\dfrac{\partial}{\partial x} \\ \mu\dfrac{\partial}{\partial x} & (\lambda+2\mu)\dfrac{\partial}{\partial y} \end{bmatrix},$$
$$\mathbf{B}^1_h = \begin{bmatrix} (\lambda+2\mu)n_x & \mu n_y \\ \lambda n_y & \mu n_x \end{bmatrix}, \quad \mathbf{B}^2_h = \begin{bmatrix} \mu n_y & \lambda n_x \\ \mu n_x & (\lambda+2\mu)n_y \end{bmatrix}. \tag{94}$$

When $N_C > N_S$, the overdetermined system can be obtained by a least-squares method with proper weights to achieve optimal solution accuracy:

$$\begin{aligned} &\sum_{I \in G_{\xi_J}} \left[\mathbf{L}^1 \Psi^{(1,0)}_I(\boldsymbol{\xi}_J) + \mathbf{L}^2 \Psi^{(0,1)}_I(\boldsymbol{\xi}_J)\right]\mathbf{u}_I = -\mathbf{b}(\boldsymbol{\xi}_J) && \forall \boldsymbol{\xi}_J \in \Omega, \\ &\sqrt{\alpha_h} \sum_{I \in G_{\xi_J}} \left[\mathbf{B}^1_h \Psi^{(1,0)}_I(\boldsymbol{\xi}_J) + \mathbf{B}^2_h \Psi^{(0,1)}_I(\boldsymbol{\xi}_J)\right]\mathbf{u}_I = \sqrt{\alpha_h}\mathbf{h}(\boldsymbol{\xi}_J) && \forall \boldsymbol{\xi}_J \in \partial\Omega_h, \\ &\sqrt{\alpha_g} \sum_{I \in G_{\xi_J}} \mathbf{B}_g \Psi_I(\boldsymbol{\xi}_J)\mathbf{u}_I = \sqrt{\alpha_g}\mathbf{g}(\boldsymbol{\xi}_J) && \forall \boldsymbol{\xi}_J \in \partial\Omega_g. \end{aligned} \tag{95}$$

For balance of errors between the domain and boundary equation, the following weights should be selected:

$$\sqrt{\alpha_h} \approx O(1), \quad \sqrt{\alpha_g} \approx O\left(\kappa a^{q-p-1}\right) \tag{96}$$

where $\kappa = \max(\lambda, \mu)$, a is the kernel support measure, p is the MLS/RK order in $\mathbf{u}^h$, and q is the order of $\mathbf{u}_x^h$ and $\mathbf{u}_y^h$. The convergence properties of G-RKCM have been shown to be as follows:

$$\left\|u - u^h\right\|_{1,\Omega} \approx O(a^{q-1}), \quad \left\|u_{,x} - u_{,x}^h\right\|_{1,\Omega} + \left\|u_{,y} - u_{,y}^h\right\|_{1,\Omega} \approx O(a^{q-1}), \tag{97}$$

$$\left\|u - u^h\right\|_{0,\Omega} \approx O(a^{q}), \quad \left\|u_{,x} - u_{,x}^h\right\|_{0,\Omega} + \left\|u_{,y} - u_{,y}^h\right\|_{0,\Omega} \approx O(a^{q}). \tag{98}$$

Remarks 4.1

1. The error estimate in (97) and (98) indicates that the convergence of G-RKCM is only dependent on the polynomial degree q in the approximation of $\mathbf{u}_{,x}$ and $\mathbf{u}_{,y}$, and is independent of the polynomial degree p in the approximation of $\mathbf{u}$. Further, $q \geq 2$ is mandatory for convergence.
2. As shown in [45], G-RKCM allows the use of $N_C = N_S$ for sufficient accuracy.

4.5 Subdomain Collocation for Heterogeneity and Discontinuities

Due to the overlapping supports of meshfree shape functions (particularly RBFs) and the high smoothness required in the strong form collocation methods, special treatments are required for problems with heterogeneity or discontinuities. The subdomain collocation method [165,166] has been introduced for this purpose.

Take a heterogeneous elastic domain as an example, as shown in Figure 17. The collocation of each subdomain is independently expressed as follows:

$$\begin{cases} \mathbf{L}^+\mathbf{u}^{h+} = -\mathbf{b}^+ & \text{in } \Omega^+ \\ \mathbf{B}_g^+\mathbf{u}^{h+} = \mathbf{g}^+ & \text{on } \partial\Omega^+ \cap \partial\Omega^g \\ \mathbf{B}_h^+\mathbf{u}^{h+} = \mathbf{h}^+ & \text{on } \partial\Omega^+ \cap \partial\Omega^h \end{cases}, \tag{99}$$

$$\begin{cases} \mathbf{L}^-\mathbf{u}^{h-} = -\mathbf{b}^- & \text{in } \Omega^- \\ \mathbf{B}_g^-\mathbf{u}^{h-} = \mathbf{g}^- & \text{on } \partial\Omega^- \cap \partial\Omega^g \\ \mathbf{B}_h^-\mathbf{u}^{h-} = \mathbf{h}^- & \text{on } \partial\Omega^- \cap \partial\Omega^h \end{cases}. \tag{100}$$

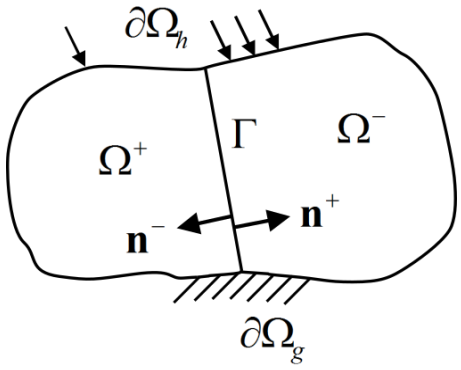

Figure 17. Two subdomains of a problem with material heterogeneity.

The approximation of **u** in each subdomain is performed by separate sets of basis functions:

$$\mathbf{u}^h(\mathbf{x}) = \begin{cases} \mathbf{u}^{h+}(\mathbf{x}) = g_1^+(\mathbf{x})\mathbf{u}_1^+ + \cdots + g_{N_S^+}^+(\mathbf{x})\mathbf{u}_{N_S^+}^+, & \mathbf{x} \in \bar{\Omega}^+ \\ \mathbf{u}^{h-}(\mathbf{x}) = g_1^-(\mathbf{x})\mathbf{u}_1^- + \cdots + g_{N_S^-}^-(\mathbf{x})\mathbf{u}_{N_S^-}^-, & \mathbf{x} \in \bar{\Omega}^- \end{cases}. \tag{101}$$

Here, Dirichlet and Neumann type interface conditions are introduced on the interface as follows for optimal convergence [166]:

$$\begin{aligned} \mathbf{u}^{h+} - \mathbf{u}^{h-} &= \mathbf{0} \quad \text{on } \Gamma \\ \mathbf{B}_h^+ \mathbf{u}^{h+} + \mathbf{B}_h^- \mathbf{u}^{h-} &= \mathbf{0} \quad \text{on } \Gamma \end{aligned}. \tag{102}$$

As before, if $N_C > N_S$ a weighted least-squared method can be applied, and the weighted discretized collocation equations read:

$$\mathbf{A}\,\mathbf{u} \equiv \begin{bmatrix} \mathbf{A}^+ \\ \mathbf{A}^- \\ \mathbf{\Lambda} \end{bmatrix} \mathbf{u} = \begin{bmatrix} \mathbf{b}^+ \\ \mathbf{b}^- \\ \mathbf{0} \end{bmatrix} \equiv \mathbf{b}\,, \tag{103}$$

with submatrices defined as:

$$\mathbf{A}^\pm = \begin{bmatrix} \mathbf{A}_L^\pm \\ \sqrt{\alpha_g^\pm}\mathbf{A}_g^\pm \\ \sqrt{\alpha_h^\pm}\mathbf{A}_h^\pm \end{bmatrix}; \mathbf{b}^\pm = \begin{bmatrix} \mathbf{b}_L^\pm \\ \sqrt{\alpha_g^\pm}\mathbf{b}_g^+ \\ \sqrt{\alpha_h^\pm}\mathbf{b}_h^+ \end{bmatrix}; \mathbf{\Lambda} = \begin{bmatrix} \sqrt{\bar{\alpha}_g}\mathbf{\Lambda}_g \\ \sqrt{\bar{\alpha}_h}\mathbf{\Lambda}_h \end{bmatrix}, \tag{104}$$

where $\mathbf{A}_L^\pm$, $\mathbf{A}_g^\pm$, and $\mathbf{A}_h^\pm$ are the matrices associated with the differential operators $\mathbf{L}^\pm$, $\mathbf{B}_g^\pm$ and $\mathbf{B}_h^\pm$, respectively; $\mathbf{\Lambda}_g$ and $\mathbf{\Lambda}_h$ are associated with the Dirichlet and Neumann type interface conditions,

respectively. For balanced errors from different terms associated with domains, boundaries, and the interface, the following weights have been derived [165]:

$$\begin{aligned}
&\sqrt{\alpha_g^+} = \sqrt{\alpha_g^-} = \sqrt{\bar{\alpha}_g} = \mathrm{O}(\bar{k} \cdot \bar{N}_s), \\
&\sqrt{\alpha_h^+} = \mathrm{O}(s^+), \\
&\sqrt{\alpha_h^-} = \mathrm{O}(s^-), \\
&\sqrt{\bar{\alpha}_h} = \mathrm{O}(1),
\end{aligned} \tag{105}$$

where $k^{\pm} = \max(\lambda^{\pm}, \mu^{\pm})$, $\bar{k} = \max(k^+, k^-)$, $\bar{N}_s = \max(N_s^+, N_s^-)$, $s^{\pm} = \bar{k} / k^{\pm}$; $\lambda^{\pm}$ and $\mu^{\pm}$ are Lamé's constants in $\bar{\Omega}^{\pm}$, and $N_s^{\pm}$ is the number of source points in $\bar{\Omega}^{\pm}$.

The L-RBCM approach, combined with the subdomain collocation method, has been applied to problems with heterogeneities (weak discontinuities) [165] and cracks (strong discontinuities) [166].

5. Reproducing Kernel Particle Method for Large Deformation Problems

5.1 Lagrangian Reproducing Kernel Approximation and Discretization

The RK approximation is constructed based on a set of points without a mesh and hence releases the strong dependence of the approximation accuracy on mesh quality. It is therefore well-suited for applications to extreme deformation problems. To illustrate, let **X** be the material coordinates for a body initially occupying the domain $\Omega_{\mathbf{X}}$ with the boundary $\Gamma_{\mathbf{X}}$, and **x** be the position of the material point **X** in the deformed configuration $\Omega_{\mathbf{x}}$ with the boundary $\Gamma_{\mathbf{x}}$ at time *t*. The position vector **x** is given by a one-to-one mapping function, $\mathbf{x} = \varphi(\mathbf{X}, t)$, and hence the Jacobian of the deformation gradient, $\det(F_{ij})$, where $F_{ij} = dx_i / dX_j$, is positive definite for problems without material damage and fragmentation.

The variational equation of motion with reference to the current configuration is:

$$\int_{\Omega_x} \delta u_i \rho \ddot{u}_i d\Omega + \int_{\Omega_x} \delta u_{i,j} \sigma_{ij} d\Omega = \int_{\Omega_x} \delta u_i b_i d\Omega + \int_{\Gamma_x^h} \delta u_i h_i d\Gamma, \tag{106}$$

where u_i is the displacement, ρ is the density of the material, σ_{ij} is the Cauchy stress, b_i is the body force, and h_i is the prescribed traction on the natural boundary Γ_x^h. In the Lagrangian formulation, the Lagrangian RK shape functions $\Psi_I^{\mathbf{X}}(\mathbf{X})$ are constructed using the material coordinates in the reference configuration to yield:

$$\Psi_I^{\mathbf{X}}(\mathbf{x}) = \mathbf{H}^T(\mathbf{0})\mathbf{M}^{-1}(\mathbf{X})\mathbf{H}(\mathbf{X}-\mathbf{X}_I)\phi_a(\mathbf{X}-\mathbf{X}_I) \tag{107}$$

where

$$\mathbf{M}(\mathbf{X}) = \sum_{I\in G_{\mathbf{X}}} \mathbf{H}(\mathbf{X}-\mathbf{X}_I)\mathbf{H}^T(\mathbf{X}-\mathbf{X}_I)\phi_a(\mathbf{X}-\mathbf{X}_I). \tag{108}$$

The discrete reproducing conditions are imposed in the reference configuration:

$$\sum_{I\in G_{\mathbf{X}}} \Psi_I^{\mathbf{X}}(\mathbf{X})\mathbf{X}_I^{\alpha} = \mathbf{X}^{\alpha}, \quad |\alpha| \le n. \tag{109}$$

The Lagrangian RK function has a deformation dependent support size when mapped to the current configuration, as shown in Figure 18(a-b).

For path-dependent materials, the discretization of (106) by the Lagrangian RK approximation requires the spatial derivatives of $\Psi_I^{\mathbf{X}}(\mathbf{X})$ as follows:

$$\frac{\partial \Psi_I^{\mathbf{X}}(\mathbf{X})}{\partial x_i} = \frac{\partial \Psi_I^{\mathbf{X}}(\mathbf{X})}{\partial X_j} F_{ji}^{-1}. \tag{110}$$

The deformation gradient **F** is first computed by taking the material spatial derivatives of $\Psi_I^{\mathbf{X}}(\mathbf{X})$, and $\mathbf{F}^{-1}$ is obtained directly by the inversion of **F**. The Lagrangian formulation breaks down when the inverse of **F** is not well conditioned. This may occur, for example, when extreme deformation leads to a non-positive definite **F** or when material separation takes place in which **F** is singular. Thus, a semi-Lagrangian RK formulation is introduced in the following section to address this issue in modeling extreme deformation problems.

5.2 Semi-Lagrangian Reproducing Kernel Approximation and Discretization

In the semi-Lagrangian RK formulation, the nodal point $\mathbf{x}_I$ associated with the RK shape functions $\Psi_I(\mathbf{x})$ follows the motion of a material point, that is, $\mathbf{x}_I = \varphi(\mathbf{X}_I, t)$, whereas the support radius in the kernel function is defined independent of material deformation as shown in Figure 18(a) and Figure 18(c).

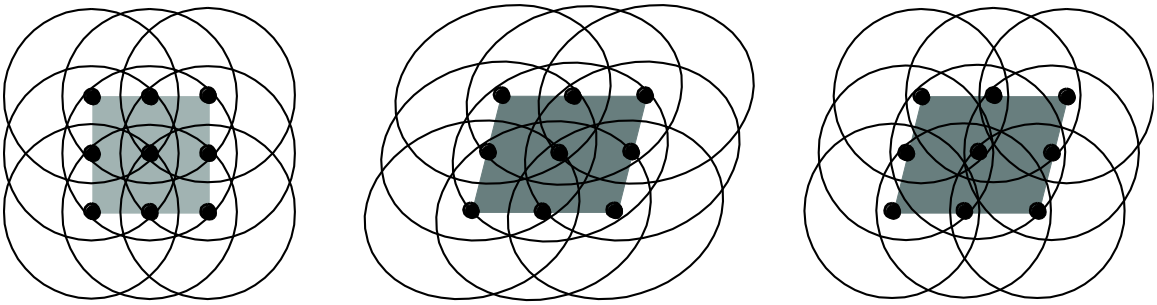

(a) (b) (c)

Figure 18. Comparison of Lagrangian and semi-Lagrangian RK kernels: (a) undeformed configuration, (b) Lagrangian RK in the deformed configuration, and (c) semi-Lagrangian RK in the deformed configuration.

The semi-Lagrangian RK shape function is then formulated in the current configuration as:

$$\Psi_I^{SL}(\mathbf{x}) = C(\mathbf{x};\mathbf{x}-\mathbf{x}_I)\phi_a(\mathbf{x}-\mathbf{x}_I) \tag{111}$$

where $\mathbf{x}_I = \varphi(\mathbf{X}_I, t)$.

It is noted that the correction function $C(\mathbf{x};\mathbf{x}-\mathbf{x}_I)$ for ensuring the reproducing condition is defined in the Lagrangian description while the kernel function in defining the locality and continuity is not purely Lagrangian. Similar to the discussion in Section 2, the coefficient vector $\mathbf{b}(\mathbf{x})$ can be determined by imposing the following discrete reproducing condition

$$\sum_{I\in G_{\mathbf{x}}} \Psi_I^{SL}(\mathbf{x})\mathbf{x}_I^{\alpha} = \mathbf{x}^{\alpha}, \quad |\alpha| \le n. \tag{112}$$

Substituting the coefficient vector $\mathbf{b}(\mathbf{x})$ into (111) yields the semi-Lagrangian reproducing kernel (semi-Lagrangian RK) shape function:

$$\Psi_I^{SL}(\mathbf{x}) = \mathbf{H}^T(\mathbf{0})\mathbf{M}^{-1}(\mathbf{x})\mathbf{H}(\mathbf{x}-\mathbf{x}_I)\phi_a(\mathbf{x}-\mathbf{x}_I), \tag{113}$$

where

$$\mathbf{M}(\mathbf{x}) = \sum_{I\in G_{\mathbf{x}}} \mathbf{H}(\mathbf{x}-\mathbf{x}_I)\mathbf{H}^T(\mathbf{x}-\mathbf{x}_I)\phi_a(\mathbf{x}-\mathbf{x}_I). \tag{114}$$

Note that the **x** coordinate in Ψ_I and $\mathbf{M}$ is also a function of time. Let the velocity v_i be the primary variable in (106) and be approximated by the semi-Lagrangian RK shape functions:

$$v_i^h(\mathbf{x},t) = \sum_{I \in G_{\mathbf{x}}} \Psi_I^{SL}(\mathbf{x}) v_{Ii}(t). \tag{115}$$

The corresponding semi-Lagrangian approximation of acceleration is given by

$$\ddot{u}_i^h(\mathbf{x},t) = \dot{v}_i^h(\mathbf{x},t) = \sum_{I \in G_{\mathbf{x}}} \left(\Psi_I^{SL}(\mathbf{x}) \dot{v}_{Ii}(t) + \breve{\Psi}_I^{SL}(\mathbf{x}) v_{Ii}(t) \right), \tag{116}$$

where $\breve{\Psi}_I^{SL}$ is the correction due to the time-dependent change of the semi-Lagrangian kernel $\dot{\phi}_a(\mathbf{x}-\mathbf{x}_I)$:

$$\breve{\Psi}_I^{SL}(\mathbf{x}) = C(\mathbf{x};\mathbf{x}-\mathbf{x}_I)\dot{\phi}_a(\mathbf{x}-\mathbf{x}_I) \tag{117}$$

where $\dot{(\,)}$ denotes the material time derivative and therefore,

$$\dot{\phi}_a(\mathbf{x}-\mathbf{x}_I) = \dot{\phi}_a\left(\frac{\|\mathbf{x}-\mathbf{x}_I\|}{a}\right) = \phi_a' \frac{\mathbf{q}\cdot(\mathbf{v}-\mathbf{v}_I)}{a} \tag{118}$$

where

$$\mathbf{q} = (\mathbf{x}-\mathbf{x}_I)/\|\mathbf{x}-\mathbf{x}_I\|, \tag{119}$$

and $\|\cdot\|$ designates the length of a vector. Note that the correction function C in (116) is used to ensure the reproducing condition of the time derivative of the semi-Lagrangian kernel $\dot{\phi}_a(\mathbf{x}-\mathbf{x}_I)$ and thus the time rate change of C is not considered.

Substituting (116) into (106) yields the following semi-discrete equation

$$\mathbf{M}\dot{\mathbf{v}} + \mathbf{N}\mathbf{v} = \mathbf{f}^{ext} - \mathbf{f}^{\text{int}}, \tag{120}$$

where

$$\mathbf{M}_{IJ} = \int_{\Omega_x} \rho \Psi_I^{SL}(\mathbf{x}) \Psi_J^{SL}(\mathbf{x}) \mathbf{I} d\Omega, \tag{121}$$

$$\mathbf{N}_{IJ} = \int_{\Omega_x} \rho \Psi_I^{SL}(\mathbf{x}) \breve{\Psi}_J^{SL}(\mathbf{x}) \mathbf{I} d\Omega, \tag{122}$$

$$\mathbf{f}_I^{ext} = \int_{\Omega_x} \Psi_I^{SL} \mathbf{b} d\Omega + \int_{\Gamma_x^h} \Psi_I^{SL} \mathbf{h} d\Gamma, \tag{123}$$

$$\mathbf{f}_I^{\text{int}} = \int_{\Omega_x} \mathbf{B}_I^T \boldsymbol{\Sigma} d\Omega. \tag{124}$$

Here, **I** denotes the identity matrix, $\mathbf{B}_I$ is the gradient matrix of $u_{(i,j)}$ associated with node *I*, $\boldsymbol{\Sigma}$ is the stress vector associated with σ_{ij}, and **b** and **h** are the body force and surface traction vectors, respectively. The temporal stability condition for the semi-Lagrangian RK formulation can be found in [215].

Remark 5.1:

> If a nodal integration scheme, such as direct nodal integration, stabilized conforming nodal integration, and stabilized non-conforming nodal integration, is employed, the diagonal terms of **N** vanish and the off-diagonal terms of **N** have relatively negligible influence over (120). Therefore, the convective effect, **Nv** in (120), can be omitted in the semi-discrete equations of motion for the sake of computational efficiency.

5.3 Kernel Contact Algorithms

In extreme deformation problems with material separation, contact surfaces are unknown and are part of the solution. As a consequence, the conventional contact algorithms, in which all possible contact surfaces are defined *a priori*, are ineffective in modeling such problems. On the other hand, kernel contact (KC) algorithms [104,216] approximate the contact condition without relying on the pre-defined contact surfaces at the pre-processing stage. The overlap between the semi-Lagrangian RK shape functions induces internal forces between particles, ensuring the impenetrability between different bodies, as shown in Figure 19, which leads to the so-called natural kernel contact algorithm. A layer of a friction-like elasto-plastic material, as shown in Figure 20, can be introduced in the "contact processing zone" to mimic the friction law, which leads to the contact algorithms in Sections 5.4 and 5.5.

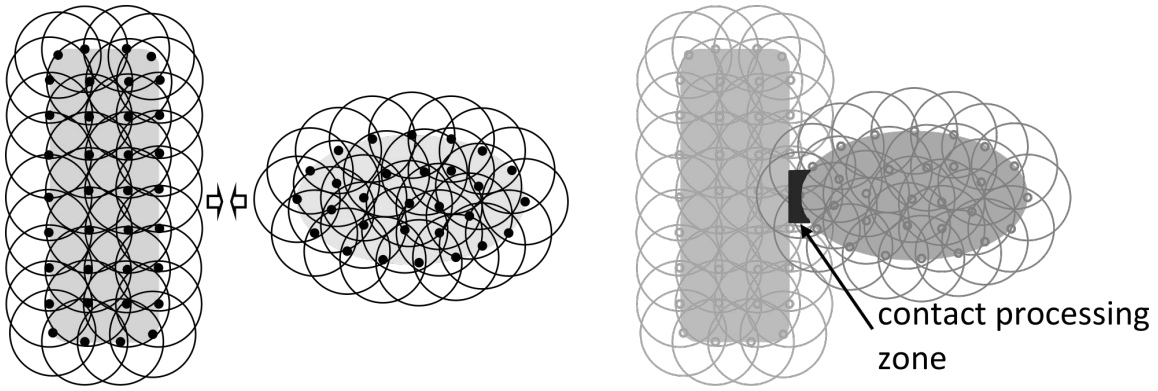

Figure 19. Natural kernel contact algorithm by kernel interaction between contacting bodies.

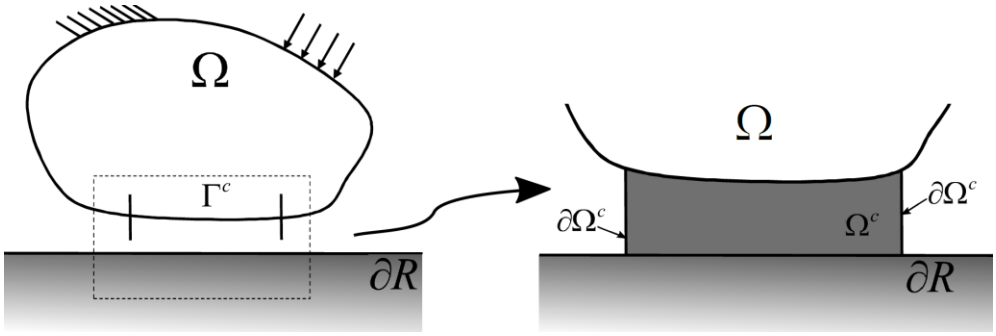

Figure 20. Schematic of a deformable body contacting with a rigid surface, and an artificial material introduced between two bodies in contact, for enforcing the contact constraints.

5.4 A Friction-Like Plasticity Model

In kernel contact, a friction-like material can be introduced between contacting bodies, Ω_c as shown in Figure 20, to mimic the frictional contact conditions. Based on the analogy between Coulomb's friction law and the elasto-plasticity flow rule, the variational contact equation leads to the constitutive equation governing the stress-strain relationship of the friction-like material such that Coulomb's friction is recovered [104,216]:

$$\boldsymbol{\sigma}_c \cdot \mathbf{n} = t_N \mathbf{n} + \mathbf{t}_T \,, \tag{125}$$

where $\boldsymbol{\sigma}_c$ is the Cauchy stress in Ω^c, $\mathbf{n}$ is the unit outward normal of the contact surface Γ^c, t_N is the normal component of the contact traction, and $\mathbf{t}_T$ is the tangential contact traction. Equation (125) indicates that the stresses in the friction-like material are in balance with t_N and $\mathbf{t}_T$ on Γ^c. Therefore, an elasto-perfectly-plastic material, in which the stress $\boldsymbol{\sigma}_c$ in Ω^c obeys (125), can be

introduced in the contact processing zone to mimic the Coulomb's friction law. To obtain $\boldsymbol{\sigma}_c$, consider the following yield function and the associated Karush-Kuhn-Tucker conditions based on local coordinates where the one-direction is aligned with the contact surface normal **n**:

$$f(\boldsymbol{\tau}) = \|\boldsymbol{\tau}\| + \mu\hat{\sigma}_{11} \le 0, \tag{126}$$

$$\dot{\mathbf{e}} = \gamma \frac{\partial f}{\partial \boldsymbol{\tau}}, \tag{127}$$

$$\gamma \ge 0, \tag{128}$$

$$\gamma f = 0, \tag{129}$$

where $\boldsymbol{\tau} = \begin{bmatrix} \hat{\sigma}_{12} & \hat{\sigma}_{13} \end{bmatrix}$, $\hat{\sigma}_{11} \le 0$ is the normal contact stress, $\dot{\mathbf{e}}$ is the tangential strain rate, $\hat{\boldsymbol{\sigma}} = \mathbf{L}\boldsymbol{\sigma}\mathbf{L}^T$ is the rotated Cauchy stress tensor onto the local coordinate system, the 2- and 3- directions are aligned with two mutually orthogonal unit vectors, **p** and **q** in the tangent plane, and $\mathbf{L} = [\mathbf{n}, \mathbf{p}, \mathbf{q}]^{\mathrm{T}}$. It is also assumed that the normal contact stress $\hat{\sigma}_{11}$ is known in (126). The yield stress $\mu|\hat{\sigma}_{11}|$ mimics the friction stress induced by the normal stress $\hat{\sigma}_{11}$, and the slip condition is represented by the yield condition in the plasticity model:

$$\begin{array}{l} f < 0, \ \text{stick condition (elastic)} \\ f = 0, \ \|\boldsymbol{\tau}\| = -\mu\hat{\sigma}_{11} \ \text{slip condition (plastic)} \end{array}. \tag{130}$$

This approach can be carried out by a predictor-corrector algorithm, in which the stresses calculated based on the overlapping supports of the contacting bodies are obtained in the predictor step, and in the corrector step, the tangential stresses are corrected according to Eqns. (126)-(129) with $\hat{\sigma}_{11}$ fixed. To enhance the iteration convergence of the two-step approach, we introduce the radial return algorithm where the trial is non-slip (elastic trial) and the violation of the yield function (interpenetration) is corrected by the return mapping algorithm. Following the radial return mapping, the corrected contact stresses $\hat{\boldsymbol{\sigma}}_c$ in the local coordinate induced by the friction-like elasto-plasticity model can be obtained as:

$$\hat{\boldsymbol{\sigma}}_c = \hat{\boldsymbol{\sigma}}^{trial} + \lambda \begin{bmatrix} 0 & \hat{\sigma}_{12}^{trial} & \hat{\sigma}_{13}^{trial} \\ \hat{\sigma}_{12}^{trial} & 0 & 0 \\ \hat{\sigma}_{13}^{trial} & 0 & 0 \end{bmatrix} \equiv \hat{\boldsymbol{\sigma}}^{trial} + \lambda\hat{\boldsymbol{\xi}}, \tag{131}$$

where $\hat{\boldsymbol{\sigma}}^{trial}$ is the Cauchy stress in the local coordinate system calculated by standard stress calculation through particle interaction without considering the artificial friction-like elasto-plasticity material and $\lambda = 0$ if $f(\boldsymbol{\tau}^{trial}) < 0$ and

$$\lambda = \frac{\mu\left|\hat{\sigma}_{11}^{trial}\right| - \left\|\boldsymbol{\tau}^{trial}\right\|}{\left\|\boldsymbol{\tau}^{trial}\right\|} \text{ if } f\left(\boldsymbol{\tau}^{trial}\right) \geq 0. \tag{132}$$

Finally, the corrected contact stress in the global coordinates is then obtained by the inverse transformation:

$$\boldsymbol{\sigma}_c = \mathbf{L}^{\mathrm{T}}\hat{\boldsymbol{\sigma}}_c\mathbf{L} \equiv \boldsymbol{\sigma}^{trial} + \lambda\boldsymbol{\xi}, \tag{133}$$

where

$$\boldsymbol{\xi} = \left(\mathbf{n}\otimes\boldsymbol{\sigma}^{trial}\cdot\mathbf{n} + \mathbf{n}\cdot\boldsymbol{\sigma}^{trial}\otimes\mathbf{n}\right) - 2t_N\mathbf{n}\otimes\mathbf{n}. \tag{134}$$

Here, the orthogonality of $\mathbf{L}$ is applied to derive the above relationship. Equation (133) can then be directly used in the calculation of the contact forces described in the next section.

5.5 Semi-Lagrangian RK Discretization and Kernel Contact Algorithms

This section describes the semi-Lagrangian-RK discretization and the contact force calculation in the KC algorithms. Consider continuum bodies Ω^A and Ω^B discretized by groups of points $G^A = \{\mathbf{x}_I \,|\, \mathbf{x}_I \in \Omega^A\}$ and $G^B = \{\mathbf{x}_I \,|\, \mathbf{x}_I \in \Omega^B\}$, respectively , with each point at $\mathbf{x}_I$ associated with a nodal volume V_I and a kernel function $\phi_a(\mathbf{x}-\mathbf{x}_I)$ with the support of radius *a* independent of material deformation. When the two bodies Ω^A and Ω^B approach each other and the semi-Lagrangian-RK shape functions form a partition of unity, the interaction between the RK points from the different bodies (Figure 19) induces stresses:

$$\boldsymbol{\sigma}(\mathbf{x}) = \sum_{I\in N^A\cup N^B} \mathbf{D}(\mathbf{x})\mathbf{B}_I(\mathbf{x})\mathbf{d}_I, \tag{135}$$

where $N^A = \{I \,|\, \mathbf{x}_I \in G^A\}$, $N^B = \{I \,|\, \mathbf{x}_I \in G^B\}$, and $\mathbf{D}$ is the material response tensor of the contacting bodies. The contact stresses between contacting bodies are obtained by (135) when $\mathbf{n}\cdot\boldsymbol{\sigma}\cdot\mathbf{n} \leq 0$ in Ω_c. With the nodal integration scheme described in Section 2.4, the internal force acting on a point *I* can then be obtained by:

$$\mathbf{f}_I = \sum_{J\in N_I^C} \mathbf{B}_I^{\mathrm{T}}(\mathbf{x}_J)\boldsymbol{\sigma}(\mathbf{x}_J)V_J, \tag{136}$$

where $N_I^C = \{J \,|\, J \in N^A\cup N^B, \phi_{a_I}(\mathbf{x}_J-\mathbf{x}_I) \neq 0, \mathbf{r}_{IJ}\cdot\boldsymbol{\sigma}(\mathbf{x}_J)\cdot\mathbf{r}_{IJ} < 0, \mathbf{r}_{IJ} = (\mathbf{x}_J-\mathbf{x}_I)/\|\mathbf{x}_J-\mathbf{x}_I\|\}$ is the set that contains the neighbor points under the support of point *I*, while the contact stress between those points and point *I* is in compression. In this approach, the pair-wise interactions due to overlapping kernel functions naturally prevent the interpenetration between different bodies. To model

the frictional contact condition, an artificial layer of material with the friction-like dissipating mechanism in the form of plasticity as presented in 5.4 is introduced. With the consideration of the frictional contact effect, the summation of the interactive forces associated with point *I* is corrected as

$$\mathbf{f}_I = \sum_{J \in N_I^C} \mathbf{B}_I^{\mathrm{T}}(\mathbf{x}_J)\boldsymbol{\sigma}_c(\mathbf{x}_J)V_J = \sum_{J \in N_I^C} (\mathbf{f}_{IJ} + \mathbf{g}_{IJ}), \tag{137}$$

where $\mathbf{f}_{IJ} = \mathbf{B}_I^{\mathrm{T}}(\mathbf{x}_J)\boldsymbol{\sigma}^{trial}(\mathbf{x}_J)V_J$, and $\mathbf{g}_{IJ} = \mathbf{B}_I^{\mathrm{T}}(\mathbf{x}_J)\lambda\boldsymbol{\xi}(\mathbf{x}_J)V_J$.

One remaining issue to implement the KC algorithm in the semi-Lagrangian formulation is to determine the contact surface and surface normal from a purely point-based discretization. A level set based method, where the level set function was chosen as the interpolant of material ID using semi-Lagrangian RK, was proposed to obtain the contact surface and surface normal under the KC contact framework (refer to [104] for details).

Example 5.1

The Taylor bar impact problem [249] was first performed by Wilkins and Guinan in [250], and subsequently by others. An aluminum bar with initial height and radius of 2.346 cm and 0.391 cm, respectively, impacts a rigid wall with an initial velocity of 373.0 m/s. For the aluminum material, J_2 plasticity with isotropic hardening is considered with material properties Young's modulus $E =$ 78.2 GPa, Poisson's ratio $\nu =$ 0.30, and density $\rho =$ 2700 kg/m^3, and the yield stress is taken as

$$K(\bar{e}_p) = \sigma_Y(1+125\bar{e}_p)^{0.1}, \tag{138}$$

where $\sigma_Y =$ 0.29 GPa.

The semi-Lagrangian formulation is considered with linear basis and quartic B-spline kernel functions with a normalized support of 2.8, and 29,637 nodes discretize the bar. The wall is also modeled and is considered frictionless, and the KC algorithms are employed for the bar-wall interaction. The four integration methods direct nodal integration (DNI), stabilized non-conforming nodal integration (SNNI), variationally consistent naturally stabilized nodal integration (VC-NSNI), and variationally consistent modified SNNI (VC-MSNNI) discussed in Section 3 are considered for comparison of the nodal integrations.

The deformed shape of the face of the bar is shown in Figure 23, with material deformation plotted for visualization purposes, in order to observe any spurious oscillations in the solution, if present. The difference in solutions is apparent; DNI and SNNI both clearly show spurious oscillatory modes in the solution as discussed in Section 3, while the stabilized methods do not.

The deformed height and radius of the bar are shown in Table 3, where it can be seen that DNI and SNNI predict a larger radius compared to the reference solutions, likely due to the very little resistance to the oscillatory mode of deformation. Another explanation is the numerical fractures in DNI and SNNI formed due to these spurious modes, as seen in Figure 22, while VC-NSNI and VC-MSNNI give stable solutions. For the deformed height of the bar, all methods give reasonable heights compared to the reference solutions except for DNI, and VC-NSNI and VC-MSNNI give the closet results to the experimental data and other methods compared.

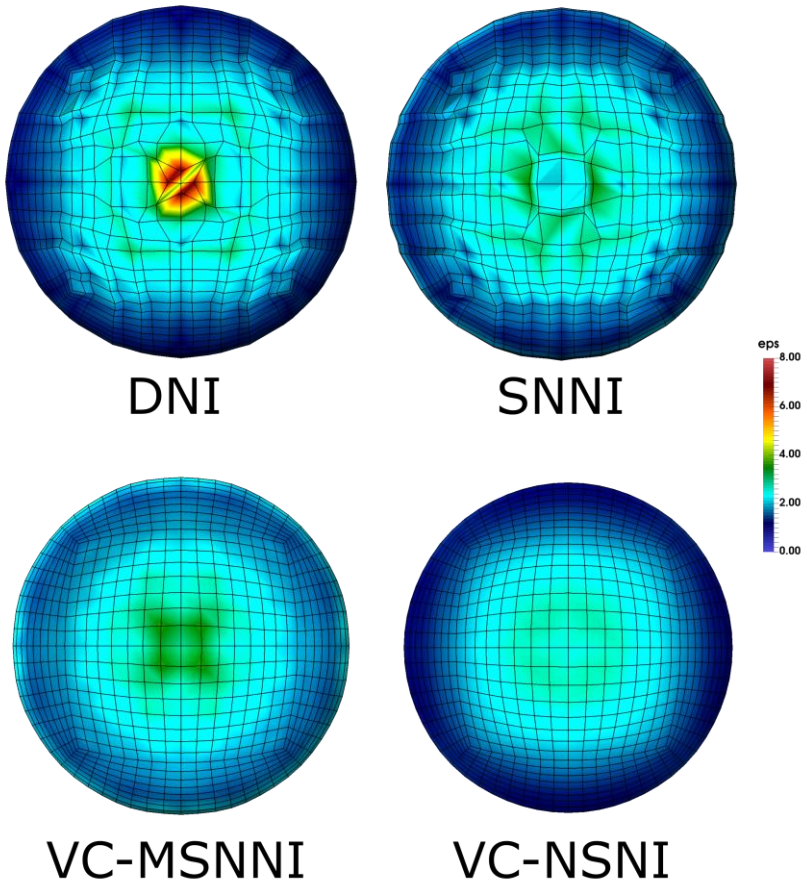

Figure 21. Final deformation on the face of the Taylor bar for various nodal integration methods.

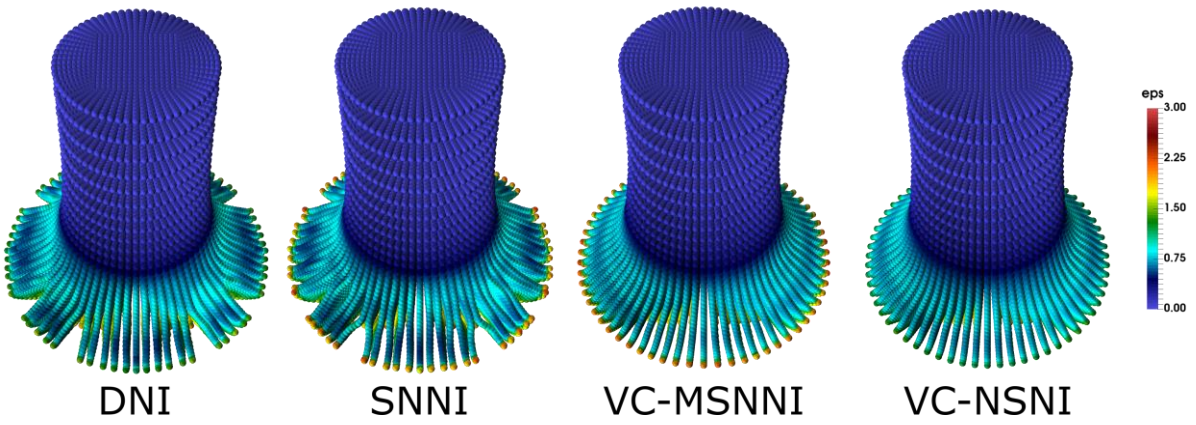

Figure 22. Final deformation of the Taylor bar for various nodal integration methods.

	Radius (cm)	Height (cm)
SNNI	0.839	1.649
DNI	0.838	1.660
VC-MSNNI	0.801	1.649
VC-NSNI	0.775	1.651
RKPM (Gauss integration) [24]	0.827	1.645
Material point method [18]	0.78	1.65
Finite element method [249]	0.742	1.652
Experimental [250]	-	1.651

Table 3. Deformed height and radius for various methods and the experiment [239].

6. Applications of Meshfree Methods

Large Deformation Meshfree methods are particularly well-suited for large deformation problems where finite element methods fail due to mesh entanglement and other mesh related issues. The Lagrangian meshfree method (106)-(110) has been applied to many different solid mechanics problems and applications, such as large deformation of hyperelastic materials and rubber [83,94,96,97], metal forming [95,98–100,102,205,255], and geomechanics problems [256], among others, showing robustness over FEM. For the presence of material separation where the Lagrangian description breaks down, the semi-Lagrangian formulation (111)-(137) was proposed [215,216,257]. Figure 23 shows the application of semi-Lagrangian RKPM to the simulation of perforation of a concrete panel by a bullet [258], and Figure 24 demonstrates a semi-Lagrangian RKPM simulation of a landslide due to the Loma Prieta earthquake. Several other researchers have developed and employed various meshfree methods discussed in Section 1 to reassociate connectivity for penetration

and fragment-impact problems [58,70,71,135,136,259–266]. On a different path, discrete bonded particle methods have been developed and coupled with FEM for similar applications [267–272] (for a review, see [273]). Recently, meshfree methods have gained traction in solving geomechanics problems with extremely large deformations such as slope stability with post-failure analysis [257,274–279]. Some recent advances in meshfree formulations for nonlinear mechanics can be found in [104,239,242,243,258,280,281].

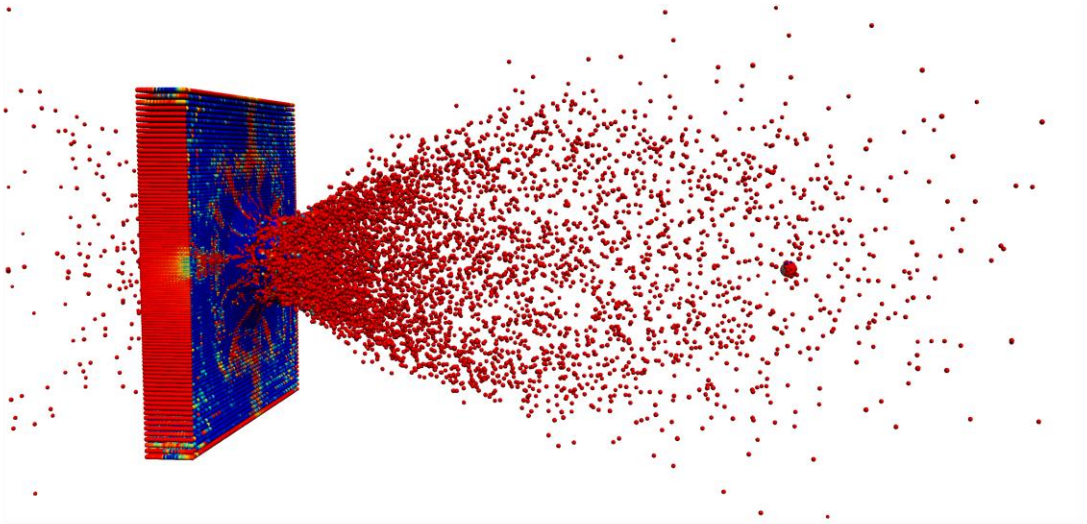

(a)

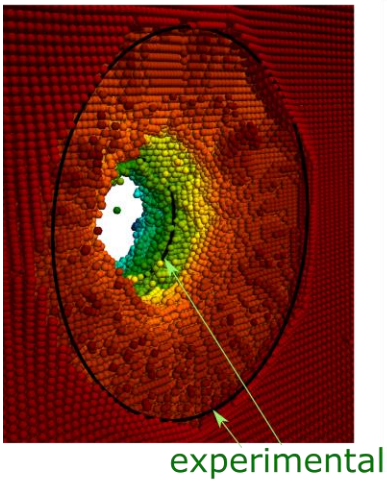

(b)

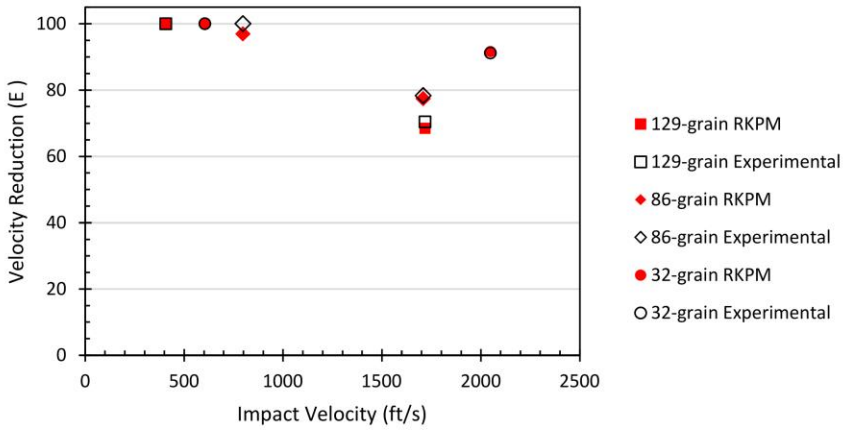

(c)

Figure 23. Semi-Lagrangian simulation of a bullet perforating a concrete panel: (a) deformed shape after impact, (b) experimental (solid blue line) and numerical crater shape, and (c) velocity reduction for different sizes of projectiles, experimental (white, no fill) versus numerical (red, solid).

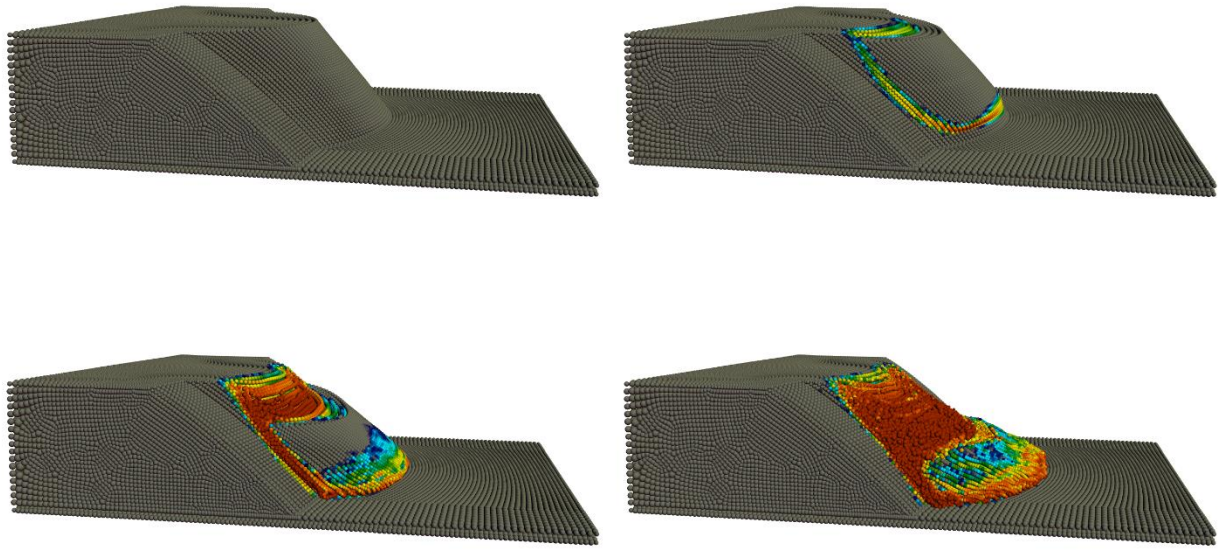

Figure 24. Simulation of a landslide triggered by the 1989 Loma Prieta earthquake using semi-Lagrangian RKPM.

Adaptive Refinement The naturally conforming properties of meshfree approximations, such as the MLS, RK, and PU approximations, allow adaptivity to be performed in a much more effective manner than the conventional finite element method [33,34,88,90,106–108,251]. Nodes can be inserted or removed with ease, and error indicators have been formulated to guide adaptive refinement. For example, the multiresolution RK-based method [84,88–90] enables the scale decomposition of the RKPM solution by using the RK function as a low-pass filter, and the high-scale solution has been used as the error indicator for adaptive refinement [23,84,252–254]. While *p*-adaptivity is not so straightforward in RK- and MLS-based methods, *hp* clouds allows the bases to vary throughout the domain such that higher order accuracy can be obtained where needed [33].

Strain Localization Researchers have employed the flexibility of meshfree methods for regularization in localization problems in [191,244,282] to circumvent ambiguous boundary conditions in gradient methods. Methods have also been developed and applied successfully to localization problems difficult for FEM [254,283–286]. More recently, the cracking particle method [287] has been developed for shear bands [108].

Fracture Mechanics Fracture mechanics is another area where meshfree methods offer a unique strength. Early on, it was recognized that meshfree formulations such as EFG could offer an effective alternative to FEM in modeling fracture by using the so-called visibility criterion (cutting the particle influence across a crack), and further provide easy adaptive refinement to attain accuracy near crack tips [13,81,82,288]. Alternatively, enrichment of the approximation functions for crack tip singularities can be considered intrinsically [289,290] or extrinsically [31,289,291]. The former approach involves some complications since MLS and RK functions in these methods cannot vary

spatially. Approaches with extrinsic enrichments have been developed for meshfree methods [15,16,292,293], including techniques for accurate closure of crack fronts in meshfree methods, with the result method termed XEFG. Tracking the geometry of evolving cracks necessary for enrichment is a difficult task, particularly in three dimensions. To circumvent this issue, a cracking particle method has been proposed, where fracture is represented by a series of discontinuities located at the particles, with arbitrary orientation [259,287,293,294]. The introduction of these discontinuities can be performed by detection of material instability. Alternatively, level-set methods for tracking of complicated crack geometry have been proposed [291,295,296].

Smooth Contact By employing the arbitrary smoothness in meshfree approximation functions, a smooth contact algorithm has been proposed where the contact surface is represented by smooth (C^2 or higher) RK approximations, which allows continuum-based contact formulations [100–102]. This in turn allows improved convergence in contact iterations versus finite element-based contact with C^0 continuity, and enables robust analysis in applications such as metal forming, as shown in Figure 25, where Lagrangian RKPM is used to model a metal extrusion processes with adaptive refinement, where points were inserted in the highly deformed region and were removed in the region undergoing elastic unloading.

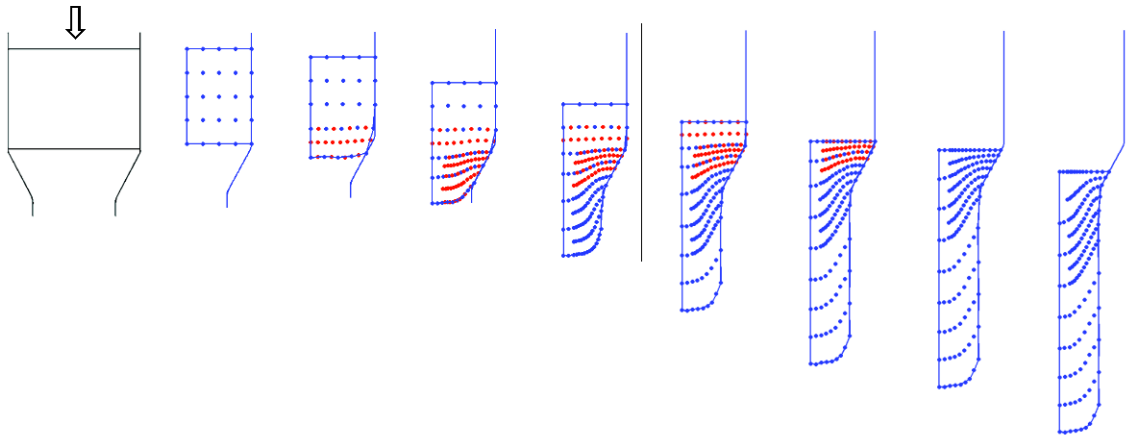

Figure 25. Metal extrusion: problem set-up, meshfree discretization, and progressive deformation.

Other Applications Meshfree methods have been developed for several other applications where they have advantages over traditional approaches. In modeling *biomaterials*, meshfree methods are well suited for *image-based modeling* by using pixels as discretization nodes without the tedious procedures in three-dimensional geometry reconstruction from the images and mesh generation. Meshfree methods can also represent the smooth transition of material properties across material interfaces in biomaterials [297,298]. Figure 26 shows how a skeletal muscle is modeled by the meshfree method, where image pixel points were used directly as the discretization points, and the associated stress distribution is computed using material properties and fiber orientations defined at the pixel points.

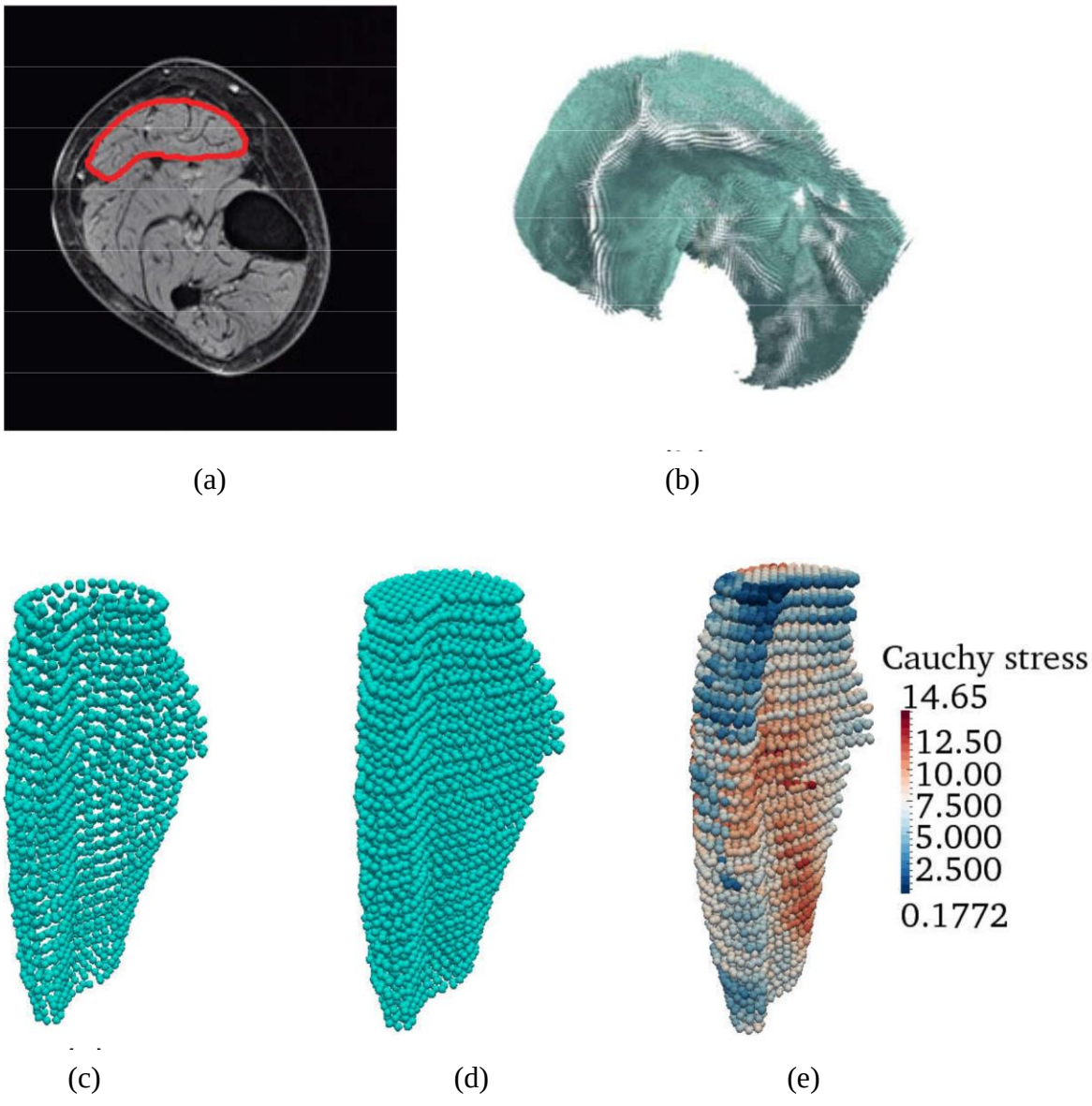

Figure 26. Image based RKCM modeling of skeletal muscle (a) MRI image; (b) DTI vector plot; (c) RK source points; (d) RK collocation points; (e) maximum principal Cauchy stress resulting from muscle contraction.

Another good application of meshfree methods is for problems that involve higher order differentiation in the PDE, such as thin *plate and shell problems* [219,220,299–303] where meshfree approximation functions with higher order continuity can be employed with virtually no additional effort. The application of the meshfree method to *quantum mechanics* has been proposed by utilizing the orbital functions as the enrichment of polynomial bases for *p*-like adaptive refinement [217].

For *shape optimization*, meshfree methods can avoid mesh distortion in the iterative process [304–306]. Meshfree methods for *fluid mechanics* [23,93,199,252,307–310] have been proposed using multi-resolution analysis in conjunction with adaptive refinement [23,252,307]. The smooth meshfree approximation functions are well suited for Petrov-Galerkin stabilization [308], and meshfree methods are more effective in handling moving domains and obstacles [309,310].

7. Conclusions and outlook

Meshfree methods offer an alternative to traditional mesh-based methods, where the conforming condition is relaxed to simply PU subordinate to open cover. Meshfree approximations can offer arbitrarily smooth or rough approximations at no cost. In meshfree approximations such as MLS and RK, the order of completeness and order of continuity in the approximations are entirely uncoupled in contrast to many other numerical methods. Because of these two properties, *h*- and *p*-refinement is simplified considerably. In addition, the strong tie between the quality of the discretization and the quality of the numerical solution to PDEs is reduced, which makes these methods well-suited for large deformation problems without cumbersome procedures such as remeshing, moving meshes, and erosion. The burden of producing an analysis suitable discretization via meshing is also greatly relieved. These features have made the application of meshfree methods widespread in the past two decades.

For the practical application of meshfree methods, efforts have been devoted to ensure solution accuracy, stability, and efficiency. To date, essential boundary condition enforcement is almost trivial in meshfree methods. The formidable computational cost of high-order quadrature has been greatly alleviated (or eliminated) through novel techniques such as SCNI and VCI, which have since been verified, showing robustness in many applications. Significant advances have also been made in spatial stability, where several accurate and efficient stabilized nodal integration methods have been developed. With the progress in nodal integration, “truly” meshless methods are now available, and they are particularly effective for problems with extreme loadings, such as fragment-impact processes.

Several issues remain, some of which are common to both mesh-based and mesh-free methods. A prime example is the simulation of high-density, three-dimensional cracking, which remains challenging, even for meshfree methods. To the authors’ knowledge, the potential to alleviate time-consuming model generation in the meshfree method has not been fully realized. The ability to collocate partial differential equations directly (strong form collocation) offers a promising avenue for meshfree methods, however, the effort devoted to advancing strong form collocation method has not been on par with the development of Galerkin meshfree methods, especially in the area of strong form collocation for large deformation, fracture mechanics, and contact-impact problems. These challenges call for future research in meshfree methods.

References

[1] O.C. Zienkiewicz, R.L. Taylor, The finite element method, McGraw-hill London, 1977.

[2] G.-R. Liu, K.Y. Dai, T.T. Nguyen, A smoothed finite element method for mechanics problems, Comput. Mech. 39 (2007) 859–877. doi:10.1007/s00466-006-0075-4.

[3] L.B. Lucy, A numerical approach to the testing of the fission hypothesis, Astron. J. 82 (1977) 1013–1024.

[4] R.A. Gingold, J.J. Monaghan, Smoothed particle hydrodynamics: theory and application to non-spherical stars, Mon. Not. R. Astron. Soc. 181 (1977) 375–389.

[5] T.J. Liszka, J. Orkisz, The finite difference method at arbitrary irregular grids and its application in applied mechanics, Comput. Struct. 11 (1980) 83–95. doi:10.1016/0045-7949(80)90149-2.

[6] T.J. Liszka, An interpolation method for an irregular net of nodes, Int. J. Numer. Methods Eng. 20 (1984) 1599–1612.

[7] E.J. Kansa, Multiquadrics—a scattered data approximation scheme with applications to computational fluid-dynamics—I surface approximations and partial derivative estimates, Comput. Math. with Appl. 19 (1990) 127–145.

[8] E.J. Kansa, Multiquadrics—A scattered data approximation scheme with applications to computational fluid-dynamics—II solutions to parabolic, hyperbolic and elliptic partial differential equations, Comput. Math. with Appl. 19 (1990) 147–161.

[9] A.S.M. Wong, Y.C. Hon, T.S. Li, S.L. Chung, E.J. Kansa, Multizone decomposition for simulation of time-dependent problems using the multiquadric scheme, Comput. Math. with Appl. 37 (1999) 23–43. doi:10.1016/S0898-1221(99)00098-X.

[10] H.-Y. Hu, J.-S. Chen, W. Hu, Weighted radial basis collocation method for boundary value problems, Int. J. Numer. Methods Eng. 69 (2007) 2736–2757.

[11] B. Nayroles, G. Touzot, P. Villon, Generalizing the finite element method: Diffuse approximation and diffuse elements, Comput. Mech. 10 (1992) 307–318. doi:10.1007/BF00364252.

[12] T. Belytschko, Y.Y. Lu, L. Gu, Element-free Galerkin methods, Int. J. Numer. Methods Eng. 37 (1994) 229–256. doi:10.1002/nme.1620370205.

[13] T. Belytschko, Y.Y. Lu, L. Gu, Crack propagation by element-free Galerkin methods, Eng. Fract. Mech. 51 (1995) 295–315.

[14] Y.Y. Lu, T. Belytschko, L. Gu, A new implementation of the element free Galerkin method, Comput. Methods Appl. Mech. Eng. 113 (1994) 397–414. doi:10.1016/0045-7825(94)90056-6.

[15] T. Rabczuk, P.M.A. Areias, A meshfree thin shell for arbitrary evolving cracks based on an extrinsic basis, C. - Comput. Model. Eng. Sci. 16 (2006) 115–130.

[16] T. Rabczuk, S.P.A. Bordas, G. Zi, A three-dimensional meshfree method for continuous multiple-crack initiation, propagation and junction in statics and dynamics, Comput. Mech. 40 (2007) 473–495. doi:10.1007/s00466-006-0122-1.

[17] D.L. Sulsky, Z. Chen, H.L. Schreyer, a Particle Method for History-Dependent Materials, Comput. Methods Appl. Mech. Eng. 118 (1994) 179–196. doi:10.1016/0045-7825(94)00033-6.

[18] D.L. Sulsky, S.J. Zhou, H.L. Schreyer, Application of a particle-in-cell method to solid mechanics, Comput. Phys. Commun. 87 (1995) 236–252. doi:10.1016/0010-4655(94)00170-7.

[19] S.G. Bardenhagen, E.M. Kober, The generalized interpolation material point method, 5 (2004) 477–495. doi:10.3970/cmes.2004.005.477.

[20] A. Sadeghirad, R.M. Brannon, J. Burghardt, A convected particle domain interpolation technique to extend applicability of the material point method for problems involving massive deformations, Int. J. Numer. Methods Eng. 86 (2011) 1435–1456.

[21] S.R. Idelsohn, N. Nigro, A. Limache, E. Oñate, Large time-step explicit integration method for solving problems with dominant convection, Comput. Methods Appl. Mech. Eng. 217-220 (2012) 168–185.

doi:10.1016/j.cma.2011.12.008.

[22] S.R. Idelsohn, J. Marti, P. Becker, E. Oñate, Analysis of multifluid flows with large time steps using the particle finite element method, Int. J. Numer. Methods Fluids. 75 (2014) 621–644. doi:10.1002/fld.3908.

[23] W.K. Liu, S. Jun, Y.F. Zhang, Reproducing kernel particle methods, Int. J. Numer. Methods Fluids. 20 (1995) 1081–1106. doi:10.1002/fld.1650200824.

[24] J.-S. Chen, C. Pan, C.-T. Wu, W.K. Liu, Reproducing Kernel Particle Methods for large deformation analysis of non-linear structures, Comput. Methods Appl. Mech. Eng. 139 (1996) 195–227. doi:10.1016/S0045-7825(96)01083-3.

[25] J. Chen, L. Angeles, Y. Wu, Stability in Lagrangian and Semi-Lagrangian Reproducing Kernel Discretizations Using Nodal Integration in Nonlinear Solid Mechanics, Appl. Sci. (2006) 1–24.

[26] J.M. Melenk, On Generalized Finite Element Methods, Ph.D. Dissertation, University of Maryland, 1995.

[27] T. Strouboulis, K. Copps, I. Babuška, The generalized finite element method, Comput. Methods Appl. Mech. Eng. 190 (2001) 4081–4193.

[28] T. Belytschko, T. Black, Elastic crack growth in finite elements with minimal remeshing, Int. J. Numer. Methods Eng. 45 (1999) 601–620. doi:10.1002/(sici)1097-0207(19990620)45:5<601::aid-nme598>3.0.co;2-s.

[29] N. Moës, J. Dolbow, T. Belytschko, A finite element method for crack growth without remeshing, Int. J. Numer. Meth. Engng. 46 (1999) 131–150. doi:10.1002/(SICI)1097-0207(19990910)46:1<131::AID-NME726>3.0.CO;2-J.

[30] S. Koshizuka, Y. Oka, Moving-particle semi-implicit method for fragmentation of incompressible fluid, Nucl. Sci. Eng. 123 (1996) 421–434.

[31] J.M. Melenk, I. Babuška, The partition of unity finite element method: Basic theory and applications, Comput. Methods Appl. Mech. Eng. 139 (1996) 289–314. doi:10.1016/S0045-7825(96)01087-0.

[32] I. Babuška, J.M. Melenk, The partition of unity method, Int. J. Numer. Methods Eng. 40 (1997) 727–758. doi:10.1002/(SICI)1097-0207(19970228)40:4<727::AID-NME86>3.0.CO;2-N.

[33] C.A.M. Duarte, J.T. Oden, An h-p adaptive method using clouds, Comput. Methods Appl. Mech. Eng. 139 (1996) 237–262. doi:10.1016/S0045-7825(96)01085-7.

[34] C.A.M. Duarte, J.T. Oden, H-p clouds-an h-p meshless method, Numer. Methods Partial Differ. Equ. 12 (1996) 673–705. doi:10.1002/(sici)1098-2426(199611)12:6<673::aid-num3>3.0.co;2-p.

[35] E. Oñate, S.R. Idelsohn, O.C. Zienkiewicz, R.L. Taylor, A finite point method in computational mechanics. Applications to convective transport and fluid flow, Int. J. Numer. Methods Eng. 39 (1996) 3839–3866. doi:10.1002/(SICI)1097-0207(19961130)39:22<3839::AID-NME27>3.0.CO;2-R.

[36] G. Yagawa, T. Yamada, Free mesh method: A new meshless finite element method, Comput. Mech. V18 (1996) 383–386. doi:10.1007/BF00376134.

[37] G.A. Dilts, Moving-Least-Squares Hydrodynamics - I. Consistency and Stability, Int. J. Numer. Methods Eng. 44 (1998) 1115–1155. doi:10.1002/(SICI)1097-0207(19990320)44:8<1115::AID-NME547>3.0.CO;2-L.

[38] S.N. Atluri, T.L. Zhu, A new Meshless Local Petrov-Galerkin (MLPG) approach in computational mechanics, Comput. Mech. 22 (1998) 117–127. doi:10.1007/s004660050346.

[39] N. Sukumar, T. Belytschko, The natural element method in solid mechanics, Int. J. Numer. Methods Eng. 43 (1998) 839–887. doi:10.1002/(SICI)1097-0207(19981115)43:5<839::AID-NME423>3.0.CO;2-R.

[40] J. Braun, M. Sambridge, others, A numerical method for solving partial differential equations on highly irregular evolving grids, Nature. 376 (1995) 655–660.

[41] M. Griebel, M.A. Schweitzer, A particle-partition of unity method for the solution of elliptic, parabolic, and hyperbolic PDEs, SIAM J. Sci. Comput. 22 (2000) 853–890.

[42] S. De, K.J. Bathe, The method of finite spheres, Comput. Mech. 25 (2000) 329–345. doi:10.1007/s004660050481.

[43] N.R. Aluru, A point collocation method based on reproducing kernel approximations, Int. J. Numer. Methods Eng. 47 (2000) 1083–1121. doi:10.1002/(SICI)1097-0207(20000228)47:6<1083::AID-NME816>3.0.CO;2-N.

[44] H.-Y. Hu, J.-S. Chen, W. Hu, Error analysis of collocation method based on reproducing kernel approximation, Numer. Methods Partial Differ. Equ. 27 (2011) 554–580.

[45] S.-W. Chi, J.-S. Chen, H.-Y. Hu, J.P. Yang, A gradient reproducing kernel collocation method for boundary value problems, Int. J. Numer. Methods Eng. 93 (2013) 1381–1402.

[46] J.-S. Chen, C.-T. Wu, S. Yoon, A stabilized conforming nodal integration for Galerkin mesh-free methods, Int. J. Numer. Meth. Eng. 0207 (2001) 435–466. doi:10.1002/1097-0207(20010120)50.

[47] J.-S. Chen, S. Yoon, C.-T. Wu, Non-linear version of stabilized conforming nodal integration for Galerkin mesh-free methods, Int. J. Numer. Methods Eng. 53 (2002) 2587–2615. doi:10.1002/nme.338.

[48] J.W. Yoo, B. Moran, J.-S. Chen, Stabilized conforming nodal integration in the natural-element method, Int. J. Numer. Methods Eng. 60 (2004) 861–890. doi:10.1002/nme.972.

[49] G.-R. Liu, Y.T. Gu, a Local Radial Point Interpolation Method (LRPIM) for Free Vibration Analyses of 2-D Solids, J. Sound Vib. 246 (2001) 29–46. doi:10.1006/jsvi.2000.3626.

[50] J.G. Wang, G.-R. Liu, A point interpolation meshless method based on radial basis functions, Int. J. Numer. Methods Eng. 54 (2002) 1623–1648. doi:10.1002/nme.489.

[51] S.R. Idelsohn, E. Oñate, N. Calvo, F. Del Pin, The meshless finite element method, Int. J. Numer. Methods Eng. 58 (2003) 893–912. doi:10.1002/nme.798.

[52] S.R. Idelsohn, E. Oñate, F. Del Pin, A Lagrangian meshless finite element method applied to fluid–structure interaction problems, Comput. Struct. 81 (2003) 655–671. doi:10.1016/S0045-7949(02)00477-7.

[53] S.R. Idelsohn, E. Oñate, F. Del Pin, The particle finite element method: A powerful tool to solve incompressible flows with free-surfaces and breaking waves, Int. J. Numer. Methods Eng. 61 (2004) 964–989. doi:10.1002/nme.1096.

[54] M. Arroyo, M. Ortiz, Local maximum-entropy approximation schemes: A seamless bridge between finite elements and meshfree methods, Int. J. Numer. Methods Eng. 65 (2006) 2167–2202. doi:10.1002/nme.1534.

[55] N. Sukumar, Construction of polygonal interpolants: A maximum entropy approach, Int. J. Numer. Methods Eng. 61 (2004) 2159–2181. doi:10.1002/nme.1193.

[56] T.J.R. Hughes, J.A. Cottrell, Y. Bazilevs, Isogeometric analysis: CAD, finite elements, NURBS, exact geometry and mesh refinement, Comput. Methods Appl. Mech. Eng. 194 (2005) 4135–4195. doi:10.1016/j.cma.2004.10.008.

[57] J.A. Cottrell, T.J.R. Hughes, Y. Bazilevs, Isogeometric analysis: toward integration of CAD and FEA, John Wiley & Sons, 2009.

[58] S.A. Silling, E. Askari, A meshfree method based on the peridynamic model of solid mechanics, Comput. Struct. 83 (2005) 1526–1535. doi:10.1016/j.compstruc.2004.11.026.

[59] S.A. Silling, M.A. Epton, O. Weckner, J. Xu, E. Askari, Peridynamic states and constitutive modeling, 2007. doi:10.1007/s10659-007-9125-1.

[60] B. Li, F. Habbal, M. Ortiz, Optimal transportation meshfree approximation schemes for fluid and plastic flows, Int. J. Numer. Methods Eng. 83 (2010) 1541–1579.

[61] J.-S. Chen, M. Hillman, M. Rüter, An arbitrary order variationally consistent integration for Galerkin meshfree methods, Int. J. Numer. Methods Eng. 95 (2013) 387–418. doi:10.1002/nme.4512.

[62] M.A. Bessa, J.T. Foster, T. Belytschko, W.K. Liu, A meshfree unification: Reproducing kernel peridynamics, Comput. Mech. 53 (2014) 1251–1264. doi:10.1007/s00466-013-0969-x.

[63] F. Auricchio, L.B. Da Veiga, T.J.R. Hughes, A. Reali, G. Sangalli, Isogeometric collocation methods, Math. Model. Methods Appl. Sci. 20 (2010) 2075–2107.

[64] D.J. Benson, Y. Bazilevs, E. De Luycker, M.-C. Hsu, M. Scott, T.J.R. Hughes, et al., A generalized finite element formulation for arbitrary basis functions: from isogeometric analysis to XFEM, Int. J. Numer.

Methods Eng. 83 (2010) 765–785.

[65] S.S. Ghorashi, N. Valizadeh, S. Mohammadi, Extended isogeometric analysis for simulation of stationary and propagating cracks, Int. J. Numer. Methods Eng. 89 (2012) 1069–1101.

[66] J.J. Monaghan, Why particle methods work, SIAM J. Sci. Stat. Comput. 3 (1982) 422–433.

[67] J.J. Monaghan, An introduction to SPH, Comput. Phys. Commun. 48 (1988) 89–96. doi:10.1016/0010-4655(88)90026-4.

[68] L.D. Libersky, A. Petschek, Smooth Particle Hydrodynamics with Strength of Materials, Lect. Notes Phys. 395 (1990) 248–257. doi:10.1007/3-540-54960-9.

[69] W. Benz, E. Asphaug, Simulations of brittle solids using smooth particle hydrodynamics, Comput. Phys. Commun. 87 (1995) 253–265.

[70] P.W. Randles, L.D. Libersky, Smoothed Particle Hydrodynamics: Some recent improvements and applications, Comput. Methods Appl. Mech. Eng. 139 (1996) 375–408. doi:10.1016/S0045-7825(96)01090-0.

[71] G.R. Johnson, R. a. Stryk, S.R. Beissel, SPH for high velocity impact computations, Comput. Methods Appl. Mech. Eng. 139 (1996) 347–373. doi:10.1016/S0045-7825(96)01089-4.

[72] J.W. Swegle, S.W. Attaway, M.W. Heinstein, F.J. Mello, D.L. Hicks, An analysis of smoothed particle hydrodynamics, Distribution. (1994). doi:10.1006/jcph.1995.1010.

[73] J.W. Swegle, D.L. Hicks, S.W. Attaway, Smoothed Particle Hydrodynamics Stability Analysis, J. Comput. Phys. 116 (1995) 123–134. doi:10.1006/jcph.1995.1010.

[74] T. Belytschko, Y. Guo, W.K. Liu, S.P. Xiao, A unifieded stability analysis of meshless particle methods, Int. J. Numer. Methods Eng. 48 (2000) 1359–1400. doi:10.1002/1097-0207(20000730)48:9<1359::AID-NME829>3.0.CO;2-U.

[75] P.W. Randles, L.D. Libersky, Normalized SPH with stress points, Int. J. Numer. Meth. Engng. 48 (2000) 1445–1462. doi:10.1002/1097-0207(20000810)48:10<1445::AID-NME831>3.0.CO;2-9.

[76] J.J. Monaghan, SPH without a Tensile Instability, J. Comput. Phys. 159 (2000) 290–311. doi:10.1006.

[77] J. Bonet, S. Kulasegaram, Correction and stabilization of smooth particle hydrodynamics methods with applications in metal forming simulations, Int. J. Numer. Methods Eng. (2000) 1189–1214. doi:10.1002/(SICI)1097-0207(20000228)47:6<1189::AID-NME830>3.0.CO;2-I.

[78] P.S. Jensen, Finite difference techniques for variable grids, Comput. Struct. 2 (1972) 17–29. doi:10.1016/0045-7949(72)90020-X.

[79] N. Perrones, R. Kao, a General-Finite Difference Method for Arbitrary Meshes, Comput. Struct. 5 (1974).

[80] P. Lancaster, K. Salkauskas, Surfaces Generated by Moving Least Squares Methods, Math. Comput. (1981) 141–158.

[81] T. Belytschko, L. Gu, Y.Y. Lu, Fracture and crack growth by element free Galerkin methods, Model. Simul. Mater. Sci. Eng. 2 (1994) 519–534. doi:10.1088/0965-0393/2/3A/007.

[82] T. Belytschko, M. Tabbara, Dynamic fracture using element-free Galerkin methods, Int. J. Numer. Methods Eng. 39 (1996) 923–938. doi:10.1002/(SICI)1097-0207(19960330)39:6<923::AID-NME887>3.0.CO;2-W.

[83] J.-S. Chen, C. Pan, C.-T. Wu, Large deformation analysis of rubber based on a reproducing kernel particle method, Comput. Mech. 19 (1997) 211–227. doi:10.1007/s004660050170.

[84] W.K. Liu, Y. Chen, C.T. Chang, T. Belytschko, Advances in multiple scale kernel particle methods, Comput. Mech. 18 (1996) 73–111. doi:10.1007/BF00350529.

[85] W.K. Liu, S. Li, T. Belytschko, Moving least-square reproducing kernel methods (I) Methodology and convergence, Comput. Methods Appl. Mech. Eng. 143 (1997) 113–154. doi:10.1016/S0045-7825(96)01132-2.

[86] W. Han, X. Meng, Error analysis of the reproducing kernel particle method, Comput. Methods Appl. Mech. Eng. 190 (2001) 6157–6181. doi:10.1016/S0045-7825(01)00214-6.

[87] J.-S. Chen, W. Han, Y. You, X. Meng, A reproducing kernel method with nodal interpolation property, Int. J.

Numer. Methods Eng. 56 (2003) 935–960. doi:10.1002/nme.592.

[88] W.K. Liu, Y. Chen, Wavelet and multiple scale reproducing kernel methods, Int. J. Numer. Methods Fluids. 2 (1995) 901–931.

[89] W.K. Liu, Y. Chen, R.A. Uras, C.T. Chang, Generalized multiple scale reproducing kernel particle methods, Comput. Methods Appl. Mech. Eng. 139 (1996) 91–157. doi:10.1016/S0045-7825(96)01081-X.

[90] W.K. Liu, W. Hao, Y. Chen, S. Jun, J. Gosz, Multiresolution reproducing kernel particle methods, Comput. Mech. 20 (1997) 295–309.

[91] S. Li, W.K. Liu, Synchronized reproducing kernel interpolant via multiple wavelet expansion, Comput. Mech. 21 (1998) 28–47. doi:10.1007/s004660050281.

[92] S. Li, W.K. Liu, Reproducing kernel hierarchical partition of unity, part I - formulation and theory, Int. J. Numer. Methods Eng. 288 (1999) 251–288. doi:10.1002/(SICI)1097-0207(19990530)45:3<251::AID-NME583>3.0.CO;2-I.

[93] S. Li, W.K. Liu, Reproducing kernel hierarchical partition of unity, Part II - applications, Int. J. Numer. Methods Eng. 45 (1999) 289–317. doi:10.1002/(SICI)1097-0207(19990530)45:3<251::AID-NME583>3.0.CO;2-I.

[94] J.-S. Chen, C.-T. Wu, On Computational Issues in Large Deformation Analysis of Rubber Bushings, J. Struct. Mech. 25 (1997) 287–309.

[95] J.-S. Chen, C. Pan, C.M.O.L. Roque, H.-P. Wang, A Lagrangian reproducing kernel particle method for metal forming analysis, Comput. Mech. 22 (1998) 289–307. doi:10.1007/s004660050361.

[96] J.-S. Chen, S. Yoon, H.-P. Wang, W.K. Liu, An Improved Reproducing Kernel Particle Method for Nearly Incompressible Finite Elasticity, Comput. Methods Appl. Mech. Eng. 181 (2000) 117–145.

[97] J.-S. Chen, H.-P. Wang, S. Yoon, Y. You, Some recent improvements in meshfree methods for incompressible finite elasticity boundary value problems with contact, Comput. Mech. 25 (2000) 137–156. doi:10.1007/s004660050465.

[98] S. Yoon, C.-T. Wu, H.-P. Wang, J.-S. Chen, Efficient Meshfree Formulation for Metal Forming Simulations, J. Eng. Mater. Technol. 123 (2001) 462. doi:10.1115/1.1396349.

[99] S. Yoon, J.-S. Chen, Accelerated meshfree method for metal forming simulation, Finite Elem. Anal. Des. 38 (2002) 937–948. doi:10.1016/S0168-874X(02)00086-0.

[100] J.-S. Chen, H.-P. Wang, Meshfree smooth surface contact algorithm for sheet metal forming, in: Proc. SAE, Detroit, 2000.

[101] H.-P. Wang, Meshfree smooth contact formulation and boundary condition treatments in multi-body contact, Ph.D. Dissertation, University of Iowa, 2000.

[102] H.-P. Wang, C.-T. Wu, J.-S. Chen, A reproducing kernel smooth contact formulation for metal forming simulations, Comput. Mech. 54 (2014) 151–169. doi:10.1007/s00466-014-1015-3.

[103] J.-S. Chen, S.W. Chi, C.-H. Lee, S.P. Lin, C. Marodon, M.J. Roth, et al., A multiscale meshfree approach for modeling fragment penetration into ultra high-strength concrete, DTIC Doc. ERDC/GSL TR-11-35. (2011).

[104] S.-W. Chi, C.-H. Lee, J.-S. Chen, P.-C. Guan, A level set enhanced natural kernel contact algorithm for impact and penetration modeling, Int. J. Numer. Methods Eng. 102 (2015) 839–866.

[105] J.A. Sherburn, M.J. Roth, J.-S. Chen, M. Hillman, Meshfree modeling of concrete slab perforation using a reproducing kernel particle impact and penetration formulation, Int. J. Impact Eng. 86 (2015) 96–110. doi:10.1016/j.ijimpeng.2015.07.009.

[106] Y. You, J.-S. Chen, H. Lu, Filters, reproducing kernel, and adaptive meshfree method, Comput. Mech. 31 (2003) 316–326. doi:10.1007/s00466-003-0434-3.

[107] T. Rabczuk, T. Belytschko, Adaptivity for structured meshfree particle methods in 2D and 3D, Int. J. Numer. Methods Eng. 63 (2005) 1559–1582. doi:10.1002/nme.1326.

[108] T. Rabczuk, E. Samaniego, Discontinuous modelling of shear bands using adaptive meshfree methods, Comput. Methods Appl. Mech. Eng. 197 (2008) 641–658. doi:10.1016/j.cma.2007.08.027.

[109] J. Dolbow, T. Belytschko, Numerical integration of the Galerkin weak form in meshfree methods, Comput. Mech. 23 (1999) 219–230. doi:10.1007/s004660050403.

[110] Q. Duan, X. Li, H. Zhang, T. Belytschko, Second-order accurate derivatives and integration schemes for meshfree methods, Int. J. Numer. Methods Eng. 92 (2012) 399–424.

[111] S.R. Beissel, T. Belytschko, Nodal integration of the element-free Galerkin method, Comput. Methods Appl. Mech. Eng. 139 (1996) 49–74. doi:10.1016/S0045-7825(96)01079-1.

[112] I. Babuška, U. Banerjee, J.E. Osborn, Meshless and generalized finite element methods: a survey of some major results, (2003) 1–20.

[113] D. Shepard, A two-dimensional interpolation function for irregularly-spaced data, 23rd ACM Natl. Conf. (1968) 517–524. doi:10.1145/800186.810616.

[114] J.T. Oden, C.A.M. Duarte, O.C. Zienkiewicz, A new cloud-based hp finite element method, Comput. Methods Appl. Mech. Eng. 153 (1998) 117–126. doi:10.1016/S0045-7825(97)00039-X.

[115] T. Strouboulis, K. Copps, I. Babuška, The generalized finite element method: an example of its implementation and illustration of its performance, Int. J. Numer. Methods Eng. (2000) 1–16. doi:10.1002/(SICI)1097-0207(20000320)47:8<1401::AID-NME835>3.0.CO;2-8.

[116] T. Strouboulis, I. Babuška, K. Copps, The design and analysis of the Generalized Finite Element Method, Comput. Methods Appl. Mech. Eng. 181 (2000) 43–69. doi:10.1016/S0045-7825(99)00072-9.

[117] V. Gupta, C.A.M. Duarte, I. Babuška, U. Banerjee, A stable and optimally convergent generalized FEM (SGFEM) for linear elastic fracture mechanics, Comput. Methods Appl. Mech. Eng. 266 (2013) 23–39. doi:10.1016/j.cma.2013.07.010.

[118] V. Gupta, C.A.M. Duarte, I. Babuška, U. Banerjee, Stable GFEM (SGFEM): Improved conditioning and accuracy of GFEM/XFEM for three-dimensional fracture mechanics, Comput. Methods Appl. Mech. Eng. 289 (2015) 355–386. doi:10.1016/j.cma.2015.01.014.

[119] V. Gupta, D.J. Kim, C.A.M. Duarte, Analysis and improvements of global-local enrichments for the Generalized Finite Element Method, Comput. Methods Appl. Mech. Eng. 245-246 (2012) 47–62. doi:10.1016/j.cma.2012.06.021.

[120] C.A.M. Duarte, D.J. Kim, Analysis and applications of a generalized finite element method with global-local enrichment functions, Comput. Methods Appl. Mech. Eng. 197 (2008) 487–504. doi:10.1016/j.cma.2007.08.017.

[121] D.J. Kim, J.P.A. Pereira, C.A.M. Duarte, Analysis of three-dimensional fracture mechanics problems: A two-scale approach using coarse-generalized FEM meshes, Int. J. Numer. Methods Eng. 81 (2010) 335–365.

[122] J. Kim, C.A.M. Duarte, A new generalized finite element method for two-scale simulations of propagating cohesive fractures in 3-D, Int. J. Numer. Methods Eng. 104 (2015) 1139–1172.

[123] J.P.A. Pereira, D.J. Kim, C.A.M. Duarte, A two-scale approach for the analysis of propagating three-dimensional fractures, Comput. Mech. 49 (2012) 99–121. doi:10.1007/s00466-011-0631-4.

[124] M. Griebel, M.A. Schweitzer, A Particle-Partition of Unity Method--Part II: Efficient Cover Construction and Reliable Integration, SIAM J. Sci. Comput. 23 (2002) 1655–1682. doi:10.1137/S1064827501391588.

[125] M. Griebel, M.A. Schweitzer, A Particle-Partition of Unity Method--Part III: A Multilevel Solver, SIAM J. Sci. Comput. 24 (2002) 377–409. doi:10.1137/S1064827501395252.

[126] M. Griebel, M.A. Schweitzer, A particle-partition of unity method-Part IV: Parallelization, in: Meshfree Methods Partial Differ. Equations, Springer, 2003: pp. 161–192.

[127] M. Griebel, M.A. Schweitzer, A particle-partition of unity method part V: boundary conditions, Geom. Anal. Nonlinear Partial …. (2003) 1–25. doi:10.1007/978-3-540-46222-4_8.

[128] S.N. Atluri, S. Shen, The meshless local Petrov-Galerkin (MLPG) method, Crest, 2002.

[129] T.L. Zhu, J.-D. Zhang, S.N. Atluri, A local boundary integral equation (LBIE) method in computational mechanics, and a meshless discretization approach, Comput. Mech. 21 (1998) 223–235. doi:10.1007/s004660050297.

[130] S. De, K.J. Bathe, The method of finite spheres with improved numerical integration, Comput. Struct. 79 (2001) 2183–2196.

[131] R. Sibson, A vector identity for the Dirichlet tessellation, Math. Proc. Cambridge Philos. Soc. 87 (1980) 151. doi:10.1017/S0305004100056589.

[132] V. V Belikov, V.D. Ivanov, V.K. Kontorovich, S.A. Korytnik, A.Y. Semenov, The non-Sibsonian interpolation: A new method of interpolation of the values of a function on an arbitrary set of points, Comput. Math. Math. Phys. 37 (1997) 9–15.

[133] E.T. Jaynes, Information theory and statistical mechanics, Phys. Rev. 106 (1957) 620.

[134] J.-D. Benamou, Y. Brenier, A numerical method for the optimal time-continuous mass transport problem and related problems, Contemp. Math. 226 (1999) 1–12.

[135] B. Li, A. Kidane, G. Ravichandran, M. Ortiz, Verification and validation of the Optimal Transportation Meshfree (OTM) simulation of terminal ballistics, Int. J. Impact Eng. 42 (2012) 25–36. doi:10.1016/j.ijimpeng.2011.11.003.

[136] B. Li, L. Perotti, M. Adams, J. Mihaly, A.J. Rosakis, M. Stalzer, et al., Large scale Optimal Transportation Meshfree (OTM) simulations of hypervelocity impact, Procedia Eng. 58 (2013) 320–327. doi:10.1016/j.proeng.2013.05.036.

[137] N. Sukumar, Quadratic maximum-entropy serendipity shape functions for arbitrary planar polygons, Comput. Methods Appl. Mech. Eng. 263 (2013) 27–41. doi:10.1016/j.cma.2013.04.009.

[138] C.J. Cyron, M. Arroyo, M. Ortiz, Smooth, second order, non-negative meshfree approximants selected by maximum entropy, Int. J. Numer. Methods Eng. 79 (2009) 1605–1632.

[139] D. González, E. Cueto, M. Doblaré, A higher order method based on local maximum entropy approximation, Int. J. Numer. Methods Eng. 83 (2010) 741–764.

[140] A. Rosolen, D. Millán, M. Arroyo, Second-order convex maximum entropy approximants with applications to high-order PDE, Int. J. Numer. Methods Eng. 94 (2013) 150–182.

[141] C.-T. Wu, C.K. Park, J.-S. Chen, A generalized approximation for the meshfree analysis of solids, Int. J. Numer. Methods Eng. 85 (2011) 693–722.

[142] X. Zhuang, H. Zhu, C. Augarde, An improved meshless Shepard and least squares method possessing the delta property and requiring no singular weight function, Comput. Mech. 53 (2014) 343–357. doi:10.1007/s00466-013-0912-1.

[143] D. Wang, P. Chen, Quasi-convex reproducing kernel meshfree method, Comput. Mech. (2014) 689–709. doi:10.1007/s00466-014-1022-4.

[144] C.-T. Wu, M. Koishi, W. Hu, A displacement smoothing induced strain gradient stabilization for the meshfree Galerkin nodal integration method, Comput. Mech. (2015). doi:10.1007/s00466-015-1153-2.

[145] D.L. Sulsky, H.L. Schreyer, Axisymmetric form of the material point method with applications to upsetting and Taylor impact problems, Comput. Methods Appl. Mech. Eng. 139 (1996) 409–429. doi:10.1016/S0045-7825(96)01091-2.

[146] F.H. Harlow, The particle-in-cell computing method for fluid dynamics, Methods Comput. Phys. 3 (1964) 319–343.

[147] J.U. Brackbill, H.M. Ruppel, FLIP: A method for adaptively zoned, particle-in-cell calculations of fluid flows in two dimensions, J. Comput. Phys. 65 (1986) 314–343. doi:10.1016/0021-9991(86)90211-1.

[148] J.U. Brackbill, D.B. Kothe, H.M. Ruppel, Flip: A low-dissipation, particle-in-cell method for fluid flow, Comput. Phys. Commun. 48 (1988) 25–38. doi:10.1016/0010-4655(88)90020-3.

[149] S.R. Idelsohn, N. Calvo, E. Oñate, Polyhedrization of an arbitrary 3D point set, Comput. Methods Appl. Mech. Eng. 192 (2003) 2649–2667.

[150] R.A. Frazer, W.N.P. Jones, S.W. Skan, Approximations to functions and to the solutions of differential equations, HSMO, 1937. doi:10.1080/14786443808562057.

[151] C. Lanczos, Trigonometric interpolation of empirical and analytical functions, J. Math. Phys. 17 (1938) 123–

199.

[152] J. Slater, Electronic Energy Bands in Metal, Phys. Rev. 45 (1934) 794–801.

[153] J. Barta, Über die Näherungsweise Lösung einiger Zweidimensionaler Elastizität Aufgaben, ZAMM - J. Appl. Math. Mech. / Zeitschrift Für Angew. Math. Und Mech. 17 (1937) 184–185.

[154] R. Franke, Scattered data interpolation: tests of some methods, Math. Comput. 38 (1982) 181–181. doi:10.1090/S0025-5718-1982-0637296-4.

[155] R.L. Hardy, Multiquadric equations of topography and other irregular surfaces, J. Geophys. Res. 76 (1971) 1905. doi:10.1029/JB076i008p01905.

[156] R.L. Hardy, Theory and applications of the multiquadric-biharmonic method 20 years of discovery 1968--1988, Comput. Math. with Appl. 19 (1990) 163–208.

[157] M.D. Buhmann, C.A. Micchelli, Multiquadric interpolation improved, Comput. Math. with Appl. 24 (1992) 21–25.

[158] C.K. Chui, J. Stöckler, J.D. Ward, Analytic wavelets generated by radial functions, Adv. Comput. Math. 5 (1996) 95–123.

[159] W.R. Madych, S.A. Nelson, Multivariate interpolation and Conditionally positive definite functions II, Math. Comput. 54 (1990) 211–230. doi:10.1090/S0025-5718-1990-0993931-7.

[160] C. Franke, R. Schaback, Solving partial differential equations by collocation using radial basis functions, Appl. Math. Comput. 93 (1998) 73–82. doi:10.1016/S0096-3003(97)10104-7.

[161] H. Wendland, Meshless Galerkin methods using radial basis functions, Math. Comput. Am. Math. Soc. 68 (1999) 1521–1531.

[162] H.-Y. Hu, Z.-C. Li, A.H.-D. Cheng, Radial basis collocation methods for elliptic boundary value problems, Comput. Math. with Appl. 50 (2005) 289–320.

[163] T. Cecil, J. Qian, S. Osher, Numerical methods for high dimensional Hamilton-Jacobi equations using radial basis functions, J. Comput. Phys. 196 (2004) 327–347. doi:10.1016/j.jcp.2003.11.010.

[164] J. Li, Mixed methods for fourth-order elliptic and parabolic problems using radial basis functions, Adv. Comput. Math. 23 (2005) 21–30. doi:10.1007/s10444-004-1807-7.

[165] J.-S. Chen, L. Wang, H.-Y. Hu, S.-W. Chi, Subdomain radial basis collocation method for heterogeneous media, Int. J. Numer. Methods Eng. 80 (2009) 163–190.

[166] L. Wang, J.-S. Chen, H.-Y. Hu, Subdomain radial basis collocation method for fracture mechanics, Int. J. Numer. Methods Eng. 83 (2010) 851–876.

[167] S.-W. Chi, J.-S. Chen, H.-Y. Hu, A weighted collocation on the strong form with mixed radial basis approximations for incompressible linear elasticity, Comput. Mech. 53 (2014) 309–324.

[168] E.J. Kansa, Y.C. Hon, Circumventing the ill-conditioning problem with multiquadric radial basis functions: Applications to elliptic partial differential equations, Comput. Math. Appl. 39 (2000) 123–137.

[169] Y.C. Hon, R. Schaback, On unsymmetric collocation by radial basis functions, Appl. Math. Comput. 119 (2001) 177–186. doi:10.1016/S0096-3003(99)00255-6.

[170] H. Wendland, Piecewise polynomial, positive definite and compactly supported radial functions of minimal degree, Adv. Comput. Math. 4 (1995) 389–396. doi:10.1007/BF02123482.

[171] G.E. Fasshauer, Solving differential equations with radial basis functions: multilevel methods and smoothing, Adv. Comput. Math. 11 (1999) 139–159. doi:10.1023/A:1018919824891.

[172] J.-S. Chen, W. Hu, H.-Y. Hu, Reproducing kernel enhanced local radial basis collocation method, Int. J. Numer. Methods Eng. 75 (2008) 600–627.

[173] E. Oñate, S.R. Idelsohn, O.C. Zienkiewicz, R.L. Taylor, C. Sacco, S. Idelsohnl, A stabilized finite point method for analysis of fluid mechanics problems, Comput. Methods Appl. Mech. Eng. 139 (1996) 315–346. doi:10.1016/S0045-7825(96)01088-2.

[174] E. Oñate, S.R. Idelsohn, A mesh-free finite point method for advective-diffusive transport and fluid flow problems, Comput. Mech. 21 (1998) 283–292. doi:10.1007/s004660050304.

[175] S. Koshizuka, A. Nobe, Y. Oka, Numerical analysis of breaking waves using the moving particle semi-implicit method, Int. J. Numer. Methods Fluids. 26 (1998) 751–769.

[176] S. Koshizuka, H. Ikeda, Y. Oka, Numerical analysis of fragmentation mechanisms in vapor explosions, Nucl. Eng. Des. 189 (1999) 423–433. doi:10.1016/S0029-5493(98)00270-2.

[177] B. Ataie-Ashtiani, L. Farhadi, A stable moving-particle semi-implicit method for free surface flows, Fluid Dyn. Res. 38 (2006) 241–256.

[178] A. Khayyer, H. Gotoh, A higher order Laplacian model for enhancement and stabilization of pressure calculation by the MPS method, Appl. Ocean Res. 32 (2010) 124–131.

[179] A. Khayyer, H. Gotoh, Enhancement of stability and accuracy of the moving particle semi-implicit method, J. Comput. Phys. 230 (2011) 3093–3118.

[180] M. Kondo, S. Koshizuka, Improvement of stability in moving particle semi-implicit method, Int. J. Numer. Methods Fluids. 65 (2011) 638–654.

[181] S.A. Silling, Reformulation of elasticity theory for discontinuities and long-range forces, J. Mech. Phys. Solids. 48 (2000) 175–209. doi:10.1016/S0022-5096(99)00029-0.

[182] T.L. Warren, S.A. Silling, A. Askari, O. Weckner, M.A. Epton, J. Xu, A non-ordinary state-based peridynamic method to model solid material deformation and fracture, Int. J. Solids Struct. 46 (2009) 1186–1195. doi:10.1016/j.ijsolstr.2008.10.029.

[183] J.T. Foster, S.A. Silling, W.W. Chen, Viscoplasticity using peridynamics, Int. J. Numer. Methods Eng. 81 (2010) 1242–1258.

[184] M.R. Tupek, J.J. Rimoli, R. Radovitzky, An approach for incorporating classical continuum damage models in state-based peridynamics, Comput. Methods Appl. Mech. Eng. 263 (2013) 20–26. doi:10.1016/j.cma.2013.04.012.

[185] S.A. Silling, R.B. Lehoucq, Convergence of peridynamics to classical elasticity theory, J. Elast. 93 (2008) 13–37. doi:10.1007/s10659-008-9163-3.

[186] A. Savitzky, M.J.E. Golay, Smoothing and differentiation of data by simplified least squares procedures., Anal. Chem. 36 (1964) 1627–1639.

[187] J.-S. Chen, T. Belytschko, Meshless and MeshfreeMethods, in: B. Engquist (Ed.), Encycl. Appl. Comput. Math., 2011: pp. 886–894. doi:10.1007/978-3-540-70529-1.

[188] S. Li, W.K. Liu, Moving least-square reproducing kernel method Part II: Fourier analysis, Comput. Methods Appl. Mech. Eng. 139 (1996) 159–193. doi:10.1016/S0045-7825(96)01082-1.

[189] S. Li, W.K. Liu, Meshfree particle methods, Springer Science & Business Media, 2007.

[190] W.K. Liu, S. Jun, S. Li, J. Adee, T. Belytschko, Reproducing kernel particle methods for structural dynamics, Int. J. Numer. Methods Eng. 38 (1995) 1655–1679.

[191] J.-S. Chen, X. Zhang, T. Belytschko, An implicit gradient model by a reproducing kernel strain regularization in strain localization problems, Comput. Methods Appl. Mech. Eng. 193 (2004) 2827–2844. doi:10.1016/j.cma.2003.12.057.

[192] W. Han, G.J. Wagner, W.K. Liu, Convergence analysis of a hierarchical enrichment of Dirichlet boundary conditions in a mesh-free method, Int. J. Numer. Methods Eng. 53 (2002) 1323–1336. doi:10.1002/nme.336.

[193] W.K. Liu, Y. Chen, S. Jun, J.-S. Chen, T. Belytschko, C. Pan, et al., Overview and applications of the reproducing Kernel Particle methods, Arch. Comput. Methods Eng. 3 (1996) 3–80. doi:10.1007/BF02736130.

[194] C.A.M. Duarte, I. Babuška, J.T. Oden, Generalized finite element methods for three-dimensional structural mechanics problems, Comput. Struct. 77 (2000) 215–232.

[195] T. Belytschko, Y. Krongauz, D. Organ, M. Fleming, P. Krysl, Meshless methods: An overview and recent developments, Comput. Methods Appl. Mech. Eng. 139 (1996) 3–47. doi:10.1016/S0045-7825(96)01078-X.

[196] G.-R. Liu, Meshfree methods: moving beyond the finite element method, Taylor & Francis, 2009.

[197] W.K. Liu, W. Han, H. Lu, S. Li, J. Cao, Reproducing kernel element method. Part I: Theoretical formulation,

Comput. Methods Appl. Mech. Eng. 193 (2004) 933–951. doi:10.1016/j.cma.2003.12.001.

[198] H.-Y. Hu, C.-K. Lai, J.-S. Chen, A study on convergence and complexity of reproducing kernel collocation method, Interact. Multiscale Mech. 2 (2009) 295–319. doi:10.12989/imm.2009.2.3.295.

[199] M. Hillman, J.-S. Chen, Nodally integrated implicit gradient reproducing kernel particle method for convection dominated problems, Comput. Methods Appl. Mech. Eng. 299 (2016) 381–400. doi:10.1016/j.cma.2015.11.004.

[200] J.-S. Chen, M. Hillman, Higher order peridynamics and accelerated derivative approximations, Under Preperation. (n.d.).

[201] T.L. Zhu, S.N. Atluri, A modified collocation method and a penalty formulation for enforcing the essential boundary conditions in the element free Galerkin method, Comput. Mech. 21 (1998) 211–222. doi:10.1007/s004660050296.

[202] F.C. Günther, W.K. Liu, Implementation of boundary conditions for meshless methods, Comput. Methods Appl. Mech. Eng. 163 (1998) 205–230. doi:10.1016/S0045-7825(98)00014-0.

[203] S.N. Atluri, H.G. Kim, J.Y. Cho, Critical assessment of the truly Meshless Local Petrov-Galerkin (MLPG), and Local Boundary Integral Equation (LBIE) methods, Comput. Mech. 24 (1999) 348–372. doi:10.1007/s004660050457.

[204] G.J. Wagner, W.K. Liu, Application of essential boundary conditions in mesh-free methods: a corrected collocation method, Int. J. Numer. Methods Eng. 47 (2000) 1367–1379. doi:10.1002/(SICI)1097-0207(20000320)47:8<1367::AID-NME822>3.0.CO;2-Y.

[205] J.-S. Chen, H.-P. Wang, New boundary condition treatments in meshfree computation of contact problems, Comput. Methods Appl. Mech. Eng. 187 (2000) 441–468. doi:10.1016/S0045-7825(00)80004-3.

[206] J. Gosz, W.K. Liu, Admissible Approximations for Essential Boundary Conditions in the Reproducing Kernel Particle Method, Comput. Mech. 19 (1996) 120–135.

[207] I. Kaljevic, S. Saigal, An improved element free Galerkin formulation, Int. J. Numer. Methods Eng. 40 (1997) 2953–2974. doi:10.1002/(SICI)1097-0207(19970830)40:16<2953::AID-NME201>3.0.CO;2-S.

[208] Y. Krongauz, T. Belytschko, Enforcement of essential boundary conditions in meshless approximations using finite elements, Comput. Methods Appl. Mech. Eng. 131 (1996) 133–145. doi:10.1016/0045-7825(95)00954-X.

[209] S. Fernández-Méndez, A. Huerta, Imposing essential boundary conditions in mesh-free methods, Comput. Methods Appl. Mech. Eng. 193 (2004) 1257–1275.

[210] J. Nitsche, Über ein Variationsprinzip zur Lösung von Dirichlet-Problemen bei Verwendung von Teilräumen, die keinen Randbedingungen unterworfen sind, in: Abhandlungen Aus Dem Math. Semin. Der Univ. Hambg., 1971: pp. 9–15.

[211] L.T. Zhang, G.J. Wagner, W.K. Liu, A Parallelized Meshfree Method with Boundary Enrichment for Large-Scale CFD, J. Comput. Phys. 176 (2002) 483–506. doi:10.1006/jcph.2002.6999.

[212] I. Babuška, Quadrature for Meshless Methods, (2007) 1–40.

[213] Y. Liu, T. Belytschko, A new support integration scheme for the weakform in mesh-free methods, Int. J. Numer. Methods Eng. 82 (2010) 699–715.

[214] Y. Krongauz, T. Belytschko, Consistent pseudo-derivatives in meshless methods, Comput. Methods Appl. Mech. Eng. 146 (1997) 371–386. doi:10.1016/S0045-7825(96)01234-0.

[215] P.-C. Guan, J.-S. Chen, Y. Wu, H. Teng, J. Gaidos, K. Hofstetter, et al., Semi-Lagrangian reproducing kernel formulation and application to modeling earth moving operations, Mech. Mater. 41 (2009) 670–683. doi:10.1016/j.mechmat.2009.01.030.

[216] P.-C. Guan, S.W. Chi, J.-S. Chen, T.R. Slawson, M.J. Roth, Semi-Lagrangian reproducing kernel particle method for fragment-impact problems, Int. J. Impact Eng. 38 (2011) 1033–1047. doi:10.1016/j.ijimpeng.2011.08.001.

[217] J.-S. Chen, W. Hu, M.A. Puso, Orbital HP-clouds for solving Schrödinger equation in quantum mechanics, Comput. Methods Appl. Mech. Eng. 196 (2007) 3693–3705.

[218] D. Wang, J.-S. Chen, Locking-free stabilized conforming nodal integration for meshfree Mindlin-Reissner plate formulation, Comput. Methods Appl. Mech. Eng. 193 (2004) 1065–1083. doi:10.1016/j.cma.2003.12.006.

[219] J.-S. Chen, D. Wang, A constrained reproducing kernel particle formulation for shear deformable shell in Cartesian coordinates, Int. J. Numer. Methods Eng. 68 (2006) 151–172. doi:10.1002/nme.1701.

[220] D. Wang, J.-S. Chen, A Hermite reproducing kernel approximation for thin-plate analysis with sub-domain stabilized conforming integration, Int. J. Numer. Methods Eng. 74 (2008) 368–390.

[221] H. Wei, J.-S. Chen, M. Hillman, A stabilized nodally integrated meshfree formulation for fully coupled hydro-mechanical analysis of fluid-saturated porous media, Comput. Fluids. 000 (2015) 1–11. doi:10.1016/j.compfluid.2015.11.002.

[222] P.-C. Guan, Adaptive Coupling of FEM and RKPM Formulations for Contact and Impact Problems, Ph. D. Dissertation, University of California, Los Angeles, 2009.

[223] G.-R. Liu, a Generalized Gradient Smoothing Technique and the Smoothed Bilinear Form for Galerkin Formulation of a Wide Class of Computational Methods, Int. J. Comput. Methods. 05 (2008) 199–236. doi:10.1142/S0219876208001510.

[224] G.-R. Liu, T. Nguyen-Thoi, Smoothed Finite Element Methods, CRC Press, New Jersey, 2010.

[225] K.Y. Sze, J.-S. Chen, N. Sheng, X.H. Liu, Stabilized conforming nodal integration: Exactness and variational justification, Finite Elem. Anal. Des. 41 (2004) 147–171. doi:10.1016/j.finel.2004.05.003.

[226] M. Rüter, M. Hillman, J.-S. Chen, Corrected stabilized non-conforming nodal integration in meshfree methods, in: Lect. Notes Comput. Sci. Eng., 2013: pp. 75–92. doi:10.1007/978-3-642-32979-1_5.

[227] M. Hillman, J.-S. Chen, Y. Bazilevs, Variationally consistent domain integration for isogeometric analysis, Comput. Methods Appl. Mech. Eng. 284 (2015) 521–540. doi:10.1016/j.cma.2014.10.004.

[228] D. Wang, J. Wu, An efficient nesting sub-domain gradient smoothing integration algorithm with quadratic exactness for Galerkin meshfree methods, Comput. Methods Appl. Mech. Eng. 298 (2016) 485–519. doi:10.1016/j.cma.2015.10.008.

[229] I. Babuška, U. Banerjee, J.E. Osborn, Q. Li, Quadrature for meshless methods, Int. J. Numer. Methods Eng. 76 (2008) 1434–1470.

[230] I. Babuška, U. Banerjee, J.E. Osborn, Q. Zhang, Effect of numerical integration on meshless methods, Comput. Methods Appl. Mech. Eng. 198 (2009) 2886–2897. doi:10.1016/j.cma.2009.04.008.

[231] T.-P. Fries, T. Belytschko, Convergence and stabilization of stress-point integration in mesh-free and particle methods, Int. J. Numer. Methods Eng. 74 (2008) 1067–1087.

[232] Q. Duan, T. Belytschko, Gradient and dilatational stabilizations for stress-point integration in the element-free Galerkin method, Int. J. Numer. Methods Eng. 77 (2009) 776–798.

[233] C.T. Dyka, P.W. Randles, R.P. Ingel, Stress points for tension instability in SPH, Int. J. Numer. Methods Eng. 40 (1997) 2325–2341. doi:10.1002/(SICI)1097-0207(19970715)40:13<2325::AID-NME161>3.0.CO;2-8.

[234] C.T. Dyka, R.P. Ingel, An approach for tension instability in smoothed particle hydrodynamics (SPH), Comput. Struct. 57 (1995) 573–580. doi:10.1016/0045-7949(95)00059-P.

[235] W.K. Liu, J.S.-J. Ong, R.A. Uras, Finite element stabilization matrices-a unification approach, Comput. Methods Appl. Mech. Eng. 53 (1985) 13–46.

[236] T. Nagashima, Node-by-node meshless approach and its applications to structural analyses, Int. J. Numer. Methods Eng. 46 (1999) 341–385.

[237] G.-R. Liu, G.Y. Zhang, Y.Y. Wang, Z.H. Zhong, G.Y. Li, X. Han, A nodal integration technique for meshfree radial point interpolation method (NI-RPIM), Int. J. Solids Struct. 44 (2007) 3840–3860. doi:10.1016/j.ijsolstr.2006.10.025.

[238] M.A. Puso, J.-S. Chen, E. Zywicz, W. Elmer, Meshfree and finite element nodal integration methods, Int. J. Numer. Methods Eng. 74 (2008) 416–446.

[239] M. Hillman, J.-S. Chen, An accelerated, convergent, and stable nodal integration in Galerkin meshfree methods for linear and nonlinear mechanics, Int. J. Numer. Methods Eng. (2015).

[240] M. Duflot, H. Nguyen-Dang, A truly meshless Galerkin method based on a moving least squares quadrature, Commun. Numer. Methods Eng. 18 (2002) 441–449. doi:10.1002/cnm.503.

[241] I. Romero, F. Armero, The partition of unity quadrature in meshless methods, Int. J. Numer. Methods Eng. 54 (2002) 987–1006. doi:10.1002/nme.455.

[242] M. Hillman, J.-S. Chen, S.-W. Chi, Stabilized and variationally consistent nodal integration for meshfree modeling of impact problems, Comp. Part. Mech. 1 (2014) 245–256. doi:10.1007/s40571-014-0024-5.

[243] C.-T. Wu, S.-W. Chi, M. Koishi, Y. Wu, Strain gradient stabilization with dual stress points for the meshfree nodal integration method in inelastic analyses, Int. J. Numer. Methods Eng. (2015).

[244] J.-S. Chen, W. Hu, M.A. Puso, Y. Wu, X. Zhang, Strain smoothing for stabilization and regularization of galerkin meshfree methods, Lect. Notes Comput. Sci. Eng. 57 (2007) 57–75. doi:10.1007/978-3-540-46222-4_4.

[245] M.A. Puso, E. Zywicz, J.-S. Chen, A new stabilized nodal integration approach, Lect. Notes Comput. Sci. Eng. 57 (2007) 207–217. doi:10.1007/978-3-540-46222-4_12.

[246] W.R. Madych, Miscellaneous error bounds for multiquadric and related interpolators, Comput. Math. with Appl. 24 (1992) 121–138. doi:10.1016/0898-1221(92)90175-H.

[247] Z. Wu, R. Schaback, Local error estimates for radial basis function interpolation of scattered data, IMA J. Numer. Anal. 13 (1993) 13–27.

[248] J. Yoon, Spectral approximation orders of radial basis function interpolation on the Sobolev space, SIAM J. Math. Anal. 33 (2001) 946–958.

[249] G. Taylor, The use of flat-ended projectiles for determining dynamic yield stress. I. Theoretical considerations, in: Proc. R. Soc. London A Math. Phys. Eng. Sci., 1948: pp. 289–299.

[250] M.L. Wilkins, M.W. Guinan, Impact of cylinders on a rigid boundary, J. Appl. Phys. 44 (1973) 1200–1206.

[251] H. Lu, J.-S. Chen, Adaptive Galerkin particle Method, Lect. Notes Comput. Sci. Eng. 26 (2002) 251–267.

[252] W.K. Liu, S. Jun, D.T. Sihling, Y.J. Chen, W. Hao, Multiresolution reproducing kernel particle method for computational fluid dynamics, Int. J. Numer. Methods Fluids. 24 (1996) 1391–1415. doi:10.1002/(SICI)1097-0363(199706)24:12<1391::AID-FLD566>3.0.CO;2-2.

[253] R.A. Uras, C.T. Chang, Y. Chen, W.K. Liu, Multiresolution reproducing kernel particle methods in acoustics, J. Comput. Acoust. 5 (1997) 71–94. doi:10.1121/1.417004.

[254] W.K. Liu, S. Jun, Multiple-scale reproducing kernel particle methods for large deformation problems, Int. J. Numer. Methods Eng. 41 (1998) 1339–1362.

[255] J.-S. Chen, C.M.O.L. Roque, C. Pan, S.T. Button, Analysis of metal forming process based on meshless method, J. Mater. Process. Technol. 80-81 (1998) 642–646. doi:10.1016/S0924-0136(98)00171-X.

[256] C.-T. Wu, J.-S. Chen, L. Chi, F. Huck, Lagrangian meshfree formulation for analysis of geotechnical materials, J. Eng. Mech. 127 (2001) 440–449.

[257] O.-L.A. Kwok, P.-C. Guan, W.-P. Cheng, C.-T. Sun, Semi-Lagrangian reproducing kernel particle method for slope stability analysis and post-failure simulation, KSCE J. Civ. Eng. 19 (2015) 107–115. doi:10.1007/s12205-013-0550-3.

[258] J.-S. Chen, E. Yreux, A Quasi-Linear Reproducing Kernel Particle Method, Accept. Int. J. Numer. Methods Eng. (2016).

[259] T. Rabczuk, T. Belytschko, A three-dimensional large deformation meshfree method for arbitrary evolving cracks, Comput. Methods Appl. Mech. Eng. 196 (2007) 2777–2799. doi:10.1016/j.cma.2006.06.020.

[260] T. Rabczuk, J. Eibl, Simulation of high velocity concrete fragmentation using SPH/MLSPH, Int. J. Numer. Methods Eng. 56 (2003) 1421–1444. doi:10.1002/nme.617.

[261] B. Ren, S. Li, Meshfree simulations of plugging failures in high-speed impacts, Comput. Struct. 88 (2010) 909–923. doi:10.1016/j.compstruc.2010.05.003.

[262] L.D. Libersky, P.W. Randles, T.C. Carney, D.L. Dickinson, Recent improvements in SPH modeling of hypervelocity impact, Int. J. Impact Eng. 20 (1997) 525–532. doi:10.1016/S0734-743X(97)87441-6.

[263] S. Ma, X. Zhang, X.M. Qiu, Comparison study of MPM and SPH in modeling hypervelocity impact problems, Int. J. Impact Eng. 36 (2009) 272–282. doi:10.1016/j.ijimpeng.2008.07.001.

[264] M.L. Parks, R.B. Lehoucq, S.J. Plimpton, S.A. Silling, Implementing peridynamics within a molecular dynamics code, Comput. Phys. Commun. 179 (2008) 777–783. doi:10.1016/j.cpc.2008.06.011.

[265] X. Zhang, K.Y. Sze, S. Ma, An explicit material point finite element method for hyper-velocity impact, Int. J. Numer. Methods Eng. 66 (2006) 689–706. doi:10.1002/nme.1579.

[266] T. Rabczuk, J. Eibl, L. Stempniewski, Numerical analysis of high speed concrete fragmentation using a meshfree Lagrangian method, Eng. Fract. Mech. 71 (2004) 547–556. doi:10.1016/S0013-7944(03)00032-8.

[267] G.R. Johnson, Linking of Lagrangian particle methods to standard finite element methods for high velocity impact computations, Nucl. Eng. Des. 150 (1994) 265–274. doi:10.1016/0029-5493(94)90143-0.

[268] G.R. Johnson, S.R. Beissel, R.A. Stryk, A generalized particle algorithm for high velocity impact computations, Comput. Mech. 25 (2000) 245–256. doi:10.1007/s004660050473.

[269] S.R. Beissel, C.A. Gerlach, G.R. Johnson, Hypervelocity impact computations with finite elements and meshfree particles, Int. J. Impact Eng. 33 (2006) 80–90. doi:10.1016/j.ijimpeng.2006.09.047.

[270] G.R. Johnson, S.R. Beissel, C.A. Gerlach, A combined particle-element method for high-velocity impact computations, Procedia Eng. 58 (2013) 269–278. doi:10.1016/j.proeng.2013.05.031.

[271] G.R. Johnson, S.R. Beissel, R.A. Stryk, An improved generalized particle algorithm that includes boundaries and interfaces, Int. J. Numer. Methods Eng. 53 (2002) 875–904. doi:10.1002/nme.316.

[272] G.R. Johnson, R.A. Stryk, J.G. Dodd, Dynamic Lagrangian computations for solids, with variable nodal connectivity for severe distortions, Int. J. Numer. Methods Eng. 23 (1986) 509–522.

[273] G.R. Johnson, Numerical algorithms and material models for high-velocity impact computations, Int. J. Impact Eng. 38 (2011) 456–472. doi:10.1016/j.ijimpeng.2010.10.017.

[274] H.H. Bui, R. Fukagawa, K. Sako, S. Ohno, Lagrangian meshfree particles method (SPH) for large deformation and failure flows of geomaterial using elastic--plastic soil constitutive model, Int. J. Numer. Anal. Methods Geomech. 32 (2008) 1537–1570.

[275] S. Andersen, L. Andersen, Modelling of landslides with the material-point method, Comput. Geosci. 14 (2010) 137–147. doi:10.1007/s10596-009-9137-y.

[276] R. Fukagawa, K. Sako, H.H. Bui, J.C. Wells, Slope stability analysis and discontinuous slope failure simulation by elasto-plastic smoothed particle hydrodynamics (SPH), Géotechnique. 61 (2011) 565–574. doi:10.1680/geot.9.P.046.

[277] D. Wang, Z. Li, L. Li, Y. Wu, Three dimensional efficient meshfree simulation of large deformation failure evolution in soil medium, Sci. China Technol. Sci. 54 (2011) 573–580.

[278] H.H. Bui, R. Fukagawa, An improved SPH method for saturated soils and its application to investigate the mechanisms of embankment failure: Case of hydrostatic pore-water pressure, Int. J. Numer. Anal. Methods Geomech. 37 (2013) 31–50.

[279] W. Chen, T. Qiu, Simulation of earthquake-induced slope deformation using SPH method, Int. J. Numer. Anal. Methods Geomech. 38 (2014) 297–330.

[280] Y. Wu, D. Wang, C.-T. Wu, H. Zhang, A direct displacement smoothing meshfree particle formulation for impact failure modeling, Int. J. Impact Eng. (2015). doi:10.1016/j.ijimpeng.2015.03.013.

[281] Y. Wu, D. Wang, C.-T. Wu, Three dimensional fragmentation simulation of concrete structures with a nodally regularized meshfree method, Theor. Appl. Fract. Mech. 72 (2014) 89–99. doi:10.1016/j.tafmec.2014.04.006.

[282] J.-S. Chen, C.-T. Wu, T. Belytschko, Regularization of material instabilities by meshfree approximations with intrinsic length scales, Int. J. Numer. Methods Eng. 47 (2000) 1303–1322. doi:10.1002/(SICI)1097-0207(20000310)47:7<1303::AID-NME826>3.0.CO;2-5.

[283] S. Li, W. Hao, W.K. Liu, Mesh-free simulations of shear banding in large deformation, Int. J. Solids Struct. 37 (2000) 7185–7206. doi:10.1016/S0020-7683(00)00195-5.

[284] S. Li, W. Hao, W.K. Liu, Numerical Simulations of Large Deformation of Thin Shell Structures Using Meshfree Methods, Comput. Mech. 25 (2000) 102–116.

[285] S. Li, W.K. Liu, A.J. Rosakis, T. Belytschko, W. Hao, Mesh-free Galerkin simulations of dynamic shear band propagation and failure mode transition, Int. J. Solids Struct. 39 (2002) 1213–1240. doi:10.1016/S0020-7683(01)00188-3.

[286] S. Li, W.K. Liu, D. Qian, P.R. Guduru, Dynamic shear band propagation and micro-structure of adiabatic shear band, Comput. Methods Appl. Mech. Eng. 191 (2001) 73–92. doi:10.1016/S0045-7825(01)00245-6.

[287] T. Rabczuk, T. Belytschko, Cracking particles: A simplified meshfree method for arbitrary evolving cracks, Int. J. Numer. Methods Eng. 61 (2004) 2316–2343. doi:10.1002/nme.1151.

[288] T. Belytschko, Y.Y. Lu, L. Gu, M. Tabbara, Element-free galerkin methods for static and dynamic fracture, Int. J. Solids Struct. 32 (1995) 2547–2570. doi:10.1016/0020-7683(94)00282-2.

[289] M. Fleming, Y.A. Chu, B. Moran, T. Belytschko, Enriched Element-Free Galerkin Methods for Crack Tip Fields, Int. J. Numer. Methods Eng. 40 (1997) 1483–1504. doi:10.1002/(SICI)1097-0207(19970430)40:8<1483::AID-NME123>3.0.CO;2-6.

[290] T. Belytschko, Y. Krongauz, M. Fleming, D. Organ, W.K. Liu, Smoothing and accelerated computations in the element free Galerkin method, J. Comput. Appl. Math. 74 (1996) 111–126. doi:10.1016/0377-0427(96)00020-9.

[291] G. Ventura, J.X. Xu, T. Belytschko, A vector level set method and new discontinuity approximations for crack growth by EFG, Int. J. Numer. Methods Eng. 54 (2002) 923–944. doi:10.1002/nme.471.

[292] T. Rabczuk, G. Zi, A meshfree method based on the local partition of unity for cohesive cracks, Comput. Mech. 39 (2007) 743–760. doi:10.1007/s00466-006-0067-4.

[293] T. Rabczuk, P.M.A. Areias, T. Belytschko, A meshfree thin shell method for non-linear dynamic fracture, Int J Numer Meth Eng. 72 (2007) 524–548. doi:10.1002/nme.2013.

[294] T. Rabczuk, G. Zi, S.P.A. Bordas, H. Nguyen-Xuan, A simple and robust three-dimensional cracking-particle method without enrichment, Comput. Methods Appl. Mech. Eng. 199 (2010) 2437–2455. doi:10.1016/j.cma.2010.03.031.

[295] S.P.A. Bordas, T. Rabczuk, G. Zi, Three-dimensional crack initiation, propagation, branching and junction in non-linear materials by an extended meshfree method without asymptotic enrichment, Eng. Fract. Mech. 75 (2008) 943–960. doi:10.1016/j.engfracmech.2007.05.010.

[296] X. Zhuang, C. Augarde, S.P.A. Bordas, Accurate fracture modelling using meshless methods, the visibility criterion and level sets: formulation and 2D modelling, Int. J. Numer. Methods Eng. 86 (2011) 249–268.

[297] J.-S. Chen, R.R. Basava, Y. Zhang, R. Csapo, V. Malis, S. Sinha, et al., Pixel-based meshfree modelling of skeletal muscles, Comput. Methods Biomech. Biomed. Eng. Imaging Vis. 1163 (2015) 1–13. doi:10.1080/21681163.2015.1049712.

[298] S.-W. Chi, Image-Based Computational Mechanics Frameworks for Skeletal Muscles, Ph. D. Dissertation, University of California, Los Angeles, 2009.

[299] P. Krysl, T. Belytschko, Analysis of thin plates by the element-free Galerkin method, Comput. Mech. 17 (1995) 26–35. doi:10.1007/BF00356476.

[300] G.-R. Liu, X.L. Chen, A mesh-free method for static and free vibration analyses of thin plates of complicated shape, J. Sound Vib. 241 (2001) 839–855. doi:10.1006/jsvi.2000.3330.

[301] P. Krysl, T. Belytschko, Analysis of thin shells by the element-free Galerkin method, Int. J. Solids Struct. 33 (1996) 3057–3078. doi:10.1016/0020-7683(95)00265-0.

[302] S. Long, S.N. Atluri, A meshless local petrov-galerkin method for solving the bending problem of a thin plate, C. - Comput. Model. Eng. Sci. 3 (2001) 53–63.

[303] D. Wang, H. Peng, A hermite reproducing kernel Galerkin meshfree approach for buckling analysis of thin plates, Comput. Mech. 51 (2013) 1013–1029. doi:10.1007/s00466-012-0784-9.

[304] N.H. Kim, K.K. Choi, J.-S. Chen, Shape Design Sensitivity Analysis and Optimization of Elasto-Plasticity with Frictional Contact, AIAA J. 38 (2000) 1742–1753. doi:10.2514/2.1163.

[305] N.H. Kim, K.K. Choi, J.-S. Chen, Die shape design optimization of sheet metal stamping process using meshfree method, Int. J. Numer. Methods Eng. 51 (2001) 1385–1406. doi:10.1002/nme.181.

[306] N.H. Kim, K.K. Choi, J.-S. Chen, Y.H. Park, Meshless shape design sensitivity analysis and optimization for contact problem with friction, Comput. Mech. 25 (2000) 157–168. doi:10.1007/s004660050466.

[307] F.C. Günther, W.K. Liu, D. Diachin, M. a. Christon, Multi-scale meshfree parallel computations for viscous, compressible flows, Comput. Methods Appl. Mech. Eng. 190 (2000) 279–303. doi:10.1016/S0045-7825(00)00202-4.

[308] A. Huerta, S. Fernández-Méndez, Time accurate consistently stabilized mesh-free methods for convection dominated problems, Int. J. Numer. Methods Eng. 56 (2003) 1225–1242. doi:10.1002/nme.602.

[309] T.-P. Fries, H. Matthias, A stabilized and coupled meshfree/meshbased method for the incompressible Navier--Stokes equations—part I: stabilization, Comput. Methods Appl. Mech. Eng. 195 (2006) 6205–6224. doi:10.1016/j.cma.2005.12.003.

[310] T.-P. Fries, H. Matthias, A stabilized and coupled meshfree/meshbased method for the incompressible Navier-Stokes equations-Part II: Coupling, Comput. Methods Appl. Mech. Eng. 195 (2006) 6191–6204. doi:10.1016/j.cma.2005.12.003.